NASA/CR—2020-220368

Small Lunar Base Camp and In Situ Resource Utilization Oxygen Production Facility Power System Comparison

Anthony J. Colozza
Vantage Partners, LLC, Brook Park, Ohio

March 2020

NASA STI Program . . . in Profile

Since its founding, NASA has been dedicated to the advancement of aeronautics and space science. The NASA Scientific and Technical Information (STI) Program plays a key part in helping NASA maintain this important role.

The NASA STI Program operates under the auspices of the Agency Chief Information Officer. It collects, organizes, provides for archiving, and disseminates NASA's STI. The NASA STI Program provides access to the NASA Technical Report Server—Registered (NTRS Reg) and NASA Technical Report Server—Public (NTRS) thus providing one of the largest collections of aeronautical and space science STI in the world. Results are published in both non-NASA channels and by NASA in the NASA STI Report Series, which includes the following report types:

- TECHNICAL PUBLICATION. Reports of completed research or a major significant phase of research that present the results of NASA programs and include extensive data or theoretical analysis. Includes compilations of significant scientific and technical data and information deemed to be of continuing reference value. NASA counter-part of peer-reviewed formal professional papers, but has less stringent limitations on manuscript length and extent of graphic presentations.

- TECHNICAL MEMORANDUM. Scientific and technical findings that are preliminary or of specialized interest, e.g., "quick-release" reports, working papers, and bibliographies that contain minimal annotation. Does not contain extensive analysis.

- CONTRACTOR REPORT. Scientific and technical findings by NASA-sponsored contractors and grantees.

- CONFERENCE PUBLICATION. Collected papers from scientific and technical conferences, symposia, seminars, or other meetings sponsored or co-sponsored by NASA.

- SPECIAL PUBLICATION. Scientific, technical, or historical information from NASA programs, projects, and missions, often concerned with subjects having substantial public interest.

- TECHNICAL TRANSLATION. English-language translations of foreign scientific and technical material pertinent to NASA's mission.

For more information about the NASA STI program, see the following:

- Access the NASA STI program home page at http://www.sti.nasa.gov

- E-mail your question to help@sti.nasa.gov

- Fax your question to the NASA STI Information Desk at 757-864-6500

- Telephone the NASA STI Information Desk at 757-864-9658

- Write to:
  NASA STI Program
  Mail Stop 148
  NASA Langley Research Center
  Hampton, VA 23681-2199

NASA/CR—2020-220368

Small Lunar Base Camp and In Situ Resource Utilization Oxygen Production Facility Power System Comparison

Anthony J. Colozza
Vantage Partners, LLC, Brook Park, Ohio

Prepared under Contract NCC12BA01B

National Aeronautics and
Space Administration

Glenn Research Center
Cleveland, Ohio 44135

March 2020

Acknowledgments

I would like to acknowledge Ian Jakupca and Bill Bennet for their technical review and Christina Gerber for her editorial review.

Level of Review: This material has been technically reviewed by expert reviewer(s).

Available from

NASA STI Program
Mail Stop 148
NASA Langley Research Center
Hampton, VA 23681-2199

National Technical Information Service
5285 Port Royal Road
Springfield, VA 22161
703-605-6000

This report is available in electronic form at http://www.sti.nasa.gov/ and http://ntrs.nasa.gov/

Contents

Small Lunar Base Camp and In Situ Resource Utilization Oxygen Production Facility Power System Comparison

Anthony J. Colozza
Vantage Partners, LLC
Brook Park, Ohio 44142

Summary

This report examines the power requirements for operating an in situ resource utilization (ISRU) oxygen production system on the lunar surface and a small six-person base camp. The baseline ISRU system produced 1.63 kg/h for a total day and night production rate of 1,154 kg. It was estimated that this plant would require 25.83 kW of power to operate. The base camp power includes auxiliary equipment as well as a communications system. The required power estimate for the base camp was 28.05 kW. This estimation was used to size a power system and determine its mass for meeting these requirements. Three types of power systems were considered: a solar photovoltaic (PV) array system using batteries for energy storage, a PV array system using a regenerative fuel cell (RFC) for energy storage, and a modular 10-kW electrical output power Kilopower reactor system. Three separate cases were examined: a stand-alone ISRU oxygen production system, a base camp, and a combined ISRU oxygen production system and base camp.

For the PV array-based system, the RFC energy storage method had a mass advantage over a battery-based energy storage system. For higher power nighttime power operation for all three cases, the RFC system's specific energy was just over 830 Wh/kg. For the lower power nighttime "keep-alive" level used as part of the Case 1 analysis, the specific energy for the RFC was 456 Wh/kg. Both of these levels are significantly above the specific energy of 200 Wh/kg for the battery. Because of this higher specific energy, the RFC-based system provided significant mass advantages over the battery-based energy storage system.

The baseline reactor system utilized shielding and separation distance to meet the desired maximum radiation dose level of 5 rem/yr for personnel operating within the vicinity of the power loads, base camp, and oxygen production facility. There are methods that could potentially be utilized to reduce the shielding requirements and separation distance. Implementing these would reduce the overall system mass for the reactor. Also, optimizing the reactor output to a specific mission would provide benefits in mass at the expense of modularity.

The results of the power system comparison between a solar PV array-based system and a Kilopower reactor-based system has shown that for missions required to operate throughout the lunar night at power levels comparable to those used during the day, the reactor-based system provides a significant mass advantage. However, for applications that can meet their mission requirements while only having to operate during the daytime with minimal power required to survive the nighttime, the PV array-based system provides a mass advantage.

1.0 Introduction

The lunar surface provides a number of challenges for both manned and unmanned missions. A key aspect to successfully operating on the lunar surface is the availability of a reliable power source that can meet the mission requirements for the duration of the mission. The power system requirements will vary considerably depending upon the type of mission (manned or robotic) as well as the individual power requirements of the components or devices associated with that particular mission or activity. The estimated power levels for some of the potential missions, devices, and vehicles are listed in Table 1. The items highlighted in gray were the missions selected for study in this report.

TABLE 1.—POWER LEVEL RANGE OF VARIOUS MISSIONS OR ACTIVITIES ON LUNAR SURFACE

Mission	Power level range, kW	Notes
Habitat/base camp power	30.0 to ≥ 100.0 (avg. 5 to 10 kW/person)	This power level is directly related to size of habitat and number of people it will need to support.
Communications system power	0.3 to 1.0 per transmitter (surface to surface and surface to orbit)	The power levels are for powering a single transmitter. The total communications system may also be powered from a central power source.
Support equipment power (vehicles, rovers, etc.)	2.0 to 10.0	This power level depends on activity that vehicle is supporting, and whether it is manned or unmanned.
Long range rover power/heavy equipment vehicle	7.0 to 30.0	For long-range pressurized rover, the power level will depend on the number of people it needs to support.
Charging station power	1.0 to 10.0	The charging station output power will vary depending on the number of vehicles charged and the desired charge time.
Electrostatic/electric field radiation shielding power (cosmic rays and solar protons)	1.0 to ≥ 10.0	A number of factors determine the power level such as distance of the field and shielding required. The shield uses very high voltage to produce deflection of particles but not much power.
In situ resource utilization (ISRU) processing heat and power (O_2 and raw material production)	10.0s to 100.0s (thermal) 10.0s to 100.0s (electrical)	Thermal and electrical power requirements are highly variable depending on process used and rate of production.
Long distance rover (magnetic field mapping, general science) power	0.1 to 5.0	Power level depends on rover size and type of science performed.
Water ice exploration and recovery heat and power	10.0s to 100.0s (thermal) 10.0s to 100.0s (electrical)	As with general ISRU, this will depend on amount of water that is to be processed.
Remote, stand-alone geology station power	0.1s to 1.0	Sensor requirements, heating for nighttime operation, and communications will determine power requirement.
Remote, stand-alone astronomy observatory power	0.1s to 1.0	Communications and nighttime operation are main power consumption items.

An in situ resource utilization (ISRU) oxygen production facility and a small lunar base camp were selected from the missions and activities listed in Table 1 for evaluation. There are a number of different types of power sources that can potentially meet the requirements of these selected mission components on the lunar surface. For this analysis, two types of power systems were selected and sized to meet their requirements; a constant power nuclear system based on the Kilopower technology and a photovoltaic- (PV-) based system utilizing either batteries or a regenerative fuel cell (RFC) for energy storage.

For comparing the power system to these mission aspects, the following assumptions were made:

- The power systems would provide power for operation over 1 day and night period. The identified systems would operate either continuously over this time period or during the daytime, approximately 354 h, and have adequate power to enable the system to survive the nighttime, also approximately 354 h.
- The ISRU production goal would be to produce at least 1,000 kg of oxygen over 1 day and night period.
- The habitat and base camp goal would be to meet the power requirements for sustaining six astronauts over a day and night period.
- The oxygen production and base camp would be located at 30° N latitude.

Figure 1.—Moon (Ref. 1).

2.0 Lunar Environment

The Moon (Figure 1) is a dry, crater-filled land with no appreciable atmosphere. The temperature difference from the sunlit areas to shadowed areas can exceed 300 K. The surface is covered with a fine powdered material called regolith made from eons of bombardment by meteors, asteroids, and comets. The successful design and operation of a lunar oxygen production system within this harsh environment will require the system to leverage the advantages of the environment (such as abundant solar energy) and minimize the disadvantages (such as temperature extremes). From the solar availability to the amount of removable oxygen in the soil, the capabilities of this system will be based on how well it is adapted to these environmental conditions.

The Moon orbits Earth every 27.3 Earth days. It is tidally locked to the Earth, therefore, it rotates at the same rate it orbits Earth. This causes the same side of the Moon to face Earth all of the time. Having the same side continually face Earth provides an advantage when it comes to communications. A device or system placed on the Earth-facing side of the Moon can be in constant communication with Earth without the need for a lunar satellite communications system. However, the day length on the Moon is 29.5 Earth days. This is the synodic period, the time it takes for the Sun to move across the sky and return to its starting point for a fixed point on the lunar surface.

Another unique orbital characteristic is its low declination angle of approximately 1.5°. This angle means that there is very little variation in solar elevation throughout the year and little seasonal effect. Because of this, locations at high elevations near the poles could be in constant sunlight throughout the year, pending local geographical obstructions. The Clementine spacecraft identified just such a location in 1994. This continuously illuminated location is on the rim of the Peary crater at the Moon's north pole (Ref. 2). Some additional physical characteristics of the Moon are listed in Table 2.

The temperature variations between the day and nighttime on the lunar surface are extreme. The hottest location on the lunar surface is during the daytime near the equator where the surface temperature can reach approximately 112 °C (385 K), whereas, that same location at night would drop to approximately –173 °C (100 K). Toward the poles, the daytime temperature does not get very high due to the low sun angles at these latitudes. The maximum surface temperature achieved at 89° latitude is around –120 °C (~153 K). These variations in temperature, as a function of latitude, can be seen in the Lunar Reconnaissance Orbiter data shown in Figure 2 (Ref. 6).

TABLE 2.—MOON'S PHYSICAL PROPERTIES[a]

Declination angle, degree, ψ_{max}	1.5
Lunar orbital eccentricity, ε_l	0.0549
Day length, t_d, h	708.33
Distance from Earth, km	
Perigee	363,300
Apogee	405,500
Total days (Earth) to revolve around the Sun	365.25
Orbital eccentricity of Earth/Moon system orbit, ε	0.0167
Average orbital radius of Earth/Moon system (about the Sun), r_{orbm}, km	1.496×10^8
Surface gravity, g, m/s^2	1.623
Lunar to Earth gravity ratio, g_r	0.165
Surface temperature min., K	102
Surface temperature max., T_{ls}, K	385
Surface daytime avg. sink temperature, T_{sd}, K	270
Surface nighttime avg. sink temperature, T_{sn}, K	84
Lunar radius, r_m, km	1,737
Lunar surface albedo, a_{ls}	0.3
The mean solar intensity (at Earth's orbital location), I_m, W/m^2	1,353

[a]References 3 to 5.

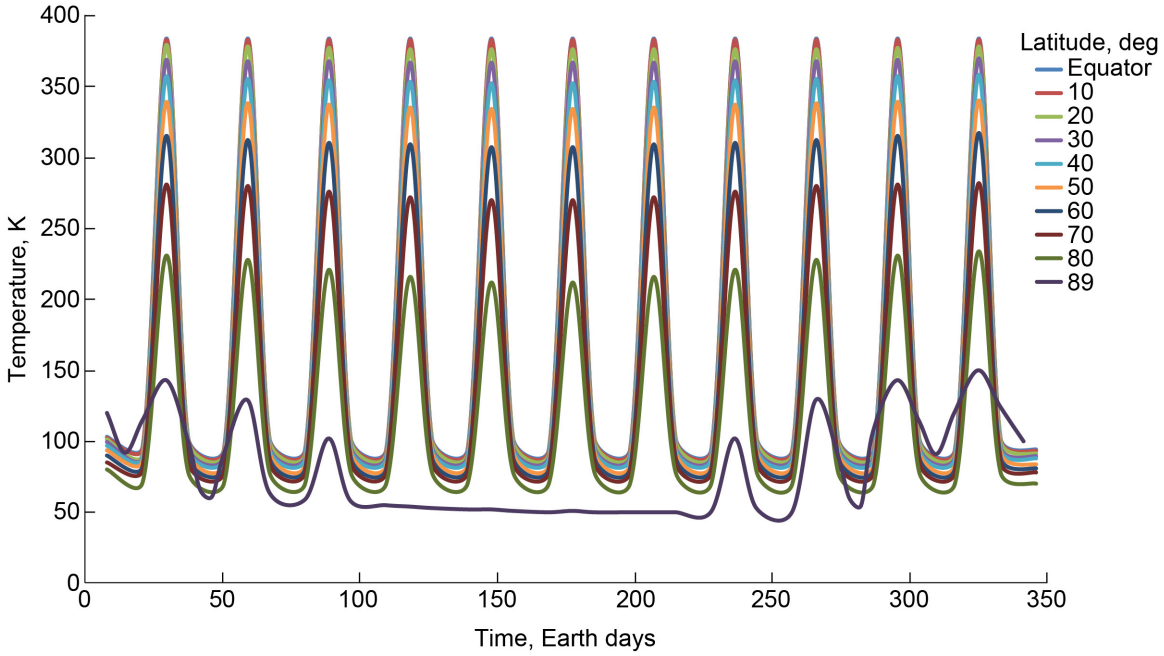

Figure 2.—Lunar Reconnaissance Orbiter lunar surface temperature data.

2.1 Surface Characteristics

The cratered highlands and the mare are the two main types of terrain on the lunar surface. The highlands are the older and significantly cratered parts of the lunar surface and appear brighter from Earth. The mare are darker regions comprising basaltic lava flows. These areas can be seen in the topographic map of the lunar surface shown in Figure 3. The blue and purple regions are the lower-lying mare regions while the red, orange, and yellow areas are the upper highland regions. The lunar regolith covering the surface of the moon consists of fragments of rocks, minerals, and glass spherules formed when meteors or other bodies impacted the surface. The regolith thickness varies greatly with location on the lunar surface. In the mare, the thickness can vary between 3 to 16 m whereas in the highlands it is at least 10 m thick (Ref. 7). The chemical and/or mineral composition of the regolith is similar to the underlying bedrock from which it was derived. There is little mixing of material between the highland and mare regions. The composition of the major materials (>1 percent of the composition) in each of these regions are given in Table 3.

The regolith is composed of fine grains of the mineral compounds given in Table 2. The grain size of the regolith varies but consists mostly of particles <1 mm in diameter. This is similar in consistency to silt or fine sand (Ref. 7). The average regolith density (ρ_r) is approximately 1,000 kg/m^3.

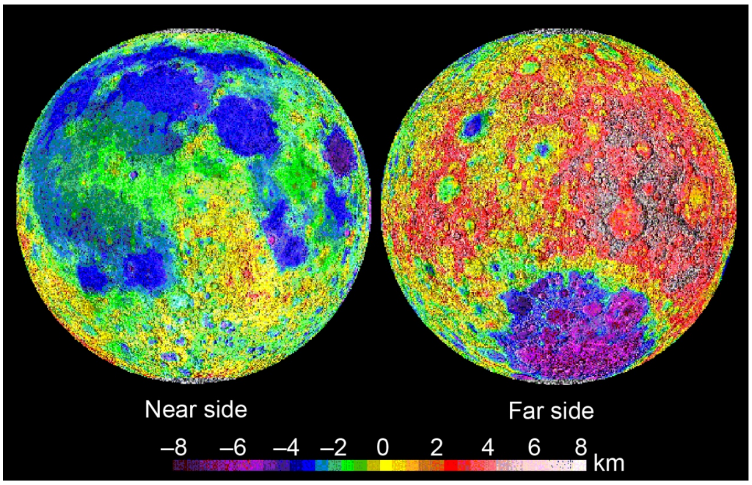

Figure 3.—Lunar Reconnaissance Orbiter lunar topographic map. Credit: NASA/Lunar and Planetary Institute (LPI). Image processing by Brian Fessler and Paul Spudis, LPI. (Used with permission.)

TABLE 3.—LUNAR SURFACE MINERAL COMPOSITION[a]

Compound	Highland, percent	Mare, percent
SiO_2	44.50	41.0
Al_2O_3	26.00	12.8
FeO	5.77	16.2
CaO	14.90	12.4
MgO	8.05	9.2
TiO_2	-------	7.3

[a]References 7 and 8.

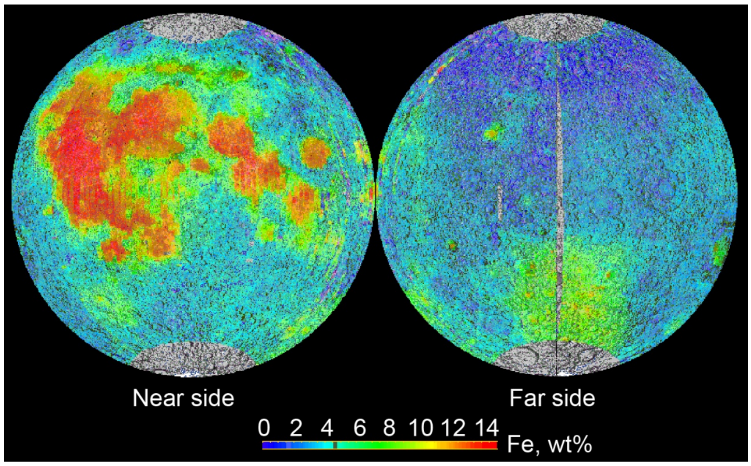

Figure 4.—Iron concentration on the lunar surface. Credit: NASA/Lunar and Planetary Institute (LPI). Image processing by Brian Fessler and Paul Spudis, LPI. (Used with permission.)

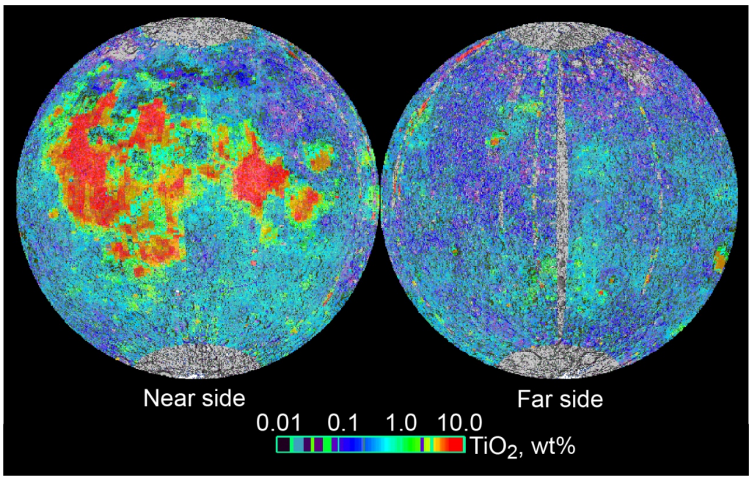

Figure 5.—Titanium concentration on the lunar surface. Credit: NASA/Lunar and Planetary Institute (LPI). Image processing by Brian Fessler and Paul Spudis, LPI. (Used with permission.)

Key compounds in the production of oxygen from lunar material are the iron oxides and titanium dioxides. Figure 4 shows the iron content on the lunar surface and Figure 5 shows a map of the titanium content. In both of these figures, higher concentrations are in red and orange and lower concentrations are in blue.

By looking at Figure 3 to Figure 5, it can be seen that the highest concentrations of iron oxide and titanium dioxide (ilmenites ($FeTiO_3$)) occur in the low-lying mare regions. Within these mare regions of high iron and titanium content, ilmenite is present in the loose regolith. About two-thirds of the ilmenite is in glassy agglutinates and basaltic rock fragments much larger than the common regolith grain size. The average amount of small grain size ilmenite available in the mare regions is approximately 7 wt% ($R_{m'}$, = 0.07) and 5 vol% ($R_{v'}$, = 0.05) of the regolith (Ref. 8).

Based on these percentages, the density of ilmenite (ρ_i) is approximately 1.4 times that of the regolith or 1,400 kg/m^3. The thermal conductivity of the fine-grained ilmenite is estimated to be 0.425 W/(m·K), which is similar to that of sand (Ref. 9). The specific heat of the ilmenite (c_p) is approximated by that of the mare regolith. The c_p as a function of temperature (T_i) is given by Equation (1) (Ref. 9).

$$c_p = -1{,}848.5 + 1{,}047.41 \log(T_i) \quad \text{(J/kg·K)} \tag{1}$$

The regolith properties described above are summarized in Table 4.

2.2 Incident Solar Radiation

With the absence of an appreciable atmosphere, the solar intensity (I_s) at the lunar surface is fairly constant. There is a slight variation throughout the year due to the Earth's orbital eccentricity about the Sun. The variation in Earth's orbital radius (r_{orb}) from the mean orbital radius (r_{orbm}, which has a value of 1.496×10^8 km) is represented by the eccentricity (ε) of Earth's orbit that has a value of 0.017 as shown in Table 2. The distance between the Moon and Earth varies between 360,300 km (at perigee) to 405,500 (at apogee). The actual solar flux, or I_s, in W/m^2 for a specific day of the year is determined by Equations (2) and (3) where γ is the day angle. This variation in I_s throughout the year is shown in Figure 6.

$$I_s = I_m \left(\frac{r_{orbm}^2}{r_{orb}^2} \right) \text{ (W/m}^2\text{)} \tag{2}$$

$$r_{orb} = \frac{1 - \varepsilon^2}{1 + \varepsilon \cos(\gamma)} \text{ (m)} \tag{3}$$

TABLE 4.—SUMMARY OF REGOLITH PROPERTIES

Granular ilmenite density, ρ_i, kg/m^3	1,400.00
Ratio of mass of ilmenite to mass of regolith, R_m	0.07
Regolith coefficient of friction, μ_r	0.40
Ilmenite particle density, ρ_{ip}, kg/m^3	4,790.00
Regolith and ilmenite surface temperature, T_{io}, K	384.00

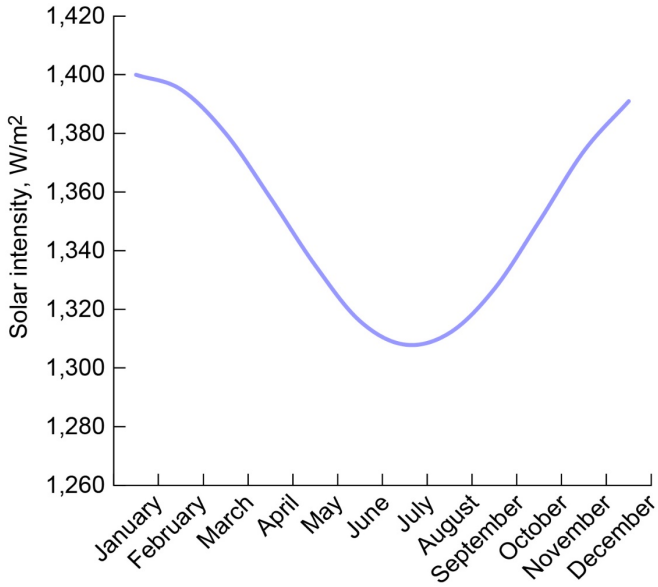

Figure 6.—Variation in solar intensity at a distance of 1 AU.

The γ used in Equation (3) is defined as 0° on January 4 (perihelion of Earth's orbit) and increases by 0.98° per day. The solar output varies from approximately 1,400 W/m^2 (on January 4) to 1,308 W/m^2 (on July 9). The variation on the I_s at the lunar surface due to the orbit of the Moon around the Earth is very slight. The maximum change in I_s resulting from the Moon's orbit about the Earth is a decrease of about 0.56 percent (~ 6 W/m^2) at the lunar surface. As the Moon orbits the Earth (defined as a lunar day), this small change in intensity will vary. Therefore, it was assumed to be negligible and the I_s at Earth's orbit was utilized in the subsequent analysis.

3.0 Oxygen Production

There are a number of potential methods for extracting oxygen from the lunar soil. Each process has significantly different power requirements, both thermally and electrically, as well as very different infrastructure requirements. Some of the more noted potential processes for removing oxygen from the lunar surface include

- Hydrogen reduction of ilmenite
- Carbothermal reduction of ilmenite and other oxides
- Hydrogen sulfide reduction of oxides
- Carbochlorination
- Fluorine exchange
- Hydrofluoric acid leach
- Direct electrolytic reduction of oxides
- Caustic solution electrolytic reduction of oxides
- Reduction of metal oxides by lithium or sodium
- Reduction of anorthite by aluminum
- Vapor phase reduction
- Ion separation
- Electrolysis of water ice

Hydrogen reduction of ilmenite is one of the more commonly proposed methods of oxygen production from lunar regolith and was the method used for this analysis. This is a fairly simple method that can be accomplished with present day technologies and uses ilmenite, an iron titanium oxide ($FeTiO_3$), as the oxygen source. Ilmenite is found throughout the lunar surface enabling the process to be utilized at almost any location. Because the reaction takes place at a relatively low temperature (~1,000 °C), below the melting point of the soil, the material compatibility and corrosiveness are not as significant an issue when compared to some of the other methods. The process utilizes hydrogen gas that will need to be supplied from Earth. However, the gas is mostly recoverable in the oxygen generation process. After the initial supply, only makeup gas will be needed to account for the gas not recovered or lost through leaking. Another advantage of this type of production is that it can utilize the surface regolith in areas that have a high iron and titanium content. This eliminates the need for the power-intensive activities of subsurface mining or processing rocks. The ability to directly utilize the surface regolith is a significant advantage for demonstrating an initial oxygen production technology or capability.

The hydrogen reduction of ilmenite is a two-step process represented by the reactions given in Equations (4) and (5) (Ref. 8). The first step in the process is the reduction of the ilmenite to iron, titanium dioxide, and water. This reaction takes place at approximately 1,000 °C. The second step is the electrolysis of the water to form hydrogen and oxygen.

$$2FeTiO_3 + 2H_2 \rightarrow 2Fe + 2TiO_2 + 2H_2O \quad (4)$$

$$2H_2O \rightarrow 2H_2 + O_2 \quad (5)$$

The overall resulting chemical reaction is given by Equation (6).

$$2FeTiO_3 + 2H_2 \rightarrow 2Fe + 2TiO_2 + O_2 + 2H_2 \quad (6)$$

The resulting oxygen will be stored for later use and the hydrogen will be recycled to perpetuate the process. The reduction process is performed in a fluidized bed reactor and the electrolysis is performed with an electrochemical electrolyzer.

A diagram of this process is given in Figure 7. This figure shows a nuclear reactor as a potential heat source. However, electrical power can drive the heaters within the oxygen reactor to maintain the temperature of the oxygen reactor. The process requires the ilmenite to remain at an elevated temperature of 1,273 K for approximately 1 h. An additional benefit of heating the ilmenite is the liberation of hydrogen. Hydrogen is present in mature lunar regolith because of exposure to the solar wind over long periods of time. The finer the particle grains, the larger the amount of hydrogen it will have trapped. This hydrogen content will range from 0.1 to 0.2 kg/m^3 of regolith. Since this hydrogen content is dependent on grain size and not material content, it is reasonable to assume the hydrogen concentration in the ilmenite is the same throughout the overall regolith. Therefore, as the ilmenite is heated, the hydrogen bonded to it will be released. It is estimated that at 900 °C, all of the hydrogen trapped with the ilmenite will be released. This released hydrogen will be utilized in the reduction of the ilmenite and will add to the overall hydrogen already in the system. It can be considered a source of makeup hydrogen to help offset any hydrogen losses from the system.

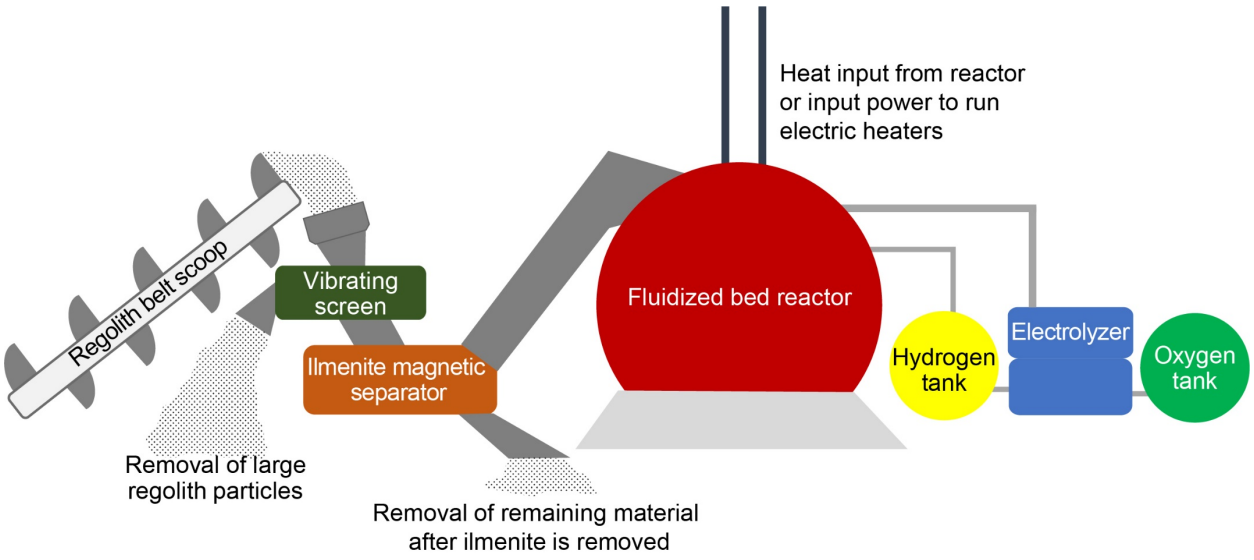

Figure 7.—Oxygen production process and components.

The sequence for the hydrogen reduction of ilmenite process illustrated in Figure 7 consists of the following:

- The regolith is scooped and transported to the screen.
- The larger regolith particles (greater than 1 mm in diameter) are separated using a vibrating screen and removed.
- The screened regolith is transported to a magnetic separator where the ilmenite is separated from the regolith.
- The ilmenite is transported to the fluidized bed reactor.
- In the reactor, the ilmenite is heated (1,273 K for 1 h) while hydrogen gas is circulated.
- The water vapor output is passed through an electrolyzer where it is separated into hydrogen and oxygen gas.
- The hydrogen gas is returned to the reactor and the oxygen is stored.

3.1 Oxygen Production System Power Analysis

An analysis was set up to evaluate the sizing of the system shown in Figure 7 for various rates of oxygen production. To perform the sizing analysis, an energy balance between the heat provided by the concentrator mirror and the requirements of the various components both thermally and electrically has to be made. Each of the components' thermal or electrical energy consumption has to be determined and scaled with the amount of regolith and/or ilmenite being processed. Since the process involves moving the material around, the height and material movement rates are needed in order to determine the energy consumption. These values can be varied to determine what effect they have on the overall system size and production rate.

The rate of ilmenite entering the reactor sets the rates for all of the other processes. This rate can be represented by the fraction of the reactor volume that is replenished each hour $\dot{V}_{ir}$. This quantity will have a value between 0 and 1. Establishing the replacement rate of the ilmenite in the reactor also sets the volume and mass flow requirements for all the other processes in the system. From this, the mass rate at which the regolith must be acquired from the surface ($\dot{M}_r$ in kg/h) can be determined. This rate is based on the total volume of ilmenite in the fluidized bed reactor and is shown in Equation (7). The reactor is assumed to be cylindrical. Its diameter (d_r) and height (h_r,) can be adjusted to increase or decrease the overall volume of ilmenite processed based on the desired oxygen production rate.

$$\dot{M}_r = \frac{\rho_i \dot{V}_{ir} \pi d_r^2 h_r}{4 R_m} \text{ (kg/h)} \tag{7}$$

The rate at which the regolith is taken from the surface defines the power required to scoop the regolith (P_{rs}) and transport it to the screen (P_{rl}) with a belt. These quantities are given in Equations (8) and (9), respectively. The P_{rs} is dependent on the distance the belt scoop travels in the regolith (d_{rs}, assumed to be 1 m) and the coefficient of friction of the regolith (μ_r). The μ_r was assumed to be 0.4, which is similar to that of sand. The power required to lift the regolith depends on the height that the scooped material is raised plus the P_{rl}. The belt power was scaled using the ratio of the lunar to Earth gravity constants and an equivalent earth power to operate a 3-m-long, 0.4-m-wide belt at an angle of approximately 30°. This height is assumed to be the height of the reactor plus the height the reactor is above the surface (h_{rs}, assumed to be 1 m). The electric motor efficiency (η_{em}) to drive the scoop and lift

the regolith is assumed to be 90 percent and the fraction of the batch time that is used to scoop the soil (t_{sc}) is assumed to be 0.01.

$$P_{rs} = \frac{\mu_r d_{rs} \dot{M}_r g}{3{,}600 t_{sc} \eta_{em}} \text{ (W)} \tag{8}$$

$$P_{rl} = \frac{(h_r + h_{rs}) \dot{M}_r g}{3{,}600 \eta_{em}} + 370 g_r \text{ (W)} \tag{9}$$

Once the regolith is picked up from the surface, the first step is to screen out the larger particles; those greater than a specific size are removed. This screening is necessary for the efficient operation of the fluidized bed reactor. The maximum particle size (d_s) and subsequent screen opening that allows for efficient fluidization is calculated in Equation (10) (Ref. 8). This equation has to be solved iteratively for the maximum particle size. It factors in a number of parameters for the operation of the fluidized bed reactor. These include the porosity of the fluidized bed (ε_p, estimated to be 0.5) and the hydrogen gas velocity within the reactor (U_{H_2}, estimated to be 0.3 m/s). Details on the hydrogen gas properties and the ilmenite are also required. These include the hydrogen gas density (ρ_{H_2}, given in Eq. (11)), hydrogen viscosity (μ_{H_2}, estimated to be 2.37×10^{-5} kg/(m·s)) (Ref. 8), ilmenite particle shape factor (τ, estimated to be that of sand, 0.83), and the ilmenite particle density (ρ_{ip}, estimated to be 4,790 kg/m^3). The ilmenite particle density is greater than that of the ilmenite in the soil. This is because the density of the ilmenite in the soil considers any spacing between the particles whereas the particle density is that of the material that makes up each particle.

$$\frac{150\rho_{H_2}(1-\varepsilon_p)U_{H_2}}{\tau^2\varepsilon_p^3\mu_{H_2}} = \frac{g\rho_{H_2}(\rho_{ip}-\rho_{H_2})}{\mu_{H_2}^2} d_s^2 - \frac{1.75\rho_{H_2}^2 U_{H_2}^2}{\tau\varepsilon_p^3\mu_{H_2}^2} d_s \tag{10}$$

The ρ_{H_2} is based on the ideal gas law (pressure (P_{H_2}) in Pascal, T_i in Kelvin, and the gas constant for hydrogen (R_{H_2}), 4,157 N·m/(kg·K)) with a compressibility factor (Z_{H_2}) for the hydrogen gas (Ref. 10).

$$\rho_{H_2} = \frac{P_{H_2}}{Z_{H_2} R_{H_2} T_i} \tag{11}$$

$$Z_{H_2} = 0.99704 + 6.4149\times10^{-9} P_{H_2} \tag{12}$$

The screening method selected for this analysis is a vibratory screen. A vibratory screening process is fairly simple. A screen with a specified mesh or opening size is vibrated as the regolith is poured onto it. The material that is less than the opening size will fall through to the next stage in the process whereas the material larger than the openings will be moved across the screen surface and discharged from one end of the screen and returned to the lunar surface. The power required to operate the vibratory screener (P_{vs}) is given by Equation (13) (Ref. 8).

$$P_{vs} = \frac{0.45\dot{M}_r}{507.72 d_s + 49.91\sqrt{d_s}} \tag{13}$$

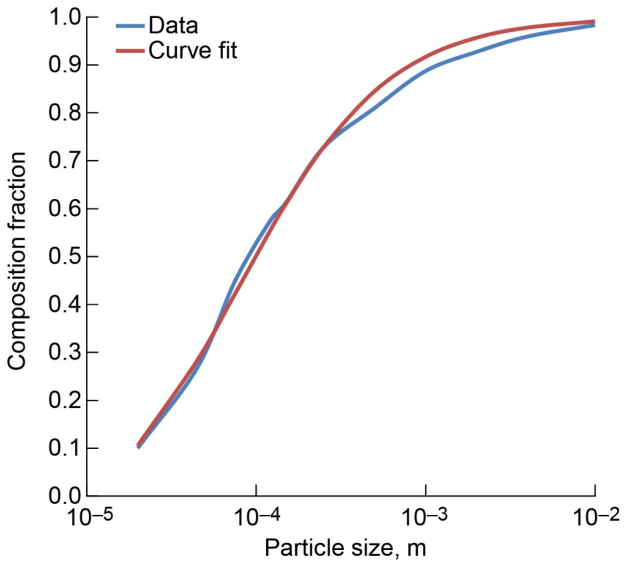

Figure 8.—Particle size distribution in the regolith.

The screening process will eliminate a portion of the regolith that was collected. The fraction of the regolith that will make it through the screen will depend on the desired maximum particle size determined by Equation (10). The particle size composition fraction (n_{ri}) of any size particle (d_i) within the regolith in meters is given by Equation (14). The composition fraction represents the fraction of regolith particles at the specified diameter or smaller within a general regolith sample. This equation is a curve fit representation of data (obtained from Ref. 8) on the percent concentration of particle size within the regolith. The particle size distribution along with the corresponding curve fit is plotted in Figure 8.

$$n_{ri} = \frac{d_i - 9.4008 \times 10^{-6}}{d_i + 8.0419 \times 10^{-6}} \tag{14}$$

The next step in the process is to separate the ilmenite from the regolith. For a smaller-scale oxygen production plant, the use of a permanent magnet or electromagnetic separator is preferred. This type of separator minimizes the power requirements compared to an induced magnetic roll separator or an electrostatic separator. The electromagnetic separator consists of a drum with alternating magnetic poles along its surface. Material is dropped over the drum as it rotates. Magnetic material will adhere to the surface where it is scraped off and captured. Nonmagnetic material will drop out of the bottom of the separator (Ref. 11). The power consumed by the separator (P_{ms}) in watts is given by Equation (15) (Ref. 8).

$$P_{ms} = 0.196 n_{ri} \dot{M}_r \tag{15}$$

The separated ilmenite has to now be lifted into the fluidized bed reactor. As in Equation (9), this distance is assumed to be the h_r plus the h_{rs}. The power required to lift the ilmenite (P_{il}) is given by Equation (16). Where the mass flow of ilmenite ($\dot{M}_i$) in kg/h is given by Equation (17). This mass flow is based on n_{ri}, which is based on d_s given by Equation (10) and used in Equation (14) for the particle size. It is assumed that the separation process is 90 percent efficient (η_s). Therefore 90 percent of the mass flow given by Equation (17) will be ilmenite. The remainder will be other materials that will not contribute to the reaction although it will go through the complete heating process.

$$P_{il} = \frac{(h_r + h_{rs})\dot{M}_i g}{3{,}600\eta_{em}} + 370 g_r \tag{16}$$

$$\dot{M}_i = n_{ri} R_m \dot{M}_r \tag{17}$$

Once the ilmenite enters the fluidized bed reactor, it is heated to 1,273 K and hydrogen gas is circulated through it. The energy to heat the soil comes from the power source. The concentrated solar radiation is focused onto a heat receiver. This heat receiver then conducts the heat into the reactor chamber where it is distributed throughout the chamber to heat the ilmenite. It is assumed that the reactor is designed to uniformly heat the ilmenite once it is in the reactor. As the ilmenite passes from the top of the reactor to the bottom, it is slowly heated. The selected rate at which the volume of ilmenite in the reactor is replaced, given previously as $\dot{V}_{ir}$, sets the amount of power needed to heat the soil. The ilmenite must be brought up to temperature and remain at temperature for a specified period of time (t_{rt}, in hours) in order for the reduction reaction (given by Eq. (6)) to take place. The time available to heat the ilmenite (t_h, in hours) is given by Equation (18). From this equation, it should be observed that there is an inherent limit on the rate at which the ilmenite is replaced and the duration at which it must be at temperature. This is because the time available to heat the ilmenite must be greater than zero.

$$t_h = \left(\frac{1}{\dot{V}_{ir}} - t_{rt} \right) \qquad \text{where} \qquad \dot{V}_{ir} t_{rt} < 1 \tag{18}$$

The thermal power required to heat the ilmenite (Q_{hi}), given by Equation (19), is dependent on this available heating time, the volume of ilmenite being heated, and the initial ilmenite properties. It is assumed that the ilmenite is initially at the illuminated surface temperature (T_{io}) of 384 K.

$$Q_{hi} = \frac{\rho_i c_p (T_i - T_{io}) \pi d_r^2 h_r \left(1 - t_{rt} \dot{V}_{ir}\right)}{14{,}400 t_h} \tag{19}$$

The ilmenite will lose heat to the surroundings (Q_{ls}) as it is being heated. To minimize this heat loss, the outside of the reactor vessel can be insulated with multilayer insulation (MLI). Because of the vacuum conditions at the lunar surface, radiation is the main heat transfer mechanism in which the reactor vessel will transfer heat to the surroundings. Therefore, multiple layers of a low emissivity (ε_i) material (such as polished nickel, $\varepsilon_i = 0.17$) that are closely layered will provide very good insulation. The greater the number of layers (n_l) and the smaller the spacing between the layers (d_{il}), the less the heat loss to the surroundings will be. The heat loss to the surroundings (at a sink temperature $T_s = 270$ K) from the insulated reactor vessel can be calculated from Equation (20) where the Stefan-Boltzmann constant (σ) has a value of 5.67×10^{-8} W/(m^2·K^4). If the reactor is constructed of a material different from that of the insulation, it will have a different emissivity (ε_{rO_2}, such as chromium $\varepsilon_{rO_2} = 0.14$).

$$Q_{ls} = \frac{\pi (d_r + n_l d_{il}) h_r \sigma \left(T_i^4 - T_{sd}^4\right)}{\left(\frac{1}{\varepsilon_{rO_2}} + \frac{2n_l}{\varepsilon_i} - n_l + 1 \right)} \tag{20}$$

In addition to the heat required to bring the ilmenite to the desired temperature and the loss of heat to the surroundings, the hydrogen reduction reaction itself will absorb heat from the system. The amount of

heat consumed (Q_r) due to the heat of reaction (H_r) is given by Equation (21). The heat of reaction for the hydrogen reduction of ilmenite is given as 294 kJ/kg (Ref. 8).

$$Q_r = \frac{H_r \eta_s \dot{M}_i}{3{,}600} \tag{21}$$

The last power-consuming component of the system is the electrolyzer. The electrolyzer's power requirement will depend on the amount of water that needs to be electrolyzed. The rate of water production ($\dot{M}_w$) is based on the ratio of the molecular weights of the reactant and product of interest, water. The rate of water production in kg/h is given by Equation (22). Subsequently, the rate of oxygen production ($\dot{M}_o$) can then be determined, which is given by Equation (23).

$$\dot{M}_w = \eta_s \dot{M}_i \frac{18}{308} \tag{22}$$

$$\dot{M}_o = \dot{M}_w \frac{16}{18} \tag{23}$$

A proton exchange membrane (PEM) electrolyzer was selected to separate the water into oxygen and hydrogen. The power required by the electrolyzer (P_e) can be calculated based on the theoretical power needed to break apart water given by the relationship for Gibbs free energy (ΔG) in Equation (24) (Ref. 12). For liquid water at 340 K (T_{H_2O}), the enthalpy change (ΔH) is 285.9 kJ/mol and the entropy change (ΔS) is the change given by Equation (25) where ΔS_{H_2O} = 69.94 (J/K)mol, ΔS_{O_2} = 205.29 (J/K)mol, and ΔS_{H_2} = 130.59 (J/K)mol. This results in an entropy change of –0.163 (kJ/K)mol. Therefore, using the previously calculated ΔH and ΔS, the available ΔG is 230.4 kJ/mol or 3,520 Wh/kg. Using this value, the mass flow rate of water, and the efficiency of the electrolyzer (η_e), the electrolyzer power can be determined as given by Equation (26).

$$\Delta G = \Delta H - T_{H_2O} \Delta S \tag{24}$$

$$\Delta S = -\Delta S_{H_2O} + \left(0.5 \Delta S_{O_2} + \Delta S_{H_2}\right) \tag{25}$$

$$P_e = \Delta G \frac{\dot{M}_w}{\eta_e} \tag{26}$$

The electrical power needed to operate the entire system, including the scoop and belt motors, the magnetic and vibratory separators, move the ilmenite, and operate the electrolyzer, is provided by the electrical power source. The required power output (P_{tO_2}) of the electrical source is given by Equation (27).

$$P_{tO_2} = P_{rs} + P_{rl} + P_{vs} + P_{ms} + P_{il} + P_e \tag{27}$$

And the total thermal power (Q_{tO_2}) output needed is given by Equation (28).

$$Q_{tO_2} = Q_r + Q_{ls} + Q_{hi} \tag{28}$$

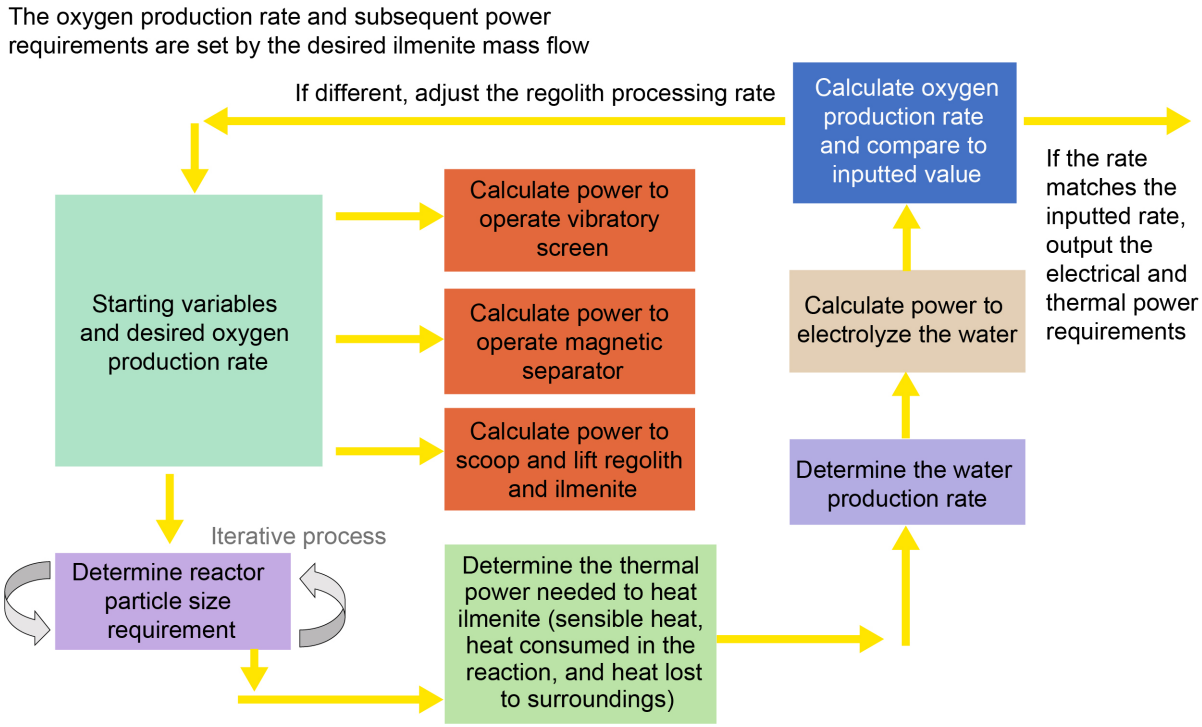

Figure 9.—Oxygen production rate analysis logic.

Equations (7) to (28) are used to size the oxygen production system and determine its power requirements. This is an iterative process that is based on selecting the desired oxygen production rate. To start the process of sizing the system to meet this oxygen production rate, a regolith processing rate is estimated. From this initial estimate, an oxygen production rate is calculated. Depending on this rate and its variation from the desired rate, the regolith processing rate is adjusted and the calculation redone. This iteration is continued until the output rate matches the desired input rate. This process is illustrated in Figure 9.

3.2 Oxygen Production System Power Requirements

Using the analysis described in Section 3.1, the required power, both electrical and thermal, was determined for the ISRU oxygen production plant. A baseline case was produced that represents the initial design and operation point for the ISRU system. The baseline assumptions used to generate this case are given in Table 5. These assumptions represent the best estimates of the performance for the various components as well as an initial sizing that is within the scope of a demonstration oxygen production system.

Using the assumptions given in Table 5, the total electrical and thermal power required for a range of oxygen production rates was determined and is shown in Figure 10. A breakdown of the thermal and electrical power requirements for the baseline oxygen production rate of 1.63 kg/h are given in Figure 11 and Figure 12, respectively. The total electrical power requirement is 9,329 W and the thermal power requirement is 16,502 W. Figure 11 shows the main thermal requirement for the system is for heating the ilmenite, as would be expected, which also demonstrates the importance of separating the ilmenite from the regolith. Since the heat required to bring the material up to the temperature where the reaction can take place is the largest power-consuming process within the system, minimizing the heating of any material that does not contribute to the oxygen production reaction is critical to minimizing the power requirements for the ISRU oxygen production system. Of the electrical power requirements shown in Figure 12, the electrolyzer uses almost all of the power to break apart water producing oxygen.

TABLE 5.—BASELINE ASSUMPTIONS FOR OXYGEN PRODUCTION PROCESS

Desired oxygen production rate, $\dot{M}_o$, kg/h	1.63
Total oxygen production over 1 day and night cycle, kg	1,154.00
Reactor diameter, dr, m	0.80
Reactor height, h_r, m	0.80
Height fluidized bed reactor is above the surface, h_{rs}, m	1.00
Distance scoop travels in the regolith, d_{rs}, m	1.00
Regolith and ilmenite conveyor belt length, L_{cb}, m	3.00
Fraction of batch time to scoop regolith, t_{sc}	0.01
Electric motor efficiency, η_{em}	0.90
Fluidized bed porosity, ε_p	0.50
Hydrogen velocity through the fluidized bed, U_{H_2}, m/s	0.30
Ilmenite particle shape factor, τ	0.83
Ilmenite hydrogen reduction reaction temperature, T_i, K	1,273.00
Ilmenite separation process efficiency, η_s	0.90
Time ilmenite is at the reaction temperature, t_{rt}, h	1.00
Number of layers of the multilayer insulation (MLI), n_l	50.00
Spacing between insulation layers, d_{il}, mm	0.10
Reactor emissivity, ε_r	0.17
Insulation layer emissivity, ε_i	0.17
Electrolyzer efficiency, η_e	0.72

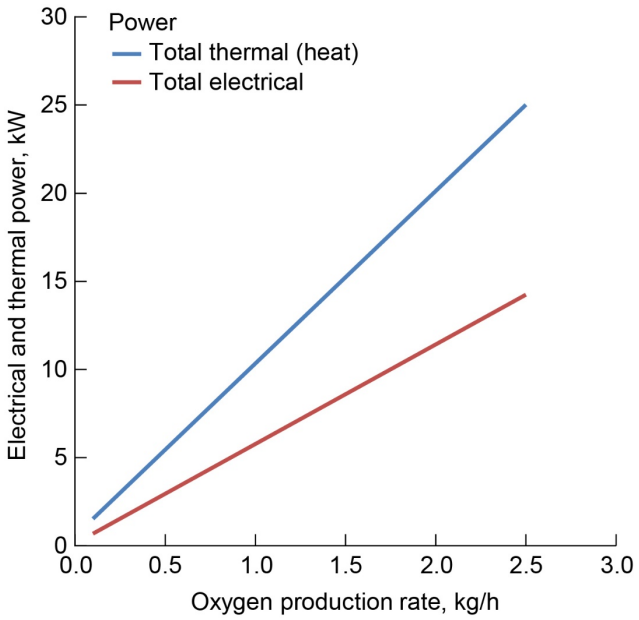

Figure 10.—Required thermal and electrical power over a range of oxygen production rates.

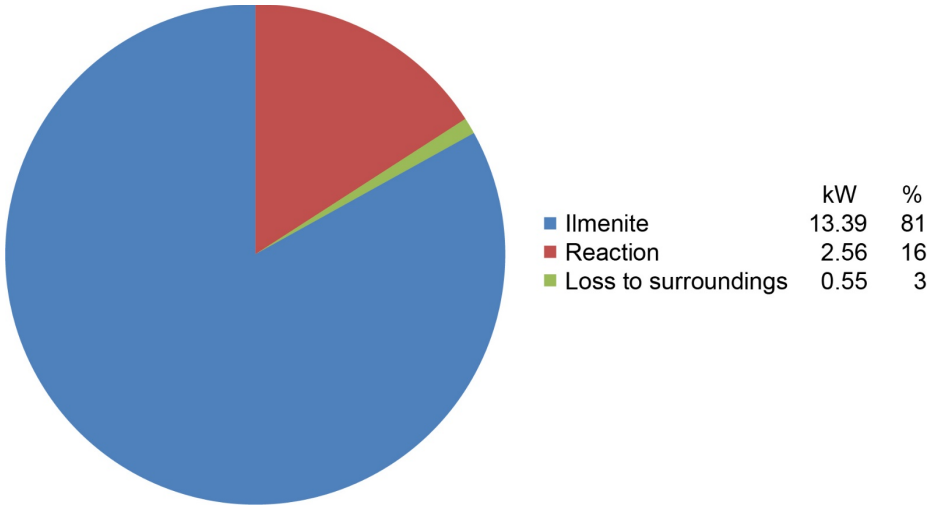

Figure 11.—Baseline oxygen production process thermal power requirements breakdown.

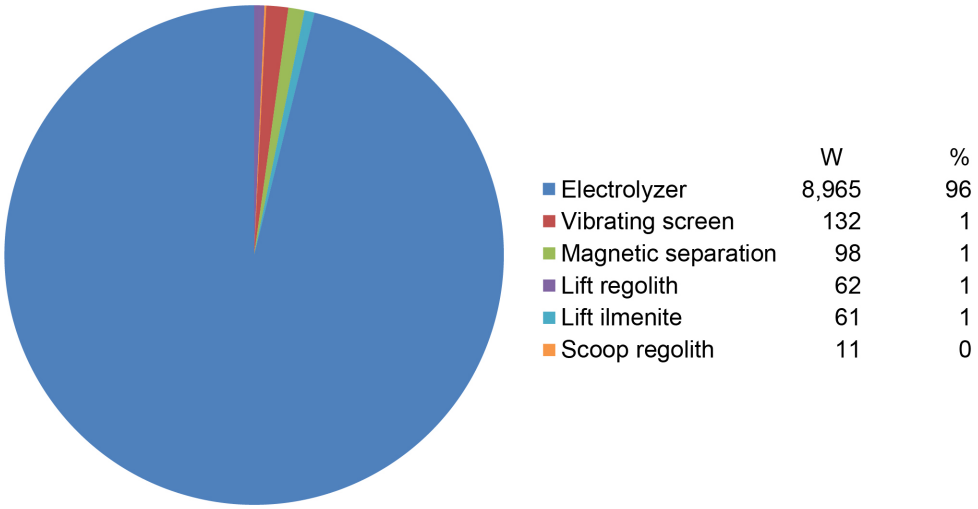

Figure 12.—Baseline oxygen production process electrical power requirements breakdown.

The thermal power can also be supplied by electrical heaters powered by an all-electric power system. For this case, a comparison of all power required by the system, both electrical and thermal, is shown in Figure 13. This comparison shows that heating the ilmenite is the largest power-consuming element comprising over 50 percent of the total system power. This power level is somewhat location and time dependent. There is a large variation in surface temperature depending on the latitude and time of year as shown in Figure 2. Operating at a time with higher surface temperatures will reduce the amount of heat needed to bring the ilmenite up to the desired temperature, whereas operating near the poles will require additional heat due to the cold surface temperatures even while sunlit. For example, operating near the poles where the surface temperature is 100 K will increase the power required to heat the ilmenite by 32 percent (from 13.4 to 17.7 kW) or a 16.5-percent increase in the total power required by the ISRU system. This approximately represents the maximum effect that site selection and time of operation can have on the system power requirement.

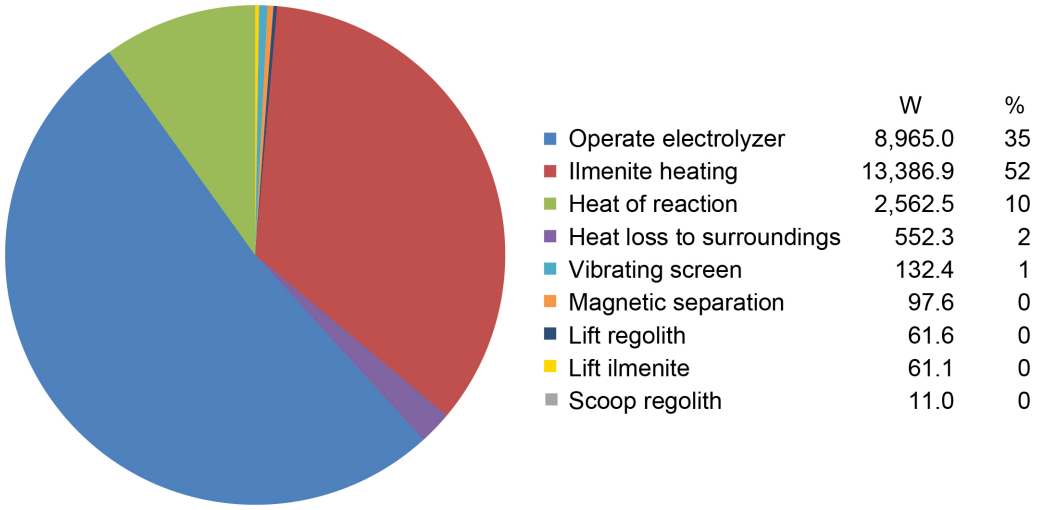

Figure 13.—Baseline oxygen production process total electrical power requirements breakdown.

TABLE 6.—ELECTROLYZER COMPONENT AND SCALING FACTOR BREAKDOWN (kg/kW)

Electrolyzer stack, S_{es}	2.00
Water tank and heater, S_{wt}	0.10
Filters, S_f	0.12
Propellant lines and fittings, S_{pl}	0.52
Controller unit, S_{cu}	0.16
Wiring, S_w	0.30
Heat exchanger, S_{he}	1.00
Water pump, S_{wp}	0.27
Check valves, S_{chv}	0.08
Flow regulators, S_{fr}	0.62
Control valves, S_{cv}	0.16
Pressure and temperature sensors, S_s	0.07
Flow sensors, S_{fs}	0.06

3.3 Oxygen Production System Mass Analysis

To accurately model the ISRU oxygen production system and the effect the power system requirements have on it, its mass must also be considered. To estimate the ISRU system mass, scaling equations were used for each of the components of the system. These equations allowed the system mass to be scaled based on their power consumption and regolith or ilmenite mass flow processed.

To size the mass of the electrolyzer (M_e), it was broken down into a number of components and scaled linearly based on its operational power level. The mass of the electrolyzer is given by Equation (29) and the components along with their scaling factors are listed in Table 6. The scaling values were based on representative commercially available components over a range of operating parameters as well as projected performance values for certain items. Linear curve fits for this data were used to generate the scaling factors.

A heat exchanger is used to precool the water vapor to a liquid and filters are used to remove any particulate matter from the liquid water prior to it entering the electrolyzer.

$$M_e = P_e\left(S_{es} + S_{wt} + S_f + S_{pl} + S_{cu} + S_w + S_{he} + S_{wp} + S_{chv} + S_{fr} + S_{cv} + S_s + S_{fs}\right) \tag{29}$$

The electrolyzer system will also require a radiator and its associated equipment to reject its waste heat during operation. The radiator mass (M_r) is calculated in a similar fashion as that described for the battery system in Section 5.1. As described in detail in Section 5.1, the required radiator area (A_r) is given by Equation (77) and its subsequent mass is given by Equation (79). The thermal power that must be rejected by the radiator (P_{te}) is given by Equation (30). This power is used as the radiator power to calculate its size. If the electrolyzer is operating only during the daytime, then louvers will be needed to reduce the heat loss from the system during the night.

$$P_{te} = 3{,}520\dot{M}_w\left(\frac{1}{\eta_e} - 1\right) \tag{30}$$

Also described in detail in Section 5.1, the mass of the remaining components of the thermal control system (MLI, cold plates, and heat pipes) are given by Equations (80) to (82), respectively, and the total thermal control system mass is given by Equation (81). The specific volume of the electrolyzer (S_{ve}) is given by Equation (88) and the corresponding area of the electrolyzer enclosure is given by Equation (89).

To minimize the mass of the reactor, hydrogen and oxygen storage tanks were spherical in shape. The total reactor tank mass (M_{rt}) is based on the mass of the reactor tank (M_t) itself plus the mass of the internal components of the tank as given by Equation (31). These internal components would include an auger mechanism to move the ilmenite while in the tank, lines to channel and distribute the hydrogen gas within the chamber, and lines to collect and channel the water vapor out of the tank as it is produced. For this analysis, these components were not sized directly. Their mass was estimated by using a scaling factor based (S_{rti}) on the reactor tank mass.

$$M_{rt} = M_t + M_t S_{rti} \tag{31}$$

The tank mass for each of the three tanks used in the system (reactor and hydrogen and oxygen storage) is determined by calculating the required wall thickness (t_t) to withstand the tank's internal pressure (P_t) while operating. The tank's wall thickness is given by Equation (32) which is based on the yield strength (σ_y) of the material used to construct the tank and the factor of safety (f_s) incorporated into the tank design.

$$t_t = \frac{P_t d_t f_s}{2\sigma_y} \tag{32}$$

The wall thickness can now be used to calculate the volume of material (V_{tm}) used to construct the tank as given by Equation (33).

$$V_{tm} = \frac{4\pi\left[\left(\frac{d_t}{2} + t_t\right)^3 - \left(\frac{d_t}{2}\right)^3\right]}{3} \tag{33}$$

With this volume, the tank mass can then be calculated based on the tank material density (ρ_{tm}) as given by Equation (34).

$$M_t = V_{tm}\rho_{tm} \tag{34}$$

The tank mass calculation, given by Equation (34), can be used to calculate the mass for the reactor tank as well as the hydrogen and oxygen storage tanks. The variables used to calculate each of the tank masses are summarized in Table 7.

The mass of the vibrating screen, which is used to separate the particles of the regolith above a specific size, is based on the size of the particle that is passed through the screen and the rate at which the material is screened. The screening rate ($\dot{R}_{vs}$) as a function of the maximum particle size is shown in Figure 14 and modeled by Equation (35), which in turn provides the required vibrating screen area (A_{vs}) given by Equation (36).

TABLE 7.—OXYGEN PRODUCTION TANK SIZING VARIABLES

Variable	Symbol	Tank		
		Reactor	Hydrogen storage[a]	Oxygen storage[b]
Pressure, psi (MPa)	P_t	147 (1)	1,350 (9.3)	1,350 (9.3)
Baseline tank diameter, m	d_t	0.8	0.8	1.27
Factor of safety	f_s	2.5	2.5	2.5
Tank material	---	Titanium alloy	Carbon composite	Carbon composite
Material yield strength, psi (MPa)	σ_y	120,000 (825)	275,000 (1,900)	275,000 (1,900)

[a]Diameter assumed to be similar to reactor tank.

[b]Diameter calculated based on the mass of the oxygen produced during 1 lunar day and night cycle.

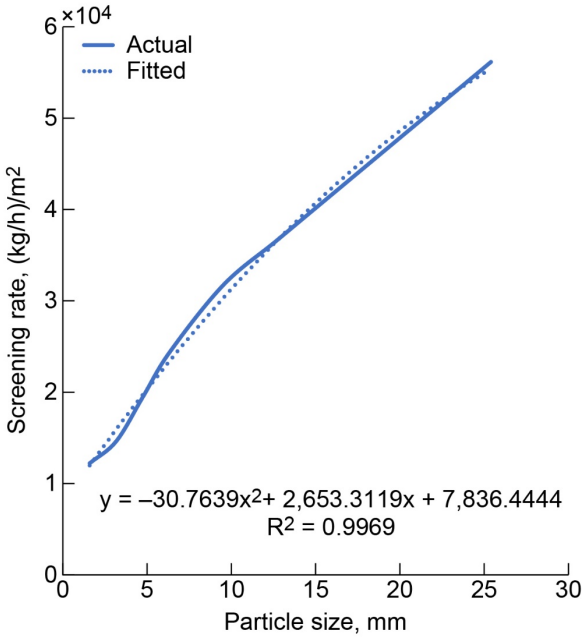

Figure 14.—Vibrating screen material flow rate versus particle size.

$$R_{vs} = -30.76 d_s^2 + 2{,}653.31 d_s + 7{,}836.44 \tag{35}$$

$$A_{vs} = \frac{\dot{M}_r}{\dot{R}_{vs}} \tag{36}$$

Using the required vibrating screen area, the mass of the vibrating screen (M_{vs}) can be estimated. This is based on the relationship between the vibrating screen area and mass given in Figure 15 and Equation (37).

$$M_{vs} = 36.35 A_{vs}^2 + 193.63 A_{vs} + 57.68 \tag{37}$$

The mass of the magnetic separator (M_{ms}), which is used to separate the ilmenite from the regolith after it is screened, is given by the relationship between the required separation rate and separator mass given in Figure 16 and Equation (38).

$$M_{ms} = 0.0497 A_{vs}^2 + 2.279 A_{vs} + 97.53 \tag{38}$$

The last items of the oxygen production system are the conveyor belts for moving the regolith to the vibrating screen and the ilmenite to the reactor. It is assumed that both belt systems are the same size and, therefore, mass. The conveyor belt mass (M_{cb}) is based on an estimate of the belts used to move rocks and soil on Earth and scaling it for operation within the lower lunar gravitational environment. This relationship is given by Equation (39).

$$M_{cb} = 51.33 g_r L_{cb} \tag{39}$$

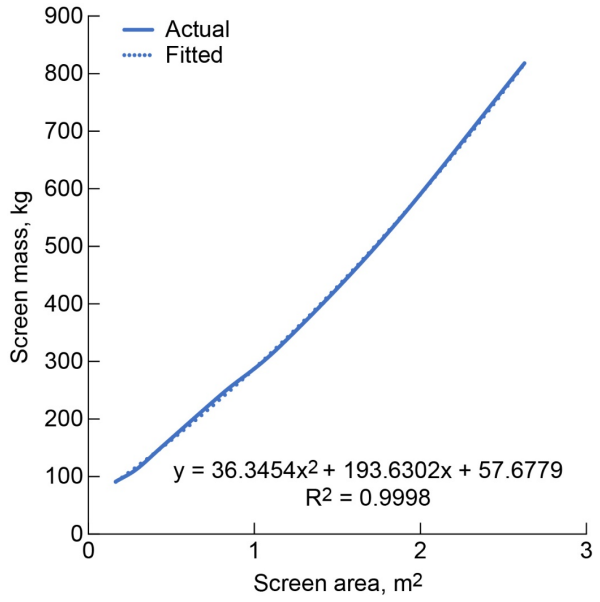

Figure 15.—Vibrating screen mass based on screen area.

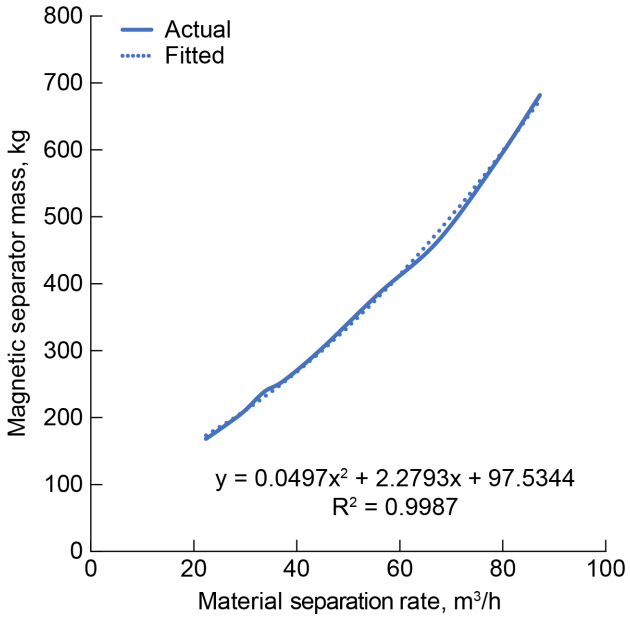

Figure 16.—Magnetic separator mass versus the separation rate.

The total oxygen production system mass as a function of the production rate is shown in Figure 17. This figure is based on the mass scaling equations given previously with a storage capacity for 1 day and night cycle's oxygen production. The mass breakdown for the baseline rate of 1.63 kg/h is shown in Figure 18. This figure shows that the largest mass component is the oxygen storage tank. The tank is sized to store 1 lunar day and night period of the oxygen produced by the system. At the baseline production rate, this is a total of 1,155 kg of oxygen.

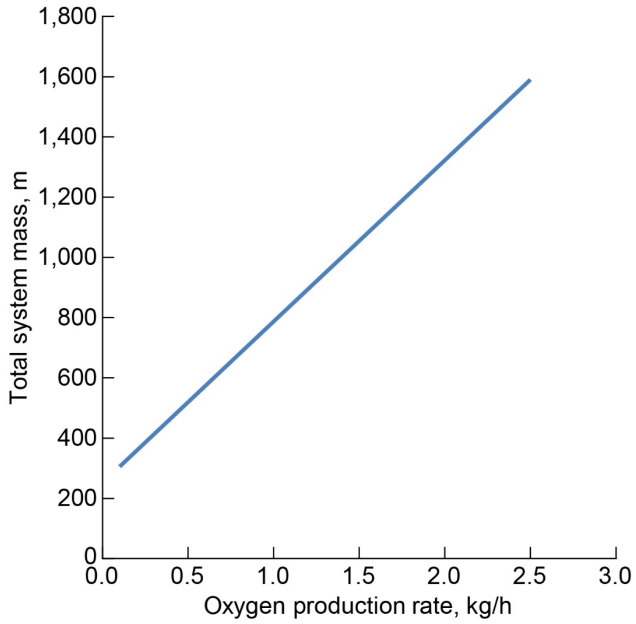

Figure 17.—Mass of the oxygen production system as a function of the production rate.

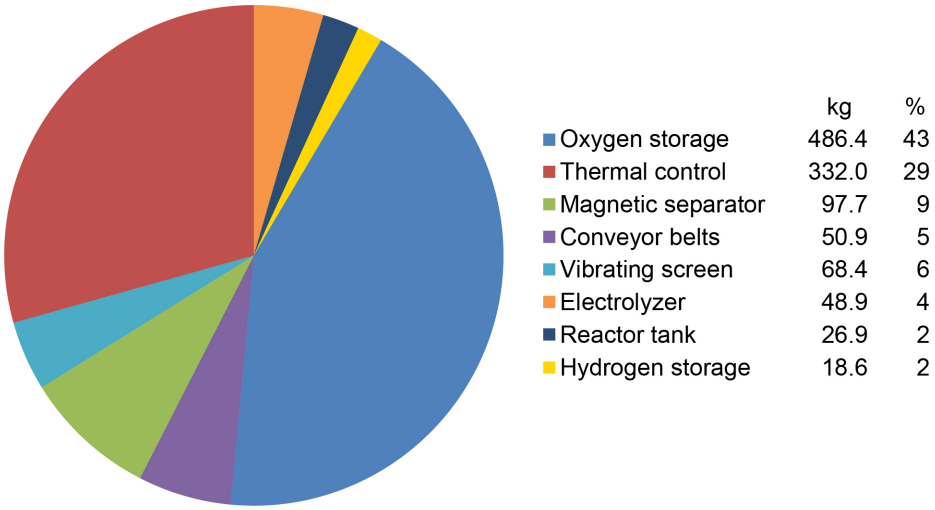

Figure 18.—Baseline oxygen production system mass breakdown.

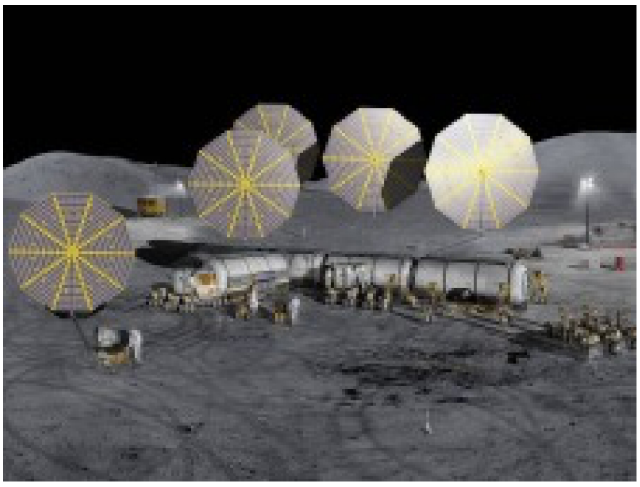

Figure 19.—Cross section of a small six-person base camp.

4.0 Habitat and Base Camp

A small base camp would consist of a habitat and support equipment needed to support the personnel and equipment used at the camp, as illustrated in Figure 19. The power requirements for the base camp can be categorized into three main areas:

1. Life support equipment (heating, cooling, air handling, and CO_2 removal)
2. Communications (equipment and displays for communications to and from Earth and to and from personnel on the surface)
3. Operational equipment (computers, science equipment within the habitat, experiments, and lighting)

In sizing the power requirements for the base camp, it was assumed that the base camp would be capable of sustaining six people for day and night operation on the lunar surface. As with the ISRU system, the operational latitude was 30° N.

4.1 Environmental Control and Life Support

The main power requirement (P_{ls}) for the habitat will be for the environmental control and life support systems (ECLSSs). This is broken down into a number of different power-consuming items that include air handling and conditioning (P_{ahc}), biomass (P_{bm}), food storage and processing (P_{fd}), thermal cooling components (P_{th}), waste processing (P_{wst}), water processing (P_{wp}), and support for extravehicular activities (P_{eva}). The total ECLSS power is given by Equation (40). It should be noted that the thermal system power identified under the habitat is for operation of the cooling system pumps and other items. Heaters for heating the habitat are not included and, as will be shown at the end of this section, not necessary since waste heat for ECLSS operation can be utilized to make up some or all of the heater power requirements.

$$P_{ls} = P_{ahc} + P_{bm} + P_{fd} + P_{th} + P_{wst} + P_{wp} + P_{eva} \tag{40}$$

Estimates for the day and night power requirements for the ECLSS of a six-person independent habitat on the lunar surface are given in Table 8.

TABLE 8.—SIX-PERSON HABITAT ENVIRONMENTAL CONTROL AND LIFE SUPPORT SYSTEM (ECLSS) POWER REQUIREMENTS (kW)[a]

Air (CO_2 removal, oxygen generation), P_{ahc}	5.85
Biomass, P_{bm}	6.10
Food, P_{fd}	4.27
Thermal, P_{th}	1.03
Waste, P_{wst}	0.01
Water processing, P_{wp}	1.29
Extravehicular activity support, P_{eva}	2.50
Total, P_{ls}	21.05

[a]Reference 13.

A thermal analysis of the heat loss that would occur during the nighttime was performed to determine if heater power was required during nighttime operation or if the waste heat from the operation of the equipment was sufficient to maintain the internal operating temperature of the habitat. It was assumed that the habitat was insulated with MLI. The heat loss paths from the habitat that were considered in the analysis included

- Through the MLI
- From passthroughs and seams in the MLI
- Out of the radiator connections
- Through the support legs of the habitat contacting the surface
- Through the airlock structure

The amount of heat lost through the insulation is dependent on the habitat geometry, environmental temperatures (desired internal habitat temperature T_{hi} and the nighttime sink temperature T_{sn}), their type, and n_l. For this analysis, the habitat was assumed to be a hemisphere. The heat loss from the habitat through the insulation is given by Equation (41). As with the reactor tank, which was also insulated with MLI, the heat loss is based on the surface area of the habit (A_h) and the emissivity of both habitat wall surface (ε_{hw}) and MLI layers (ε_l).

$$Q_{hi} = \frac{A_h \sigma \left(T_{hi}^4 - T_{sn}^4 \right)}{\left(\frac{1}{\varepsilon_{hw}} \right) + \left(\frac{2n_l}{\varepsilon_i} \right) - (n_l + 1)} \tag{41}$$

The surface area for the hemisphere is dependent on its diameter (d_h) as given by Equation (42).

$$A_h = \frac{\pi d_h^2}{2} \tag{42}$$

The MLI is very good at resisting heat flow. However, the majority of heat leak through the insulation occurs from passthroughs and seams (Q_{ps}) in the insulation covering. This heat leak is approximated by Equation (43), which is based on the mean insulation temperature (T_m) given by Equation (44) and passthrough constants 1 and 2 (f_n and f_p), given by Equations (45) and (46).

$$Q_{ps} = 0.664 \left(\frac{0.000136}{4\sigma T_m^2} + 0.000121 T_m^2 \right) f_p f_n A_h \sigma \left(T_{hi}^4 - T_{sn}^4 \right) \tag{43}$$

$$T_m = \left[\frac{\left(T_{hi}^2 + T_{sn}^2\right)\left(T_{hi} + T_{sn}\right)}{4} \right]^{1/3} \tag{44}$$

The f_p is based on the presence of passthrough area (A_{pt}) of items such as wires or tubes that pass through the insulation. This area is given in percent value, for example, if the estimated passthrough area is ½ percent, 0.5 is used as the percent passthrough area.

$$f_p = 0.73 + 0.27 A_{pt} \tag{45}$$

$$f_n = 4.547 - 0.501 n_i \tag{46}$$

The values used for the variables in determining the heat loss through the passthroughs and seams are given in Table 9.

During the night, the coolant loop will be turned off to minimize the heat loss from the radiator. Since there is no longer any heat flow to the radiator, it will drop in temperature to match that of the surroundings over the night period. Therefore, the heat leak from the habitat to the radiator (Q_{ra}) will be dependent on the conduction down the coolant tubes that connect the radiator to the habitat. This is similar to the heat loss that occurs through the support legs (Q_{sl}) and the airlock structure (Q_{as}). The heat leak (Q_{cp}) through conduction from these sources is given by Equation (47), which is dependent on the number of conductive paths (n_{cp}), the thermal conductivity of the material (k), the cross-sectional area of the material normal to the direction of the heat flow (A_{cp}), and the length of the conductive path (L_{cp}).

$$Q_{cp} = \frac{n_{cp} k A_{cp} \left(T_{hi} - T_{sn}\right)}{L_{cp}} \tag{47}$$

The cross-sectional area for the conductive paths is given by Equation (48). It was assumed that all of the paths considered could be represented by a hollow cylinder shape with a specified inner diameter (d_{icp}) and wall thickness (t_{cp}) where the cross-sectional area of that shape is normal to the flow of heat from the interior of the habitat to the surroundings.

$$A_{cp} = \pi \left[\left(\frac{d_{icp}}{2} + t_{cp} \right)^2 - \left(\frac{d_{icp}}{2} \right)^2 \right] \tag{48}$$

The variables used to determine the heat leak for each of the identified conductive paths are summarized in Table 10.

TABLE 9.—HABITAT PASSTHROUGH AND SEAMS HEAT LEAK VARIABLES

Habitat wall emissivity, ε_{hw}	0.07
Insulation emissivity, ε_i	0.07
Number of layers of insulation, n_l	25.00
Habitat diameter, m, d_h	8.00
Percent of passthrough area, A_{pt}	1.00

TABLE 10.—HABITAT CONDUCTIVE PATH HEAT LEAK VARIABLES

Variable	Symbol	Radiator coolant lines	Support legs	Airlock structure
Number of conductive paths	n_{cp}	16	10	2
Material	---	Stainless steel	Titanium alloy Ti-6Al-4V	Stainless steel
Thermal conductivity, W/(m·K)	k	19.00	6.70	19.00
Inner diameter, m	d_{icp}	0.02	0.46	1.48
Thickness, cm	t_{cp}	0.10	2.00	10.00
Length, m	L_{cp}	0.10	1.00	0.25
Interior temperature, K	T_{hi}	295.00	295.00	295.00
Surrounding sink temperature, K	T_{sn}	84.00	84.00	84.00

TABLE 11.—HABITAT NIGHTTIME HEAT LOSS SUMMARY (W)

Insulation, Q_i	245
Passthroughs and seams, Q_{ps}	1,883
Radiator, Q_{ra}	42
Support legs, Q_{sl}	426
Airlock structure, Q_{as}	1,500
Total, Q_h	4,096

The total heat loss from the habitat to the surroundings during nighttime operation (Q_h) is given by Equation (49) and summarized in Table 11.

$$Q_h = Q_i + Q_{ps} + Q_{ra} + Q_{sl} + Q_{as} \tag{49}$$

Since the power required to make up the heat loss (Table 11) is less than that of the ECLSS (Eq. (50)), the additional heater power (P_{ht}) needed to maintain the habitat at its operating temperature is set to zero. The waste heat from the other systems can be used to maintain the habitat temperature during the nighttime period.

$$Q_h < (P_{ls} - P_{th}) \therefore P_{ht} = 0 \tag{50}$$

4.2 Communications

To support the surface operations, a communications station, as shown in Figure 20, will be needed by the base camp to provide a data link between the base camp on the lunar surface, orbiting satellites, and Earth. Examples of the data rate communications requirements are shown in Table 12.

To provide the types of communications links shown in Table 12, the base camp communications system will be required to both transmit and relay data to points on the surface or in orbit. This type of system would be very similar to a cellular phone transmission tower system. As with the habitat itself, the communications system will need to operate continuously throughout the day and night.

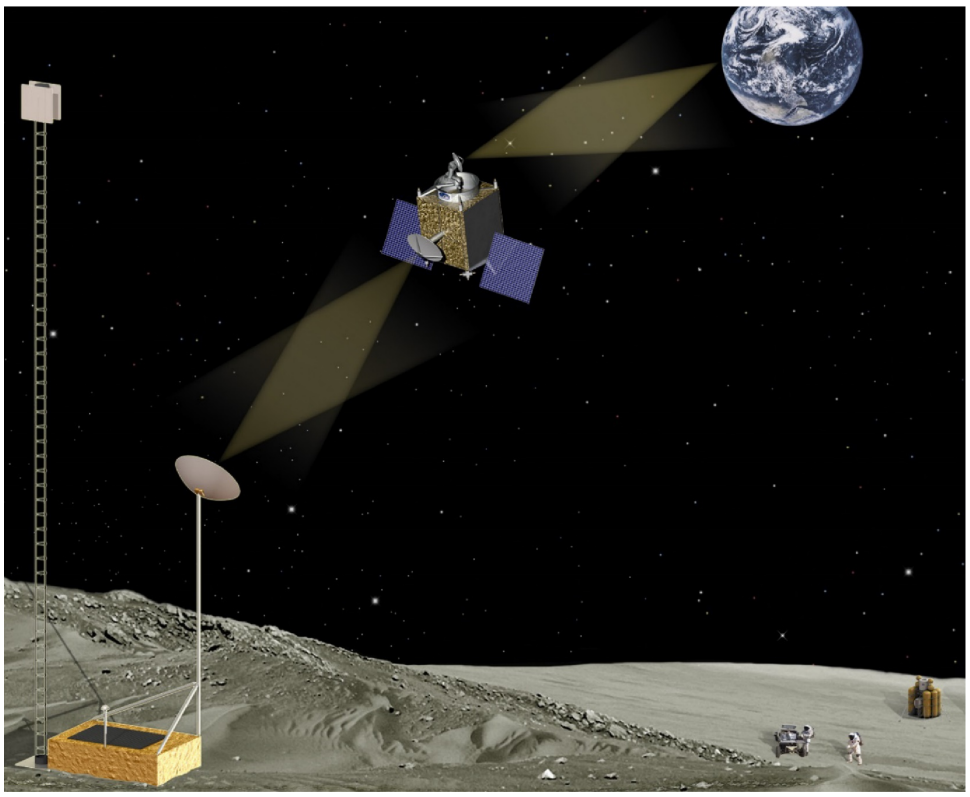

Figure 20.—Lunar surface communications station.

TABLE 12.—COMMUNICATIONS REQUIREMENTS
FOR VARIOUS LUNAR APPLICATIONS[a]

Application	Data rate, Mbps	Transmission distance, km
Lunar surface-to-spacecraft relay	1,000	6,500
Lunar surface low-rate communications	10	2,700
Surface-to-lunar science orbiter	100	2,700
Lunar surface human outpost	1,000	2,700

[a]Reference 14.

For surface-to-surface transmissions, the required power level for the transmitter (P_{tm}) and the signal strength at the receiver must be determined (P_{ss}). From the receiver power level, the maximum transmission data rate can be determined. For transmission over the lunar surface, the power at the receiver is given by Equation (51) (Ref. 15), which is dependent on the transmission centerline frequency (f_{cl}), the transmitter height above the surface (h_t), the receiver height above the surface (h_{re}), and the distance between the transmitter and receiver (d_{tr}). The value for the speed of light (c) is 2.998×10^8 m/s.

$$P_{ss} = \frac{P_{tm} c \left| \sin \frac{2\pi f_{cl} h_t h_{re}}{c d_{tr}} \right|}{2\pi d_{tr} f_{cl}} \tag{51}$$

The maximum transmission distance ($d_{tr_{\max}}$) will be limited by the curvature of the lunar surface. This distance is given by Equation (52) where the radius of the Moon (r_m) is 1,737.5 km. Due to interaction with the surface, the signal can, however, travel beyond the line of sight distance. This increase in transmission can be represented by an adjustment factor (K = 1.33) (Ref. 4).

$$d_{tr_{\max}} = K r_m \cos^{-1}\left(\frac{r_m}{r_m + h_t}\right) \tag{52}$$

The receiver power for a transmission from the surface to an orbiting satellite (P_{ro}) is based on the free-space loss due to dispersion of the signal as it travels from the transmitter to the receiver. Equation (53) calculates the surface-to-satellite receiver power.

$$P_{ro} = \frac{P_{tm} c}{4\pi d_{tr} f_{cl}} \tag{53}$$

The maximum achievable data rate ($R_{\max}$) can be calculated based on the receiver power as shown in Equation (54). Expressed as thermal noise, the data rate is based on the bandwidth of the transmission (B_w) and the noise power level (P_n) illustrated in Equation (55) (Ref. 16). The thermal noise is a function of temperature of the transmission and receiving system and the bandwidth of the transmission. For this analysis, the daytime sink temperature is used as a worst-case thermal noise temperature. The Boltzmann constant (k_b) has a value of 1.3803×10^{-23} J/K.

$$R_{\max} = B_w \log_2\left(1 + \frac{P_{ro}}{P_n}\right) \tag{54}$$

$$P_n = k_b T_{sd} B_w \tag{55}$$

The baseline assumptions used to determine the data rate capability and power requirements for the communications system are given in Table 13. From these assumptions, the required transmitter power and corresponding maximum data transfer rate were calculated for the lunar surface-to-lunar orbit, lunar surface-to-lunar surface, and lunar surface-to-Earth communications and are shown in Figure 21 to Figure 23, respectively. For the surface-to-surface communications, the maximum transmission distance, as calculated by Equation (51), was 11.1 km.

Based on the data rates shown in Table 12 and the communications power (P_{com}) required to achieve these data rates for both communications from the lunar surface (to orbit or Earth), a power level of 1 kW was assumed for the base camp communications system.

TABLE 13.—COMMUNICATIONS SYSTEM BASELINE

Transmitter and receiver tower height, h_t, m	10
Center operating frequency, f_{cl}, GHz	30
Effective noise temperature, T_{sd}, K	270

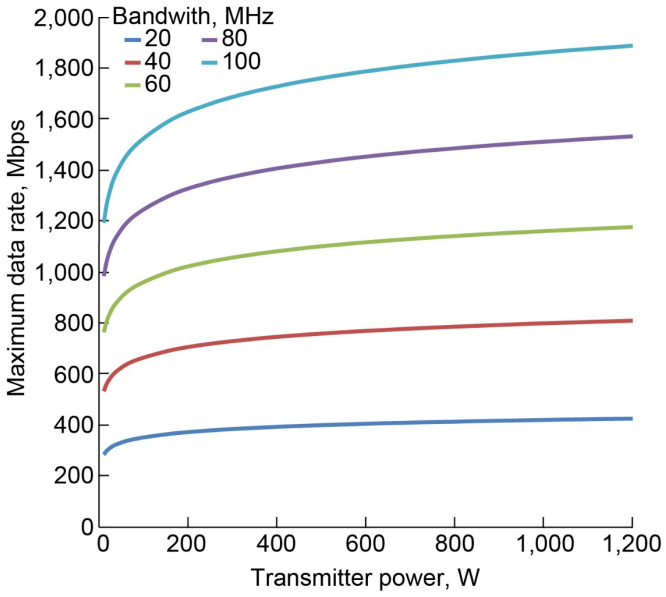

Figure 21.—Transmission power and data rate for lunar surface-to-lunar orbit (6,500 km) transmission bandwidths.

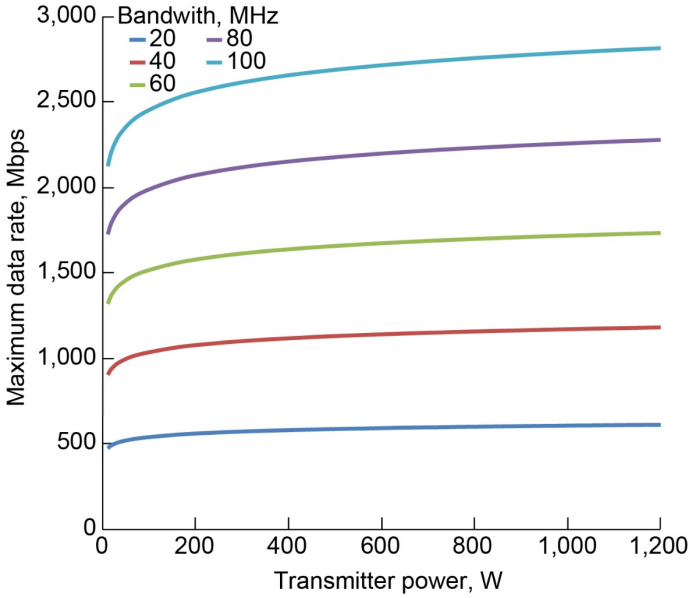

Figure 22.—Transmission power and data rate for lunar surface-to-lunar surface (11.1 km) transmission bandwidths.

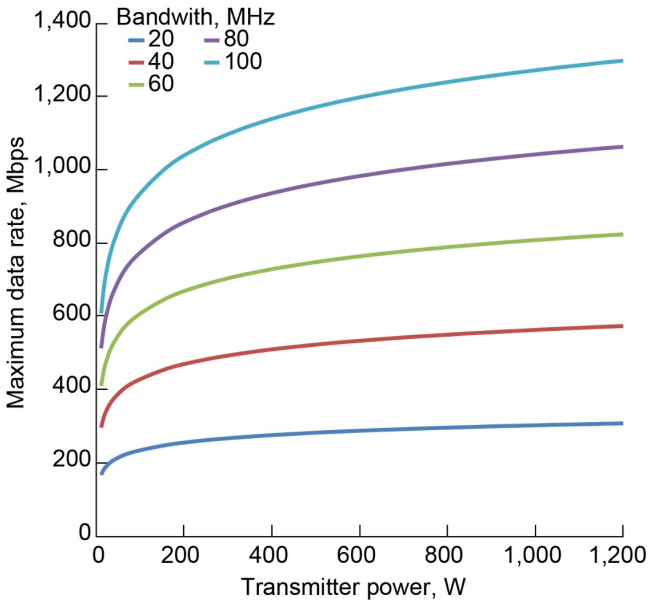

Figure 23.—Transmission power and data rate for lunar surface-to-Earth (384,400 km) transmission bandwidths.

4.3 Operational Equipment

Operational equipment within the habitat includes all of the power-consuming items that are utilized by the personnel as well as any experimental equipment and general habitat operations and maintenance equipment. The types of items that would consist of the operational equipment include

- Lights
- Computers
- Networking equipment
- Cameras
- Displays
- Experiments
- Sensors
- Food preparation
- Maintenance equipment (tools, vacuum, etc.)

Data taken at the Desert Research and Technology Studies (Desert RATS) campaign was used to estimate the operational power for these components. Under this program, an operational habitat demonstration unit (HDU), as shown in Figure 24, was constructed and operated for a number of weeks at the Black Point Lava Flow outside of Flagstaff, Arizona. The Desert RATS program was conducted annually with the goal to provide analog testing of different mission elements operating together in an environment similar to that of an actual lunar mission to evaluate the interactions between the different elements.

The power distribution system within the Deep Space Habitat (DSH) consisted of six power distribution units (PDUs). Each PDU had 12 controllable outlets. The power flow from each outlet was monitored to track the power consumption of individual items or systems as well as the total power consumed by the habitat during operation. The output power throughout the day for each day of operation of the habitat during one of the testing periods is shown in Figure 25. This power consumption represents all of the equipment utilized within the habitat and is a good representation of the operational equipment power usage for a small habitat.

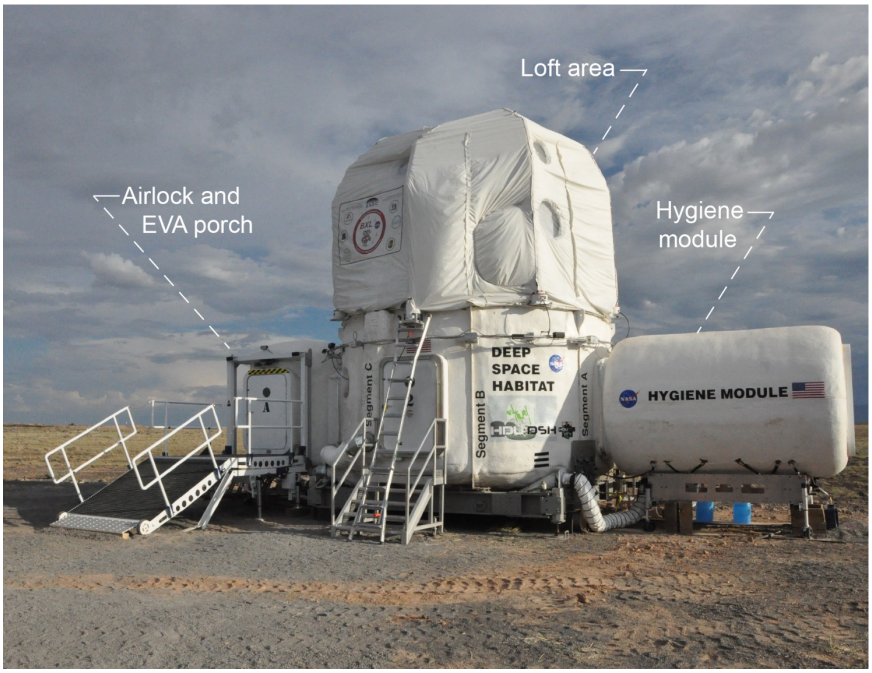

Figure 24.—Deep Space Habitat (DSH) testing at Desert Research and Technology Studies (Desert RATS) 2011. Extravehicular activity is EVA.

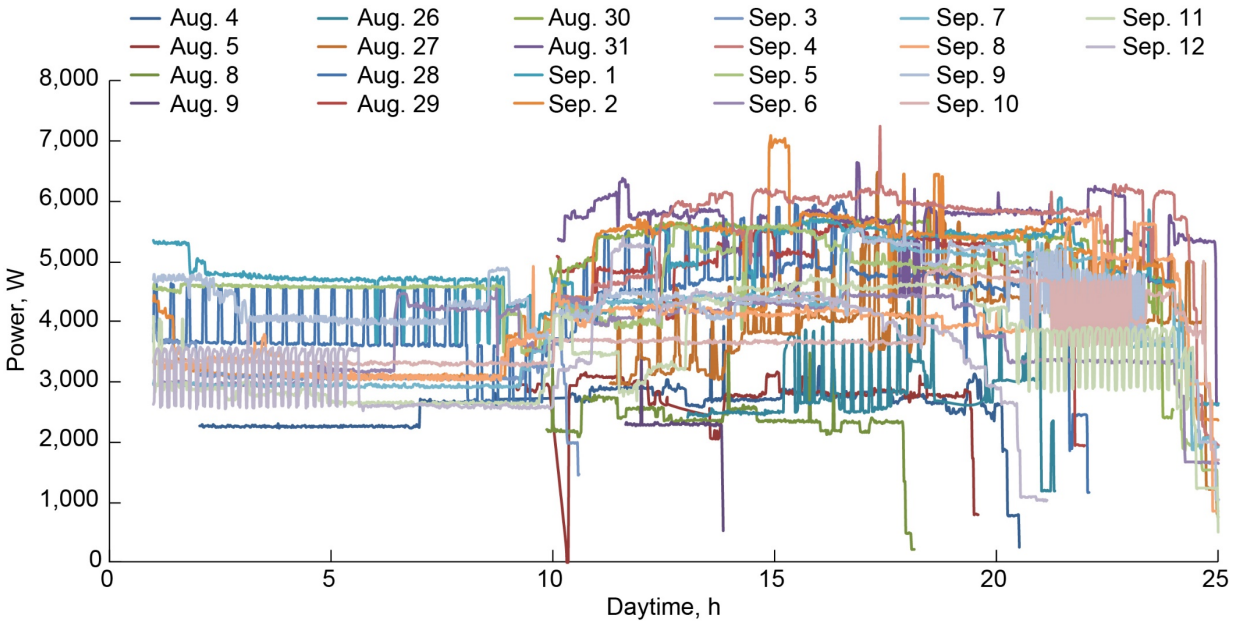

Figure 25.—Daily Deep Space Habitat (DSH) power consumption.

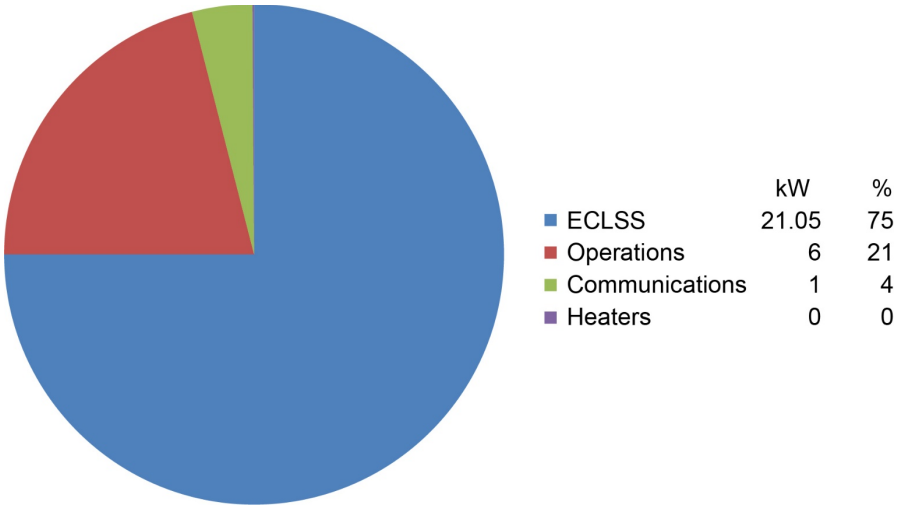

Figure 26.—Base camp power breakdown. Environmental control and life support system is ECLSS.

The data shown in Figure 26 can be used to estimate the operational equipment power (P_{oe}) requirements for the habitat. The data shows a power consumption range of 2.5 to 7.0 kW over the total period of operation of the habitat. Based on this, a conservative power consumption estimate of 6 kW was selected to represent the ancillary operational equipment power level.

4.4 Base Camp Total Power Requirement

Using the power estimates for the different components that make up the base camp, a total power requirement (P_{bc}) can be determined as given by Equation (56). This power requirement is continuous through both the day and nighttime periods. Since the habitat and its support equipment for the base camp have to sustain the six-person crew, there is no decrease in power during the nighttime period. The power requirement summary for the base camp is shown in Figure 26.

$$P_{bc} = P_{ls} + P_{ht} + P_{com} + P_{oe} \tag{56}$$

It should be noted that there was no heater power required for the habitat. The heat leak from the habitat during the nighttime was estimated to be 4,096 W. However, the waste heat generated by the other systems within the habitat (ECLSS and operations) is much greater than this level. Therefore, it is assumed that the waste heat can be utilized to maintain the internal habitat temperature during the night at the desired 295 K without the need for heaters.

5.0 Power System Sizing

To provide power for the ISRU oxygen production system and the base camp, both a PV array-based power system and Kilopower reactor-based system were considered. The power systems were sized to meet the electrical and thermal power requirements for both applications. While the power systems were both sized to operate within the vicinity of the base camp and ISRU system, the Kilopower system was also sized to operate a distance away to minimize the shielding requirements.

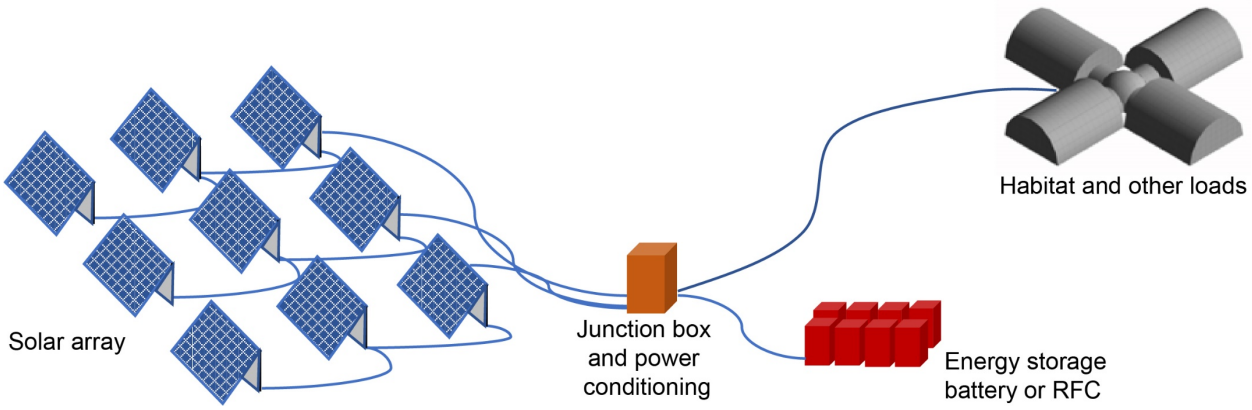

Figure 27.—Photovoltaic (PV) array-based power system layout. Regenerative fuel cell (RFC).

5.1 Photovoltaic Array Power System

The PV power system consists of a fixed PV array and energy storage system, either a battery or RFC, to meet the needs of the ISRU system and base camp as illustrated in Figure 27. An RFC system consists of an electrolyzer as described previously in Section 3.0 and a fuel cell, which is used to provide the nighttime power output. The fuel cell is an electrochemical device that produces electricity through the electrochemical recombination of hydrogen and oxygen. It does not "burn" the hydrogen as a conventional engine would. Instead, it combines it electrochemically to produce electricity and water as given by Equation (57). The water is subsequently stored and then broken apart into hydrogen and oxygen gas by the electrolyzer, reversing the direction of the reaction given by Equation (57), during the day when solar power is available.

$$2H_2(g)+O_2 \rightarrow 2H_2O \tag{57}$$

PV power systems are the most common type of space-based power system currently used. This type of system's advantages and disadvantages for the ISRU and base camp power include

Advantages:

- High technology readiness level (TRL) mainly for the PV and battery system; RFC system is lower.
- Power production is applicable to other mission aspects and will likely be utilized on other vehicles or installations. This provides a synergy in the power source design and the commonalty of the power system application could have additional benefits, such as cost, repair parts, and multiple system integration.

Disadvantages:

- Depending on location and power requirements, it may be limited to daytime operation only due to the excessive energy storage requirements of operating during the 14-Earth-day lunar night.
- Large size to achieve high power levels.
- The electrical conversion to heat reduces the overall efficiency of systems such as the oxygen production plant that requires significant amounts of high-quality heat.

The PV system sizing is heavily dependent on its operational environment. Items such as the time of year, latitude, and array orientation significantly influence its output power and sizing. For the PV array sizing, it was assumed that the array was south facing and fixed at a given inclination angle. The array was sized to provide enough power to meet both the day and nighttime power requirements specified for each of the cases examined. This was accomplished through an energy balance between the energy collected by the array during the day and the energy stored in the battery or RFC system for use at night. The array did not track the Sun, therefore the output power of the array varied throughout the day due to the changing Sun angle relative to the array surface. The fixed array was chosen since it utilized a simple lightweight structure and is less complicated to install and operate than a tracking array. It was also assumed that no applicable dust coverage was allowed to accumulate on the array surface. The power system assumptions used to size the array are given in Table 14.

The eccentricity of the Earth and Moon system orbit about the Sun causes the I_s to vary throughout the year, as shown in Figure 6. The vernal equinox was selected as the baseline operational date with an I_s of 1,359 W/m^2.

It is assumed that the array is at a fixed inclination angle and facing south (for Northern Hemisphere operation). The input to the array will consist of the direct beam component normal to the array surface as illustrated in Figure 28. Since there is no atmosphere, there is no diffuse component of the solar radiation.

TABLE 14.—VARIABLES USED TO SIZE SOLAR ARRAY POWER SYSTEM

Latitude	30° N was selected as the operational latitude for all cases
Date	March 21 (vernal equinox), day number 80
Solar cell efficiency, η_{sc}, percent	28
Battery discharge efficiency, percent	Up to 99 (rate dependent)
Battery charge efficiency, η_{bc}, percent	99
Fuel cell efficiency, η_{fc}, percent	65
Electrolyzer efficiency, η_e, percent	85
Array inclination angle and orientation, β	30°, south facing
Array solar cell fill factor, f_{sc}	0.89

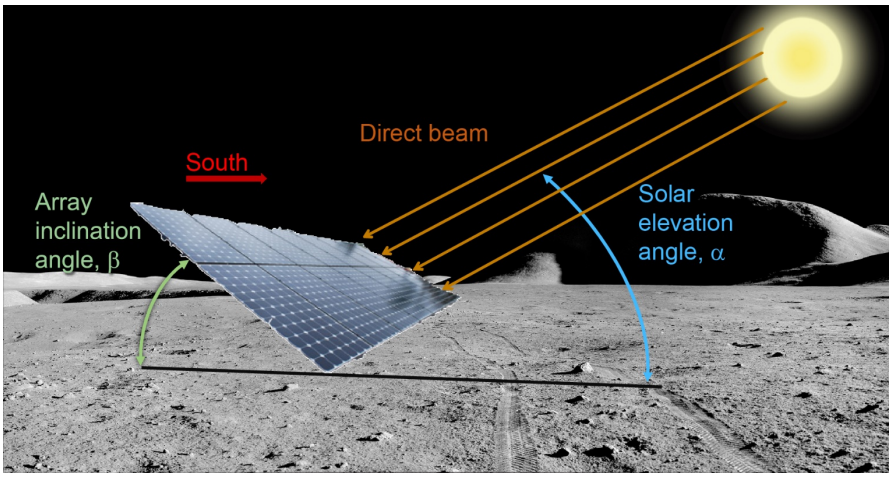

Figure 28.—Solar array orientation on lunar surface.

The array output power (P_a) can be calculated from Equation (58), which is based on the solar cell efficiency (η_{sc}), the area of the solar array (A_a), and the fill factor (f_{sc}) or ratio of the solar cell area to the array area.

$$P_a = (1-\chi_d)\, f_{sc}\eta_{sc} A_a I_s \sin(\alpha+\theta) \tag{58}$$

From a fixed point on the lunar surface, the rotation of the Moon causes the Sun to move in an arc through the sky above that point. That arc describes the elevation angle of the Sun from that fixed point on the surface. The solar elevation angle (α), given by Equation (59), varies throughout the day from dawn to dusk at a given latitude (ϕ).

$$\alpha = \frac{\pi}{2} - \cos^{-1}\left[\sin(\phi)\sin(\psi) - \cos(\phi)\cos(\psi)\cos\left(\frac{2\pi t_i}{t_d}\right)\right] \tag{59}$$

The lunar declination angle (ψ) throughout the year is given by Equation (60). The ψ is much less than that of Earth. Therefore, the seasonal variation in solar elevation angle is much less on the Moon than on Earth. Since the Earth and Moon system orbits the Sun with the same period, the day number (d_n) to indicate the position in orbit about the Sun and the total number of days (d_{nt}) needed to make one revolution about the Sun are based on Earth days.

$$\psi = \psi_{\max}\sin\left(\frac{2\pi d_n}{d_{nt}}\right) \tag{60}$$

The angle of the incident solar flux onto the array surface is a combination of the hour angle (θ) and the α. The θ is given by Equation (61) which is based on the inclination angle of the array (β) and the ratio of the instantaneous lunar day time (t_i in hours) to the total hours in the lunar day (t_d from Table 2).

$$\theta = \tan^{-1}\left[\tan(\beta)\cos\left(\left|\frac{2\pi t_i}{t_d} - \pi\right|\right)\right] \tag{61}$$

The maximum α for each day throughout the year is plotted in Figure 29 for a number of latitudes. From this figure, it can be seen how small the variation is throughout the year.

Dust buildup on the array, represented by the percent of dust coverage (χ_d), would reduce the output of the solar array over time. However, since this is a manned base camp, it was assumed that the array would be periodically cleaned and therefore there would be no significant dust buildup during the operation. The percent of dust coverage was assumed to be zero ($\chi_d = 0$).

The η_{sc} of 28 percent was selected as representative of near-term solar array efficiency capabilities for large-scale space-based arrays. Current research cells can achieve efficiencies greater than this for single samples under laboratory conditions as shown in Figure 30. However, for large-scale production and use in a large array system, the overall efficiency will be less than the research sample cells. The efficiency and areal density (ρ_a) of different array and solar cell types are listed in Table 15. It should be noted that the efficiencies listed are the overall array efficiency, which accounts for the fill factor that is used to adjust from the cell efficiency to the array efficiency.

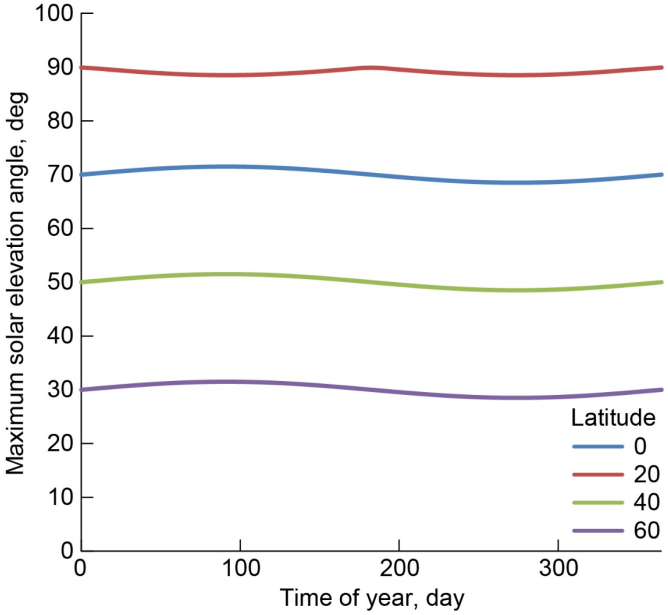

Figure 29.—Maximum daily solar elevation angle throughout year at various latitudes on lunar surface.

TABLE 15.—EFFICIENCY AND AERIAL DENSITY OF DIFFERENT ARRAY AND PHOTOVOLTAIC (PV) CELL COMBINATIONS[a]

Array type[b]	Cell type	Array efficiency, percent	Areal density, kg/m^2
UltraFlex	Thin film	11.5	0.80
UltraFlex	Multijunction	25.0	1.59
RAPDAR	Thin film	8.5	0.33
RAPDAR	Thin film	11.5	0.42
RAPDAR	Multijunction	25.0	1.79
Ridged panel	Multijunction	25.0	3.12

[a]Reference 18.

[b] UltraFlex (AEC-Able Engineering Company, Inc.). Rollout and passively deployed array (RAPDAR).

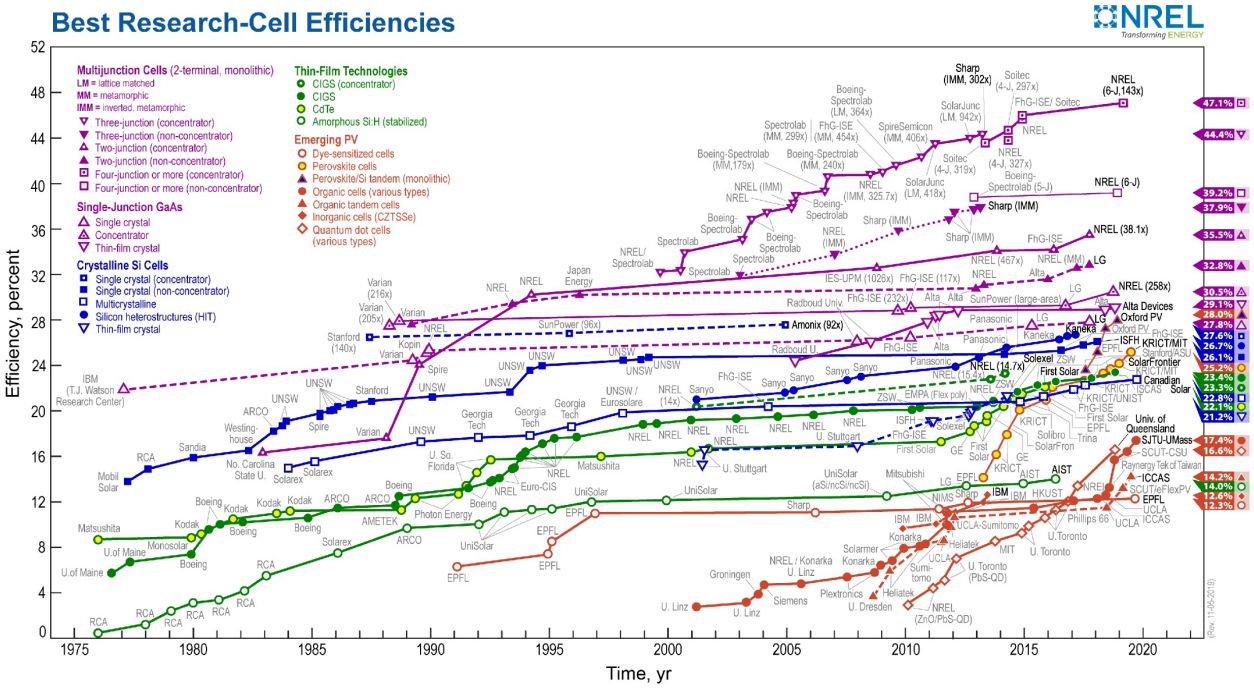

Figure 30.—Research photovoltaic (PV) cell efficiencies over time from National Renewable Energy Laboratory (NREL) part of the Department of Energy (DOE) (Ref. 17).

The A_a needed to provide the necessary output to meet the day and night power requirements is determined through an energy balance between the array output and the day and nighttime power requirements. An example of this type of energy balance is shown in Figure 31. The energy produced by the solar array (E_a) is equal to the area under the array output curve, as given by Equation (62). Similarly, the energy required by the loads during the day (E_d) is the area under the load power curve for the daytime period, as given by Equation (63) and is based on the daytime operating time for the loads and their power level (P_{dl}). For this analysis, it is assumed that the daytime load is constant at any given time (t_i) over the time period it is operational.

$$E_a = \int_0^{t_d} P_a \, dt_i \tag{62}$$

$$E_d = \int_0^{t_d} P_{dl} \, dt_i \tag{63}$$

The nighttime power is provided by the energy storage system. The energy stored in either the batteries or the RFC system is the area under the nighttime power (E_n) curve, as given by Equation (64), and is based on the nighttime power loads (P_{nl}).

$$E_n = \int_0^{t_d} P_{nl} \, dt \tag{64}$$

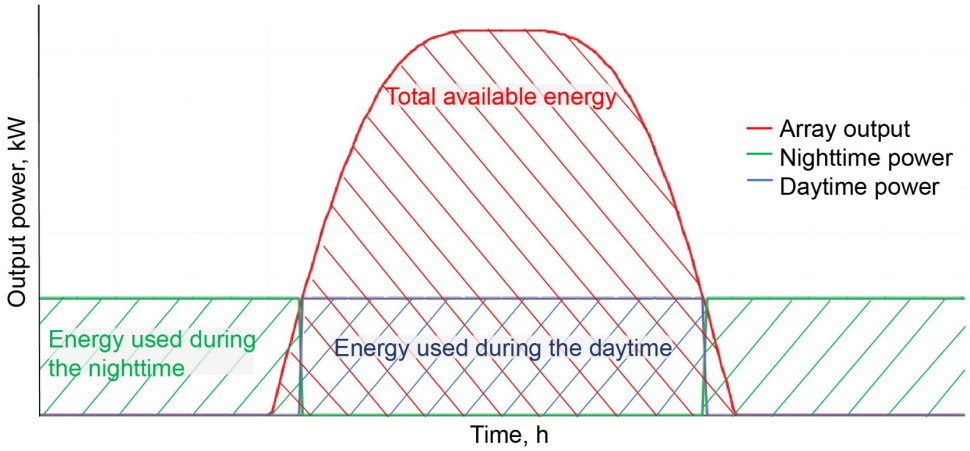

Figure 31.—Baseline production-rate energy balance for operating oxygen production plant continuously day and night.

Therefore, to be able to recharge the energy storage system (batteries or RFC) from the array, the array has to produce excess energy, beyond what is used for daytime operation, equivalent to what is consumed from the batteries during the night multiplied by the charge (η_c) and discharge (η_d) efficiencies. The energy produced by the solar array used to charge the batteries is given by the area under the array output curve minus the area under the daytime power curve. This relationship is given by Equation (65).

$$E_n = (E_a - E_d)\eta_c\eta_d \tag{65}$$

This relationship is solved by iterating on the array area until the nighttime energy requirement (left side of the equation) is equivalent to the excess energy produced during the day, factoring in the charge and discharge inefficiencies (right side of the equation). This approach, iterating on the array area, is utilized if the day and nighttime power levels are similar, as in the power requirements for the base camp or if the oxygen production plant was operated continuously day and night.

There are other operational approaches for situations where a large discrepancy in the day and nighttime power requirements exists. This discrepancy would occur, for example, if the oxygen production plant was operated only during the day in order to reduce the need for larger nighttime energy storage. While the nighttime power requirements would be minimal, just enough to provide “keep-alive” power for the equipment, the plant would have to operate at a much higher production rate to produce the same output of oxygen. In this situation, the goal would be to match the total energy required (as if the oxygen production system was running continuously day and night) with an equivalent amount of energy being produced during only a portion of the daytime period. This operational situation is shown in Figure 32. To accomplish this, the array is oversized to provide all of the daytime power to the oxygen production system running at the higher production rate and its corresponding higher power level than the system designed to operate continuously day and night. Since the goal is to match the total energy of the ISRU process, the iteration is based on both the array area and the operational power level. The array area sets the total array output’s power curve, and the operational power level sets the total usable energy for the process within that power curve. The majority of the array output during the morning and evening is less than the operating power level of the oxygen production plant, which prevents it from being utilized. Also, the majority of the power produced during midday, in excess of the amount needed for the oxygen production plant, is not utilized. Some of this excess power is used to recharge the batteries for the nighttime keep-alive power, but this amount is minimal compared to the total excess power available. To solve this situation’s energy balance discrepancy, a two-step iteration on the required operational power level and the total array area is required.

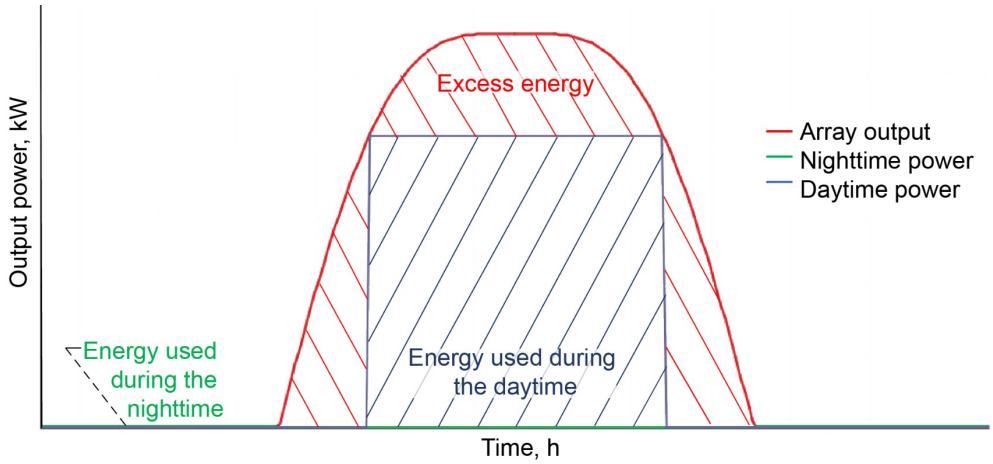

Figure 32.—Baseline production-rate energy balance for operating oxygen production plant during only the daytime.

Based on the required array area determined through the energy balance, the mass of the array can be calculated. The array blanket mass (M_{apv}), given by Equation (66), is also based on the areal density of the array given in Table 15. For this analysis, the UltraFlex multijunction array (AEC-Able Engineering Company, Inc.) areal density of 1.59 kg/m^2 is used.

$$M_{apv} = A_a \rho_a \tag{66}$$

The array structure mass (M_{as}) was based on a fixed carbon composite structure. The structure had an estimated specific mass (ρ_{as}) of 0.55 kg/m^2 based on the array area (Refs. 19 and 20). The array structure mass is given by Equation (67).

$$M_{as} = A_a \rho_{as} \tag{67}$$

The wiring mass (M_w) to connect the arrays is based on the number of wire runs between the arrays and junction box (n_w) given by Equation (68). The average spacing between the arrays (S_a) was estimated to be 3 m with the average length of each of the wire runs (L_w) given by Equation (69).

$$n_w = \left(\frac{\sqrt{A_a}}{S_a} \right)^2 \tag{68}$$

$$L_w = \frac{\sqrt{A_a}}{2} \tag{69}$$

The specific mass of the wire (M_{sw}) in kg/m is given by Equation (70), which is a curve fit of the data in Figure 33. The M_{sw} is based on the required wire gauge (G_w). The G_w is in turn based on the current level (I_w) per wire run. This current is given by Equation (71) for an array bus voltage (V_a) and total current to accommodate the P_a. Depending on how the system is operating, to size the G_w, either the P_{dl} or the maximum array output power ($P_{a_{max}}$), determined from the array output power curve, is used. If the power system is operating as shown in Figure 31 where the total output energy of the array is utilized to operate the loads and recharge the energy storage system, then the wire is sized for maximum array output. If the system operates as shown in Figure 32, where the maximum power transmission is based on the daytime load power demand, then the daytime load power is used.

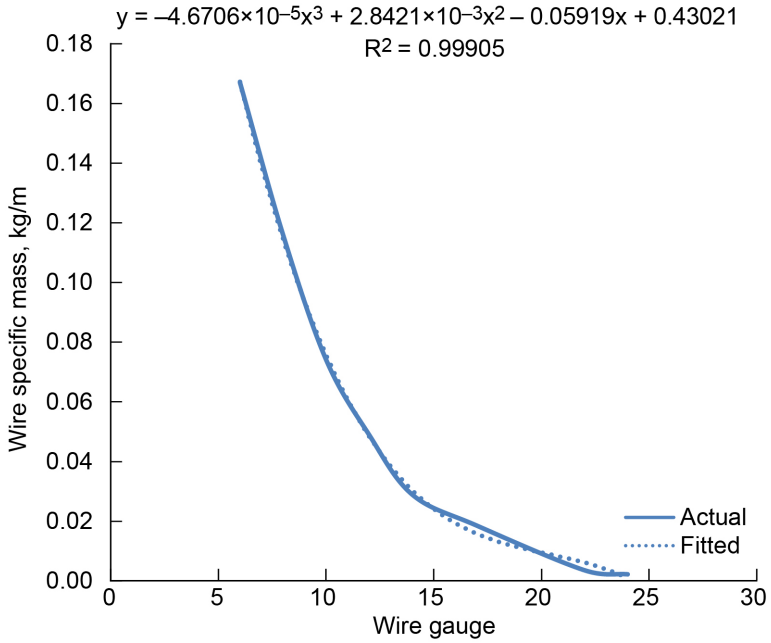

Figure 33.—Power transmission wire specific mass versus wire gauge.

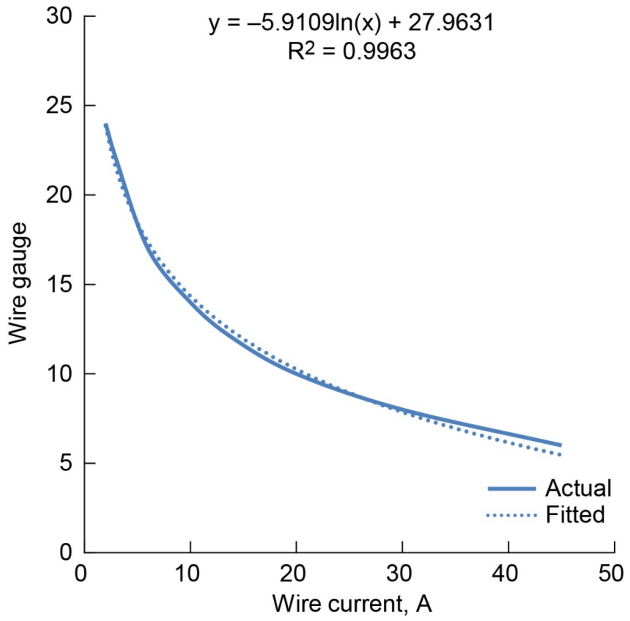

Figure 34.—Required wire gauge for maximum current level.

$$M_{sw} = -\left(4.671\times10^{-5}\right)G_w^3 + \left(2.842\times10^{-3}\right)G_w^2 - 0.0592G_w + 0.4302 \tag{70}$$

$$I_w = \frac{P_a}{V_a n_w} \tag{71}$$

The corresponding G_w needed to carry the required I_w as calculated by Equation (71) is shown in Figure 34 and corresponding Equation (72). The I_w versus G_w relationship is for a wire in a vacuum environment.

$$G_w = -5.911 \ln(I_w) + 27.963 \tag{72}$$

Since wire gauges are given in whole numbers, the output of Equation (72) is rounded up to the next highest whole number based on the I_w. This also provides a small amount of margin in the wire size calculation and provides a conservative estimate of the required G_w.

Once the G_w is known, the M_{sw} can be determined. The M_{sw} is based on using bare, uninsulated wire. For operation in vacuum on the lunar surface, the bare wires will need to be held apart with spacers at increments along their length. A benefit of bare wire is the amount of current that can be carried by the wire since it will reject heat to the surroundings at higher rates than insulated wires. The wires can be painted or coated to provide a high emissivity for enhanced heat rejection to the environment. In addition, there are several other drawbacks to using insulated wire. These include the increased mass of the wire due to the added insulation, insulation damage due to long-term ultraviolet (UV) exposure on the lunar surface, and the thermal expansion mismatch between the insulation and the wire material, which could cause failure of the insulation due to the large temperature swings seen on the lunar surface.

The corresponding total M_w for power transmission wire mass can now be calculated from the M_{sw}, n_w, and L_w as given by Equation (73).

$$M_w = M_{sw} n_w L_w \tag{73}$$

The power wires coming from the array are run to a breaker switch box and then connected to the remainder of the system. The mass of the breaker box (M_{bb}) is scaled from commercially available breaker boxes based on the number of connections the box can handle. This relationship is shown in Figure 35 and expressed by Equation (74).

$$M_{bb} = 9.6736 \ln(n_w) - 13.897 \tag{74}$$

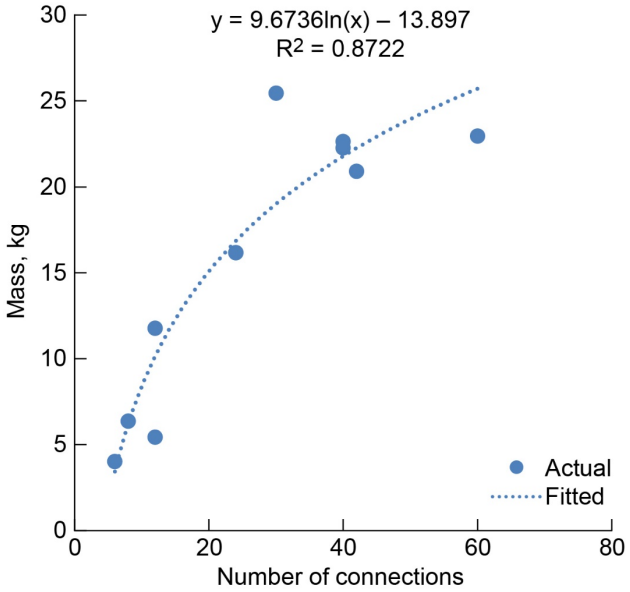

Figure 35.—Breaker box and switch mass versus number of wire connections.

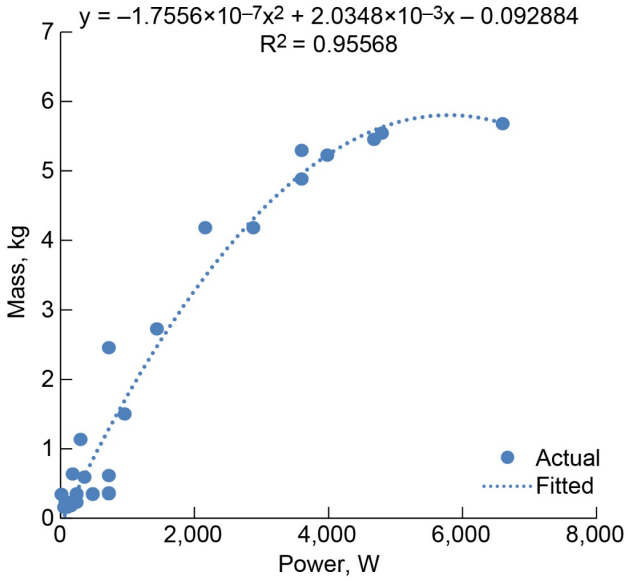

Figure 36.—Battery charge controller mass as a function of battery operating power.

For the power system utilizing a battery as the energy storage medium, the mass of the battery charge controller (M_{bcc}) can be estimated from data on commercially available battery charge controllers. The battery charge controller mass is based on the operating power level of the battery. This relationship is shown in Figure 36 and expressed in Equation (75).

$$M_{bcc} = -1.756 \times 10^{-7} P_{nl}^2 + 2.035 \times 10^{-3} P_{nl} - 0.09288 \tag{75}$$

The energy storage mass (M_{es}) consists of either the battery mass (M_b) or the RFC system mass (M_{rfc}). The M_b is based on the specific energy (in Wh/kg) of the battery type utilized for energy storage. The specific energy ranges for various battery types are shown in Figure 37. The sodium sulfur battery, which has the highest specific energy, is a type of thermal battery and is not commonly used for long-duration operation. Therefore, it is not applicable for use during the lunar nighttime. The lithium-ion battery has space heritage and is commonly used in aerospace applications, which is why it was chosen for use as an energy storage medium for the PV array and powering the loads during the lunar night. Based on the lithium-ion battery specification shown in Figure 37, a battery specific energy (S_b) of 200 Wh/kg was used for the battery. This value represents the specific energy of a packaged battery system comprising multiple cells. The battery mass also depends on the maximum acceptable battery depth of discharge (B_{dod}) during anticipated operation. The B_{dod} represents the percentage of energy that can be extracted from the battery relative to its total energy capacity. The B_{dod} is directly related to the lifetime charge and discharge cycles the battery can achieve as shown in Figure 38. Although the nighttime periods that the battery must operate through are very long, the expected number of cycles for the system are very low. For an estimated 15-yr lifetime, the batteries would experience only 196 cycles. Therefore, to reduce battery mass, the batteries can use a high B_{dod} of 80 percent or 0.8. Using this battery type's specific energy, the required M_b to meet the nighttime lunar energy requirements is given by Equation (76). It should be noted that due to the low number of operating cycles and prolonged periods of operation, the battery lifetime may be affected by other failure mechanisms such as material degradation. However, estimating these other failure mechanisms is out of the scope of this study.

$$M_b = \frac{E_n}{S_b B_{dod}} \tag{76}$$

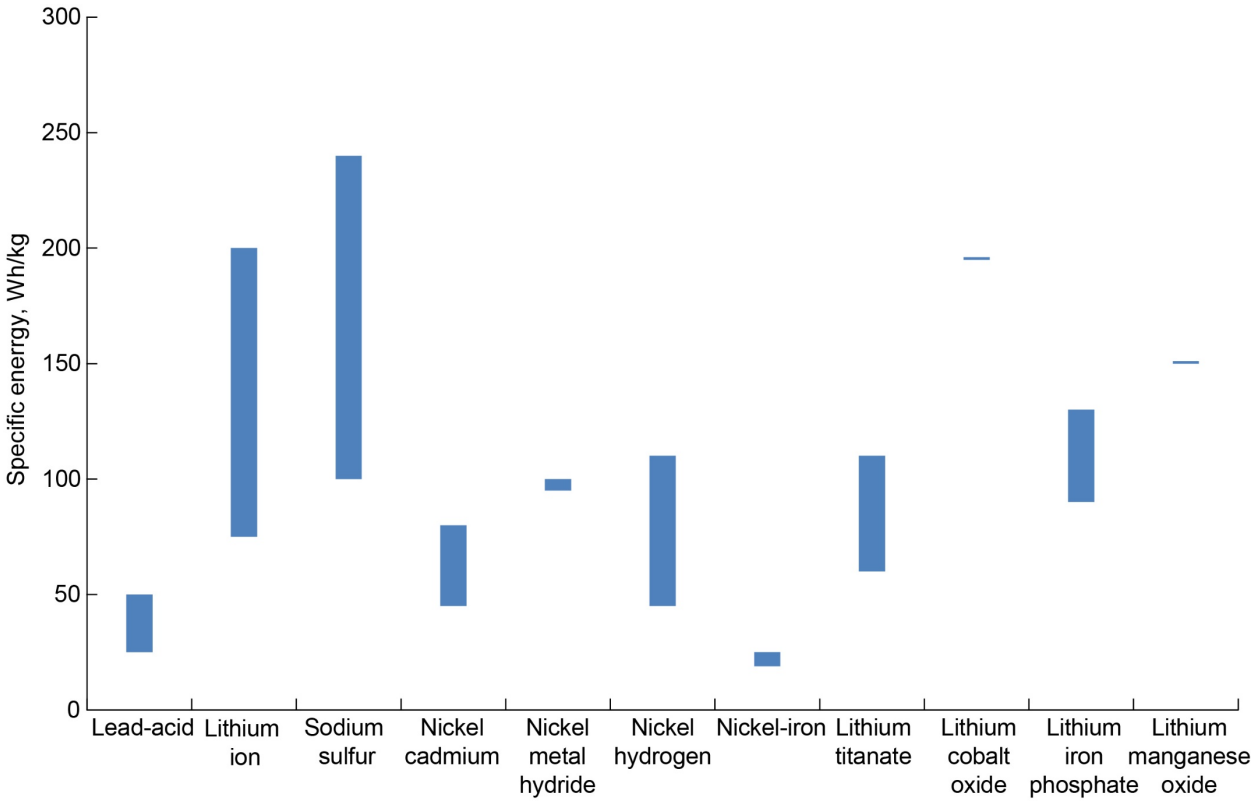

Figure 37.—State-of-the-art battery specific energy for various battery types (Refs. 21 and 22).

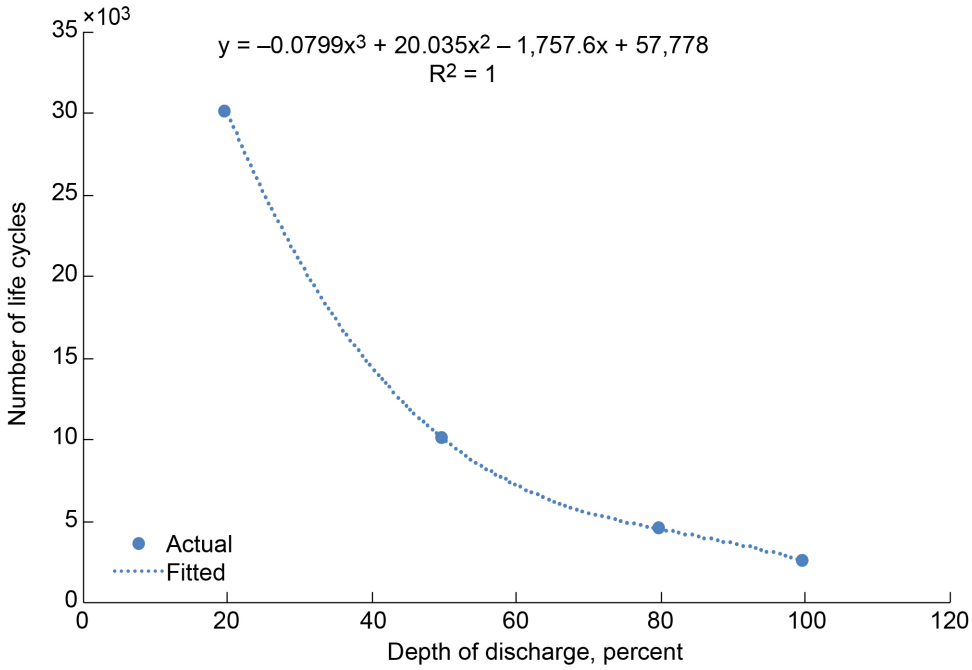

Figure 38.—Lithium-ion battery depth of discharge effect on cycle life (Ref. 23).

The last component of the battery system is the thermal control to maintain the battery and charging electronics within their operating temperature range. The thermal control system consists of the following components:

- Radiator
- MLI
- Heat pipes
- Cold plates

The required A_r, as given by Equation (77), is determined by the thermal power that needs to be rejected (P_r). The radiator is sized using given variables (described in Table 16) based on the worst-case operating conditions.

$$A_r = \frac{P_r F_{al}}{\sigma\left(\varepsilon_r T_r^4 - \alpha_{rls} f_{ls} T_{ls}^4\right) - \alpha_{rs} I_s \left(\cos\left(\theta_{rs}\right) + f_{ls} a_{ls}\right)} \tag{77}$$

Since the worst-case operating condition for the radiator sizing will occur during the daytime, the P_r used to size the radiator is based on the power and efficiency used to charge the battery. The charging power is the difference between the $P_{a_{\max}}$ obtained from the array output on the energy balance diagram and the P_{dl}. Using the energy balance diagram shown in Figure 31, the heat that has to be rejected by the radiator is given by Equation (78).

$$P_r = \eta_{bc}\left(P_{a_{\max}} - P_{dl}\right) \tag{78}$$

An estimate of the M_r can be made based on its required area. The radiator structure can be separated into a number of components with a scaling coefficient for each component to linearly scale the mass based on the required A_r. These coefficients, listed in Table 17, were derived from satellite and spacecraft radiator mass data. The total M_r is given by Equation (79).

$$M_r = C_p A_r + C_c A_r + C_t A_r + C_h A_r + C_a A_r + C_s A_r + C_{at} A_r + C_{lv} A_r \tag{79}$$

The last term in Equation (79) represents the louvers. Louvers are used to insulate the radiator when it is not in use during nighttime operation. They are required to reduce the heat loss to the environment during this time. Utilizing louvers on the radiator will increase the required A_r needed, due to the reduced view factor of the radiator to deep space or other cold surfaces to reject heat. This is represented by the louver area adjustment factor (F_{al}) given in Table 16 and is estimated to increase the A_r by 30 percent.

TABLE 16.—RADIATOR SIZING VARIABLES

Emissivity, ε_r	0.84
Temperature, T_r, K	300
Lunar surface absorptivity, α_{rls}	0.3
View factor to lunar surface, f_{ls}	0.5
Solar absorptivity, α_{rs}	0.14
Maximum Sun angle to radiator, θ_{rs}, deg	75
Louver area adjustment factor, F_{al}	1.3

TABLE 17.—RADIATOR MASS SCALING COEFFICIENTS (kg/m^2)

Panels, C_p	3.30
Coating, C_c	0.42
Tubing, C_t	1.31
Header, C_h	0.23
Adhesives, C_a	0.29
Stingers, C_s	1.50
Attachment, C_{at}	0.75
Louvers, C_{lv}	4.50

TABLE 18.—MULTILAYER INSULATION MASS SCALING COEFFICIENTS (kg/m^2)

Spacer, C_{sp}	0.0063
Reflective layer, C_{rl}	0.0550
Outer cover, C_{oc}	0.1100
Inner cover, C_{ic}	0.0500
Attachment and seals, C_{as}	0.1000

The insulation mass to enclose the batteries is based on the surface area of the battery enclosure (A_{be}). The specific volume of the selected lithium-ion batteries (S_{vb}) is estimated to be 5.5×10^{-4} m^3/kg (Ref. 24). Using the battery's specific volume and required M_b, the A_{be}, which is also the insulation surface area, can be determined, as given by Equation (80).

$$A_{be} = 6\left(M_b S_{vb}\right)^{2/3} \tag{80}$$

The corresponding mass of the MLI (M_{mli}) is based on the area to be insulated and scaling relationships for the components that make up the MLI as given by Equation (81). The scaling coefficients for the insulation are given in Table 18.

$$M_{mli} = \left\{\left[\left(C_{sp} + C_{rl}\right)n_l + C_{oc} + C_{ic}\right]A_{be}\right\}\left(1 + C_{as}\right) \tag{81}$$

The cold plates and heat pipes are used to remove the heat from the batteries and transfer it to the radiators. The number of cold plates needed and their mass (M_{cp}) can be estimated based on the surface area of the battery enclosure as given by Equation (82) with the variables used to size the cold plates given in Table 19.

$$M_{cp} = A_{be} C_{cf} t_c \rho_c \tag{82}$$

The last component of the thermal system is the heat pipes used to move the heat from the cold plates to the radiators. It is assumed that the radiators are located just outside of the battery enclosure. Therefore, the average heat pipe length is estimated to be half the distance from the center of the enclosure to the outer wall. The mass of the heat pipes (M_{hp}) is given by Equation (83), and the heat pipe (C_{hp}) and cold plate (C_{cf}) coefficients are given in Table 19.

$$M_{hp} = \frac{C_{cf} C_{hp} A_{be}^{1.5}}{1.225 w_c L_c} \tag{83}$$

TABLE 19.—COLD PLATE COMPONENT MASS SCALING COEFFICIENTS

Cold plate coverage coefficient, C_{cf}	0.25
Cold plate thickness, t_c, m	0.005
Cold plate width, w_c, m	0.1
Cold plate length, L_c, m	0.1
Cold plate material	Aluminum
Cold plate density, ρ_c, kg/m^3	2,700
Heat pipe mass coefficient, C_{hp}, kg/m	0.15

The relations for the individual thermal control system component masses can then be summed to provide the total thermal control system mass (M_{tc}) needed to maintain the battery temperature at its desired level as given in Equation (84).

$$M_{tc} = M_r + M_{mli} + M_{cp} + M_{hp} \tag{84}$$

The array power system using the battery as the energy storage medium consists of the PV array blanket and structure, battery charge controller, wire, junction box, and battery. The mass of these components, as previously outlined, are summed to provide the total array and battery power system mass (M_{ab}) as given by Equation (85).

$$M_{ab} = M_{apv} + M_{as} + M_{bcc} + M_w + M_{bb} + M_b + M_{tc} \tag{85}$$

The mass of the RFC system consists of the reactants masses with significantly smaller contributions from the mass of the fuel cell (M_{fc}) and the M_e. The M_e is calculated in the same manner as that given in Section 3.3 for the electrolyzer used with the oxygen production system. For use with the PV array system, its sizing is represented by Equation (26). Because the array output is not constant throughout the day and not all of the solar array power will be used to drive the electrolyzer, the electrolyzer has to be sized to take advantage of the maximum amount of output power that is available after primary daytime functions in order for the energy balance to work. Therefore, the P_e used to size the electrolyzer is the difference between the $P_{a_{\max}}$ and the required P_{dl} as given by Equation (86).

$$P_e = P_{a_{\max}} - P_{dl} \tag{86}$$

The thermal control for operating the electrolyzer during the daytime is similar to that for the battery and can be calculated using Equations (77) to (84). Where the radiator thermal power to be dissipated would be given by Equation (87). The S_{ve} is given by Equation (88), and the corresponding area of the electrolyzer enclosure (A_{ee}) is given by Equation (89).

$$P_r = \eta_e \left(P_{a_{\max}} - P_{dl} \right) \tag{87}$$

$$S_{ve} = \left(1 \times 10^{-4}\right) - \left[\left(5 \times 10^{-10}\right) P_r\right] \tag{88}$$

$$A_{ee} = 6\left(M_e S_{vb}\right)^{2/3} \tag{89}$$

The M_{fc} is calculated in a similar manner as that for the electrolyzer. To size the M_{fc}, it was broken down into a number of components and scaled linearly based on nighttime operational power level (Table 20). The M_{fc} is given by Equation (90). It is beyond the scope of this study to investigate the nonlinearity of the

TABLE 20.—FUEL CELL COMPONENT AND SCALING FACTOR BREAKDOWN (kg/kW)

Fuel cell stack, S_{fc}	2.00
Hydrogen separation tank, S_{hst}	0.20
Filters, S_f	0.12
Propellant lines and fittings, S_{pl}	0.52
Controller unit, S_{cu}	0.16
Wiring, S_w	0.30
Heat exchanger, S_{he}	1.00
Water pump, S_{wp}	0.27
Check valves, S_{chv}	0.08
Flow regulators, S_{fr}	0.62
Control valves, S_{cv}	0.16
Pressure and temperature sensors, S_s	0.07
Flow sensors, S_{fs}	0.06
Hydrogen phase separator, S_{hps}	0.07
Hydrogen regulator, S_{hr}	0.05
Oxygen separation tank, S_{ost}	0.18
Oxygen regulators, S_{or}	0.09

individual components scaling factors for an electrochemical stack power level. The process fluid conditions of pressure, flow rate, pressure drop, and temperature strongly influence these scaling factors and impose a level of uncertainty.

$$M_{fc} = P_{nl}\left(S_{fc} + S_{hst} + S_f + S_{pl} + S_{cu} + S_w + S_{he} + S_{wp} + S_{chv} + S_{fr} + S_{cv} + S_s + S_{fs} + S_{hps} + S_{hr} + S_{ost} + S_{or}\right) \tag{90}$$

Since the scaling factors used to size the electrolyzer (Table 6) and fuel cell (Table 20) are linear, they are not representative of lower power RFC systems below 500 W. This is due to practical concerns such as structures and attachments that are utilized to manufacture the system that become a larger fraction of the total mass producing a nonlinear scaling at lower power levels. The RFC reactant tanks are also sized in a similar method to the tanks for the ISRU system. The volume of hydrogen and oxygen gas stored is dependent on the total mass of hydrogen and oxygen that is needed to operate the RFC system throughout the nighttime. To determine the reactant mass, the flow rate of the reactants is needed to produce the desired nighttime power.

The flow rate of hydrogen and the subsequent total mass of hydrogen (M_{H_2}) needed, can be calculated from Equation (91) using the total required E_n from Equation (64) and the η_{fc} given in Table 14. This relationship is based on Faraday's constant (96,485 As/mol or C/mol), the hydrogen charge transfer of 2 electrons per mole, and a theoretical cell operational voltage of 1.48 V since the product, water, is produced in the liquid state.

$$M_{H_2} = \frac{\left(1+R_{H_2}\right)\left(E_n, \text{Wh}\right)\left(3{,}600\frac{\text{s}}{\text{h}}\right)\left(2.02\frac{\text{kg}}{\text{kmol}}\right)}{\left(2\frac{\text{e}^-}{\text{mol H}_2}\right)\left(\eta_{fc}\cdot 1.48\right)\left(96{,}485\frac{\text{C}}{\text{mol}}\right)\left(1{,}000\frac{\text{mol}}{\text{kmol}}\right)} = \frac{E_n\left(1+R_{H_2}\right)}{39{,}273\eta_{fc}} \tag{91}$$

The mass of oxygen needed (M_{O_2}) to react with the hydrogen can be determined from the basic chemical reaction of combining hydrogen and oxygen to form water, given in Equation (56). Based on this chemical reaction, 2 mol of hydrogen are required to react with 1 mol of oxygen. Since a mole of diatomic oxygen gas is 8 times that of a mole of diatomic hydrogen gas, the required oxygen mass is one-eighth that of the hydrogen as shown in Equation (92). It should be noted for this analysis that a residual of 20 percent (R_{res} = 0.2) for both hydrogen and oxygen by mass was added to the total amount required to account for reactants and water left in the lines and tanks of the system.

$$M_{O_2} = 8M_{H_2} \tag{92}$$

As with the tanks for the ISRU oxygen production system, it was assumed that the storage tanks for both the hydrogen and oxygen gases were spherical. The hydrogen (V_{H_2t}) and oxygen (V_{O_2t}) tank volumes, given by Equations (93) and (94), respectively, and the corresponding diameters (d_{H_2t} and d_{O_2t}), given by Equations (95) and (96), respectively, are determined from the M_{H_2} and M_{O_2} that need to be stored from Equations (91) and (92). The tank volumes are based on the gas constants for hydrogen and oxygen, 4,157.2 and 259.84 (J/kg)K, respectively.

$$V_{H_2t} = \frac{4{,}157.2 Z_{H_2} M_{H_2} T_{sd}}{P_t} \tag{93}$$

$$V_{O_2t} = \frac{259.84 M_{O_2} T_{sd}}{P_t} \tag{94}$$

$$d_{H_2t} = 2\sqrt[3]{\frac{3V_{H_2t}}{4\pi}} \tag{95}$$

$$d_{O_2t} = 2\sqrt[3]{\frac{3V_{O_2t}}{4\pi}} \tag{96}$$

Using the d_{H_2t} and d_{O_2t} from Equations (95) and (96), the subsequent tank masses, M_{H_2t} and M_{O_2t}, can be calculated using Equations (31) to (34). The variables used in these equations for sizing the hydrogen and oxygen storage tanks are given in Table 21.

The total M_{rfc} is given by Equation (97).

$$M_{rfc} = M_e + M_{fc} + M_{O_2} + M_{H_2} + M_{O_2t} + M_{H_2t} + R_{res}M_{O_2} + R_{res}M_{H_2} \tag{97}$$

TABLE 21.—REGENERATIVE FUEL CELL (RFC)
REACTANT STORAGE TANK SIZING VARIABLES

Variable	Symbols	Hydrogen storage tank	Oxygen storage tank
Pressure, psi (MPa)	P_t	2,000 (13.8)	2,000 (13.8)
Factor of safety	f_s	2.0	2.0
Tank material	--	Carbon composite tank	Carbon composite tank
Material yield strength, psi (MPa)	σ_y	275,000 (1,900)	275,000 (1,900)

The array power system using the RFC as the energy storage medium consists of the PV array blanket and structure, wire, junction box, and RFC system. The mass of these components, as outlined previously, are summed to provide the total array power system mass (M_{arfc}) as given by Equation (98).

$$M_{arfc} = M_{apv} + M_{as} + M_{w} + M_{bb} + M_{rfc} + M_{tc} \tag{98}$$

5.2 Nuclear Kilopower Reactor Power System

Nuclear power systems for space applications have mainly been radioisotope-based systems. Radioisotope power systems utilize the radioactive decay of an isotope to produce heat through α emissions. Plutonium is an ideal isotope for this type of application. Isotope-based power systems have been used extensively since the early days of space exploration with recent use on a number of deep space missions such as NASA's Cassini probe and Mars Curiosity rover. However, isotope-based power systems are not practical for power requirements greater than approximately 1 kW due to the amount of isotope required to produce the electrical power. Therefore, radioisotope power is not considered a viable option for the ISRU oxygen production and base camp applications.

As an alternative to a solar-based power source, a nuclear system that utilized fission instead of radioactive decay would be applicable to the proposed mission. This type of system advantages and disadvantages for providing the ISRU and base camp power are listed as follows.

Advantages:

- Fission-reactor power systems can scale to very high output power levels and meet the power demands of the ISRU oxygen production system and base camp.
- The fission power system can operate day and night with no operational constraints.
- The operation of the fission power system is location independent and can be designed (mainly by adjusting the radiator sizing) to operate anywhere on the lunar surface with little impact on the system mass.

Disadvantages:

- Fission power systems currently have a low TRL and would need development to be brought up to flight status.
- The shielding requirements for the reactor can be significant, especially for an inhabited base camp. Reactor shielding may require infrastructure be available to enable regolith use as a shielding material, or the reactor may need to be placed a considerable distance away from the base camp and power loads. This would require the deployment of long cable runs to provide power from the reactor to the loads.

Since the beginning of space exploration, reactor power systems have always been considered as a viable option for space power. The first U.S.-based reactor development took place in the 1950s and 1960s under the Systems for Nuclear Auxiliary Power (SNAP) program (Ref. 25). Under this program, the U.S. flew its first space nuclear reactor SNAP–10A in 1965, which produced 500 W of electrical power using thermoelectric (thermal to electric) energy conversion. In conjunction with the SNAP program, a nuclear reactor for nuclear thermal propulsion was being developed under the Project Rover program. This program resulted in some ground testing of the Kiwi reactor designs but did not continue on to flight tests. This transitioned into the Nuclear Engine for Rocket Vehicle Application (NERVA) program in the 1960s, which continued the ground testing and the development of the nuclear rocket design. The NERVA program did result in a successful ground demonstration of a 1,000 MWth nuclear rocket engine. Additional

development continued with the Phoebus reactor design, which was the most powerful space reactor successfully ground tested at 4,000 MWth. Between the Project Rover and NERVA programs, 17 reactors were developed and tested (Ref. 25).

After the Project Rover and NERVA programs ended in the early 1970s, space reactor development was halted until 1979 when the Department of Energy (DOE) began the Space Power Advanced Reactor (SPAR) program development. The SPAR was designed to produce 1,200 kWth power at a temperature of 1,500 K. The SPAR program transitioned to the NASA-led space power reactor program (SP–100) to develop a 100-kW electric space reactor in the mid-1980s. The SP–100 reactor was capable of producing 2.4 MWth power at a temperature of 1,350 K. By the early 1990s, NASA and DOE began to look into scaling down the SP–100 reactor to produce between 5- and 20-kW electrical output using either thermoelectrics or a closed-cycle Brayton power conversion system. The SP–100 program was eventually canceled in 1994 before any full-scale reactor tests were performed. In 1985, the DOE and Strategic Defense Initiative Office (SDIO) began a program concurrent with the SP–100 program to construct a larger multimegawatt space reactor termed the Multimegawatt Space Reactor (MMW) program. This program was also canceled in 1990 before reactor tests begun. In this same time period, DOE began a program to develop and test thermionic energy conversion for space applications and constructed a test reactor termed a Training, Research, Isotopes, General Atomic (TRIGA) reactor. This program was ended in 1993 (Ref. 25).

During the late 1980s and early 1990s, additional space reactor programs were also underway. The Russians were developing a thermionic reactor called TOPAZ. The first generation of this reactor was flown and powered two satellites in 1987. The second-generation TOPAZ reactor was designed to produce a 6-kW electrical output from a 15-kWth heat generation. The Department of Defense under the SDIO started a program to evaluate the Russian reactors termed the Thermionic System Evaluation Test (TSRT). Under TSRT, the TOPAZ–II reactor was slated to be used for providing power for a satellite electric propulsion system. This in turn became the Nuclear Electric Propulsion Space Test Program (NEPSTP). This would have been the first U.S. launch of a reactor since the SNAP–10A in 1965. However, the program was canceled in 1996 before the flight tests could take place. In addition, DOE was looking into a particle bed reactor for space nuclear thermal propulsion applications termed Timberwolf. It was renamed the Space Nuclear Thermal Propulsion (SNTP) when it was transferred to the Air Force. This reactor design was different from the design used under the NERVA program for nuclear propulsion. SNTP was mainly a technology development program and was canceled in 1996 (Ref. 25).

The next significant effort in developing a space nuclear reactor began in 2003 under the Prometheus program funded by NASA. The main objective for the development of this reactor was the Jupiter Icy Moons Orbiter (JIMO) mission. The Prometheus reactor was to provide at least 200 kW electrical power output from over 1 MWth power output. The Prometheus reactor design was new and developed by the DOE Office of Naval Reactors (DOE–NR). Due to changing priorities within NASA, the program was canceled in 2005 before conducting any reactor testing (Ref. 25).

The latest and ongoing space reactor development effort is the Kilopower program, which began in 2015 (Ref. 26). This program initially began its development with a 1-kW electrical output space power reactor based on a 4-kWth power production utilizing Stirling engines for the thermal to electrical energy conversion. The current development focus is now on a 10-kW electrical output reactor based on a 43-kWth power output. The reactor is being developed jointly between NASA and DOE's National Nuclear Security Administration (NNSA). The reactor utilizes a highly enriched uranium core to generate heat and uses sodium heat pipes to move the generated heat from the core to eight Stirling engines (Ref. 27). The Stirling engines then reject their waste heat to a radiator using water heat pipes. To simplify the reactor system design, the reactor core uses an existing reactor fuel form and the Stirling engine converters based on the Advanced Stirling Radioisotope Generator (ASRG) design. The reactor system is illustrated in Figure 39 with a fixed radiator and in Figure 40 with a deployable radiator system.

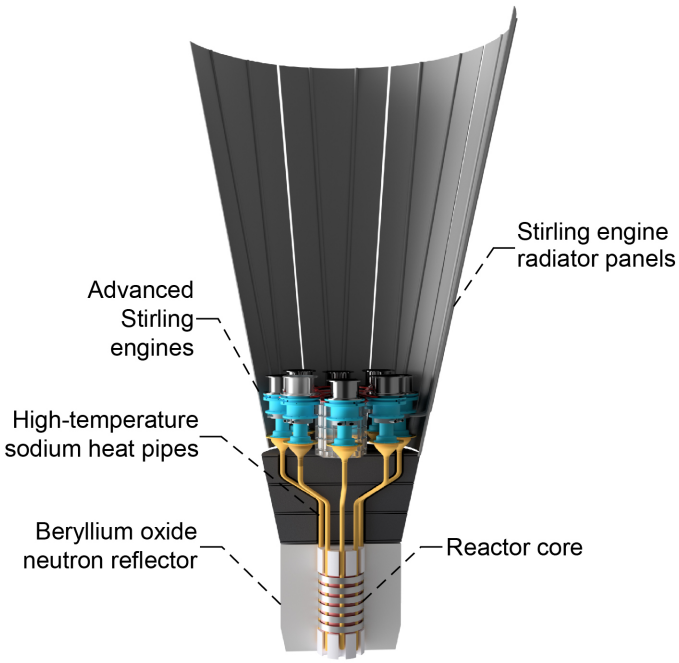

Figure 39.—Kilopower reactor system with fixed radiator (Ref. 26).

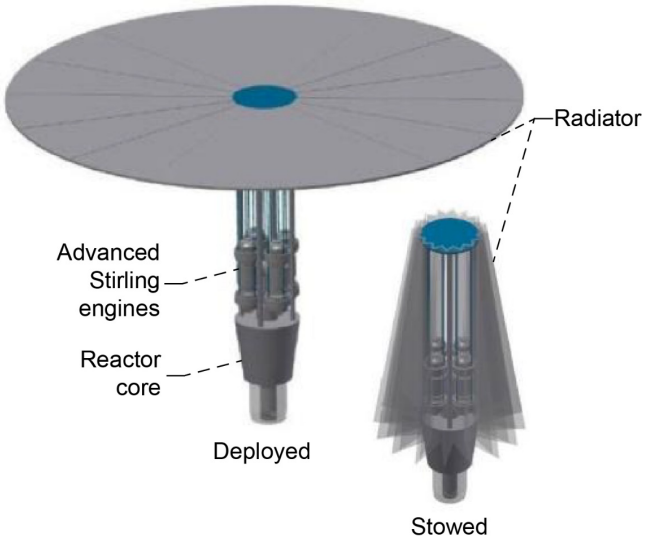

Figure 40.—Kilopower reactor system with deployable radiator (Ref. 28).

The Kilopower reactor system is intended to provide reliable power for extended operation in space as well as on planetary surfaces such as the Moon. Multiple units can be “ganged” together to modularly build up output power capability, as illustrated in Figure 41. To install the Kilopower reactors, it is envisioned that they would be robotically placed at a safe separation distance from the power loads with a power transmission cable spooled out as the reactor is moved to its operating location. After placement on the surface, potentially behind a berm or natural feature to reduce separation distance from the load, any required radiators are deployed before activating the units. Full power is available in 4 to 6 h, depending on the size of the reactor. Following shutdown, robotic operations may commence in close proximity to the Kilopower reactor units within 1 day, or 1 week for crewed operations. This enables relocating the systems to a new location if desired (Ref. 28).

It is envisioned that the current electric Kilopower reactor design can be easily scaled from the test, validated a 1-kW design to a 10-kW electric system with minor changes to the size of the reactor core and integrating the heat pipes into the core rather than mounting them on the exterior of the core. Table 22 contains the specifications of the 1- and 10-kWe Kilopower reactor systems along with specifications for a next-generation advanced reactor system which, if developed, would benefit the integrated operation of the ISRU oxygen production and base camp.

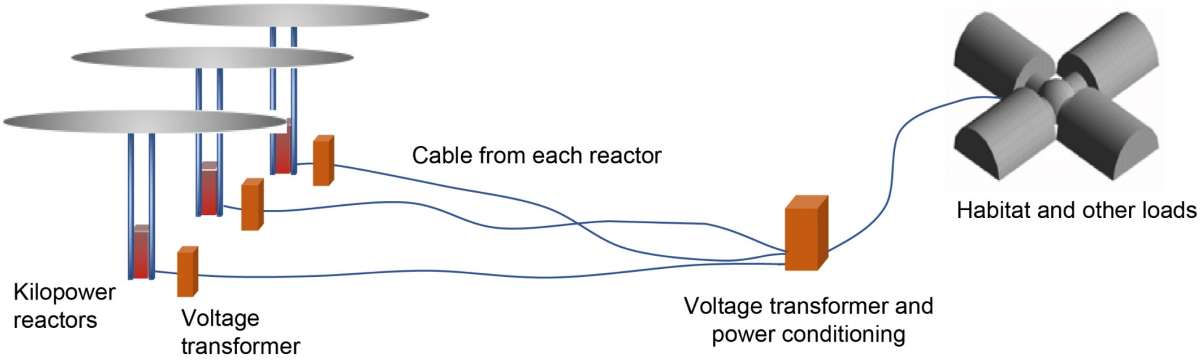

Figure 41.—Kilopower fission-based power system layout.

TABLE 22.—ELECTRIC KILOPOWER REACTOR SPECIFICATIONS[a]

Parameter	1-kWe reactor	10-kWe reactor baseline	10-kWe core-based advanced
Nuclear fuel	93 percent enriched solid cast U-235 Mo alloy		
Reactor type	Fast spectrum, Be reflector, and single centered control rod		
Design life	>10 yr		
Reactor operating temperature, °C	800	800	1,000
Advanced Stirling engine efficiency, percent	23	23	35
Reactor thermal power output, kW	4.3	43.3	43.3
Electrical output power, kW	1	10	10
Output power voltage, Vdc	120	120	120
Distance (dose rate of 26.3 rem/yr), m	100	500	500
Distance (dose rate of 5 rem/yr), km	0.23	1.15	1.15
Reactor radiator area, m^2	3.2	20	20
Stowed diameter, m	1.1	1.5	1.5
Stowed height (fixed radiator), m	3.0	7.3	7.3
Stowed height (deployable radiator), m	2.0	3.3	3.3
Reactor mass (M_{fr}), kg	136	235	235
Shield mass (M_{frs}), kg	148	547	547
Balance-of-plant mass (M_{frb}), kg	122	763	763
Total mass, kg	406	1,545	1,545

[a]Reference 28.

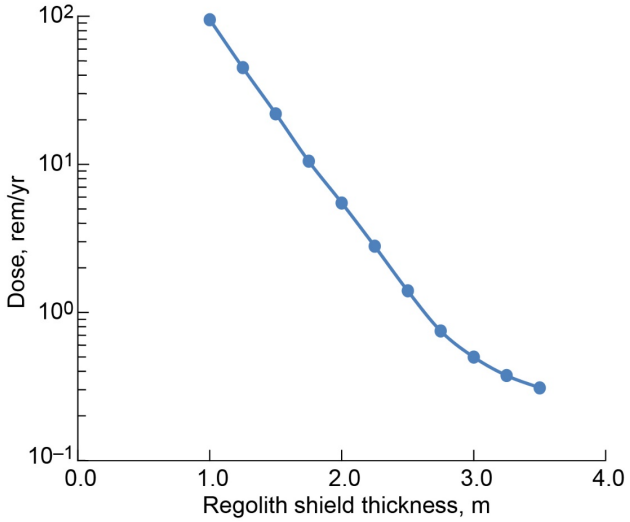

Figure 42.—Effect of regolith thickness on radiation dose.

The baseline reactor shielding mass given in Table 22 provides a yearly dose rate for personnel of 26.3 rem at a distance of 500 m for the 10-kWe output reactor. The current guidelines for radiation workers are a whole-body dose limit of 5 rem/yr (Ref. 29). This is significantly less than values shown in Table 22. However, this exposure rate can be reduced by increasing the separation distance between the reactor and the personnel. The dose rate can be scaled based on Equation (99). This equation approximates the reduction in radiation intensity based on the spherical area as the distance from the reactor changes from the initial radius (r_1) with a known dose (d_1) to the desired distance (r_2) and subsequent dose (d_2).

$$d_2 = d_1\left(\frac{r_1^2}{r_2^2}\right) \tag{99}$$

Using Equation (99), the minimum required distance from the 10-kWe reactor necessary to reduce the dose rate below the specified 5 rem/yr is 1.15 km. This required distance presumes a direct line of sight between the reactor and the location where people will be working such as the base camp. Another approach to reduce this minimum separation distance while maintaining the dose rate limit protection is to impose a physical barrier. The regolith material itself is a good radiation shielding material and can be used as a low-cost and mass solution. The dose received through a range of regolith thicknesses from an unshielded reactor at a distance of 1 km is shown in Figure 42.

Figure 42 shows that the radiation dose drops off significantly with increasing regolith material thickness. The regolith itself can be built up around the reactor using the Kilopower robotic deployment systems to move and pile the regolith or by constructing blocks or bags of regolith and stacking them around the reactor. This approach is illustrated in Figure 43. Using the regolith to shield the reactor in this manner has the following requirements and limitations:

- Access to the equipment is needed to pile the regolith to a sufficient height and thickness.
- The area above the reactor will still be exposed when required to be left open. If it can be closed, a fixed shield will need to be placed over the reactor. Another option would be to place a container over the reactor to support and pile the regolith on top of the container to provide complete shielding of the reactor.

- Variations of the mounded regolith shielding can be considered:
  - Partial shielding, where only a certain area around the reactor is shielded; the unshielded areas would be off limits to personnel.
  - Utilizing a natural feature such as an outcrop as part of the shielding. In this situation, the reactor will be placed near an outcrop and the regolith piled up around the exposed areas of the reactor. This will reduce the amount of regolith required to be moved.
  - A final variation for utilizing the regolith directly as a shielding material is to change its form by melting the regolith into blocks or filling up bags with the regolith. The blocks or bags can then be stacked to form a radiation shield. The blocks or bags may be easier to handle and provide a more accurate shielding design.

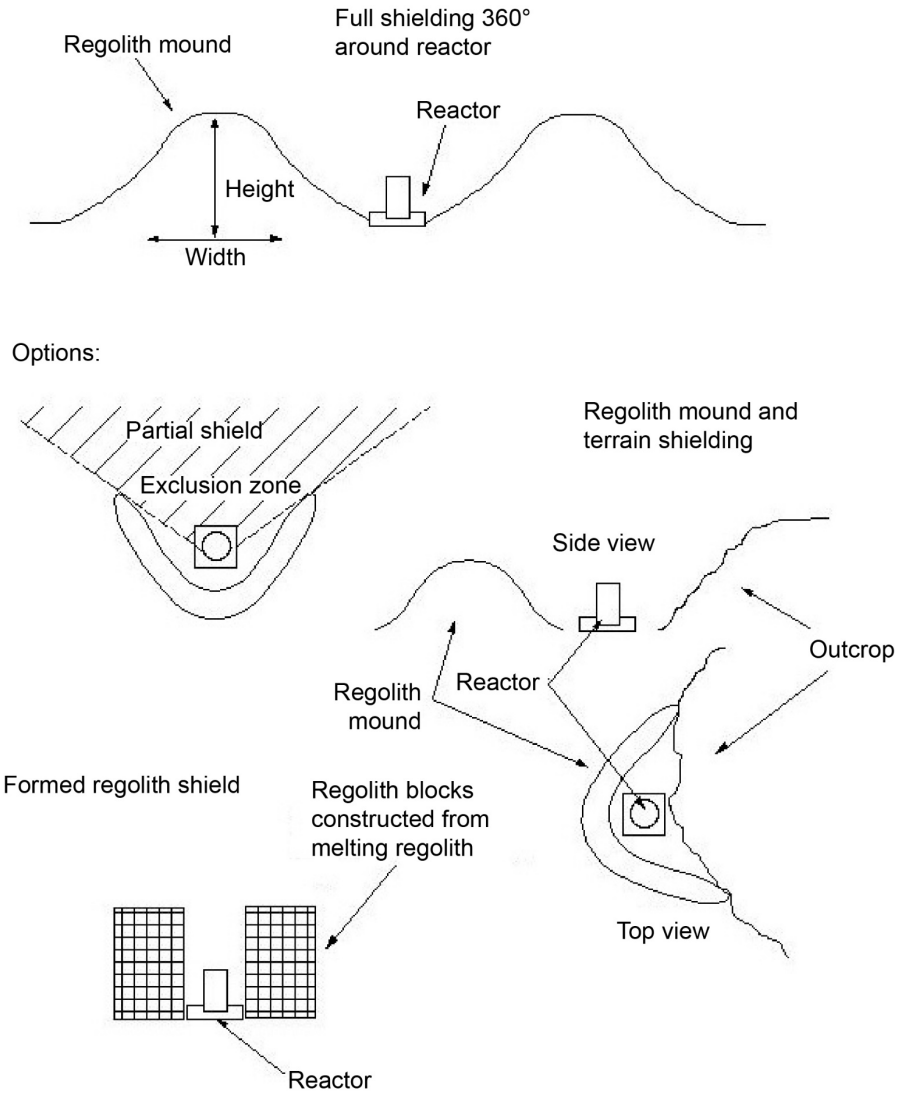

Figure 43.—Reactor shielding using loose regolith.

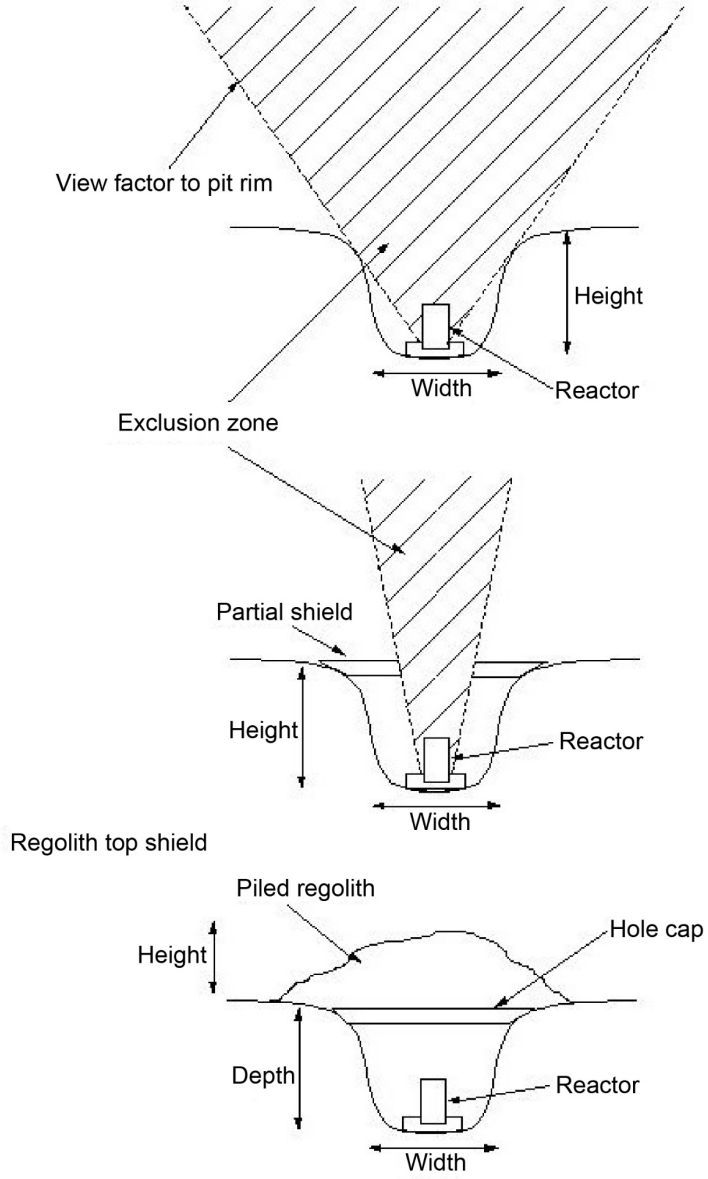

Figure 44.—Reactor shielding by burying reactor.

Another shielding option is to bury the reactor by digging a pit and placing the reactor in it. This approach is illustrated in Figure 44. Placing the reactor in a constructed pit can provide a significant amount of shielding. The following are some concerns or considerations for this approach:

- The pit dimensions, particularly the depth, will determine the feasibility of this type of shielding. The depth requirement will be set by the location of the reactor core and the desired exclusion range from the pit.
- Excavation equipment needed to prepare the pit will require an alternate power source before the reactor is operational.

- Neither the regolith depth nor density is uniform over the surface of the Moon. This may limit the reactor location to areas where there is sufficient depth of lunar regolith with adequate consistency to place the pit.
- The ability to place the reactor into the pit and provide all the necessary thermal and electrical connections to components on the surface.
- Since the reactor will be below grade, there may be a need to provide shielding over the pit depending on activity within and above the area where the reactor is located. Options for the pit top include
    - Maintain a keep-out zone above the reactor site
    - Utilize a partial shield around the perimeter of the pit
    - To place a cover over the reactor pit and utilize loose regolith to shield the top of the pit

The last option is to utilize the terrain for shielding the reactor. A crater or depression in the terrain can be used to provide shielding as illustrated in Figure 45. This is the least intrusive method and does not require any equipment to prepare the site. However, it does limit the potential locations for the reactor as well as the mission and equipment supported by the reactor power. Some considerations for this type of shielding include

- A crater with sufficient depth is needed to meet the shielding requirements at or near the location where the proposed mission is to take place.
- The ability to place the reactor into the crater and provide all of the necessary thermal and electrical connections is needed.
- The crater width and therefore wall steepness will affect the ability to access the reactor as well as the need for additional shielding on the reactor.
- As with the pit shielding, the area above the crater will need to be a keep-out zone for personnel.
- Additional shielding can be applied to reduce or eliminate any operating concerns with activity taking place over the crater. This can be accomplished by placing a cone shield on top of the reactor to enable personnel to move to the crater edge or over the crater.

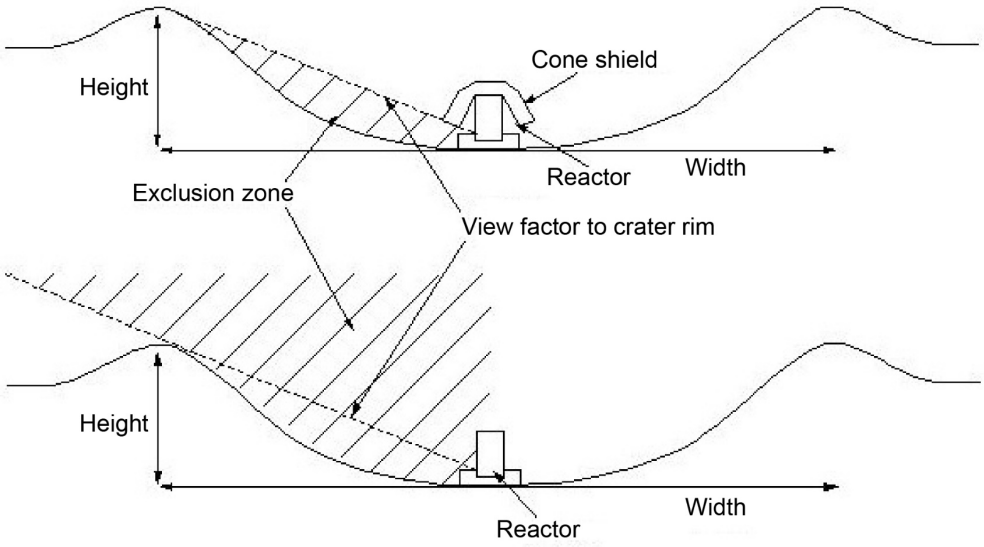

Figure 45.—Reactor terrain shielding by placing it in crater.

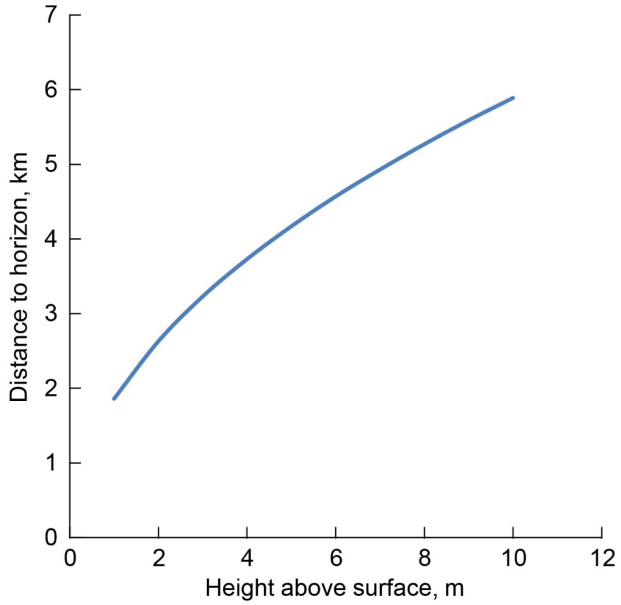

Figure 46.—Distance to horizon versus height above lunar surface.

Similar to the terrain shielding by using a crater to shield the reactor, another approach would be to place it over the horizon from where the base camp and personnel will be. This would require a cable to be deployed from the reactor to the power loads, so distance is a considerable factor. However, due to the smaller lunar radius, this distance is not as significant as it would be on Earth. The distance to the horizon (d_{hr}) for a given height above the lunar surface (h) is given by Equation (100) and plotted in Figure 46.

$$d_{hr} = \sqrt{h(2r_m + h)} \tag{100}$$

If the h of the personnel or components requiring protection is on the order of 3 m or less, the horizon distance is approximately 3 km. This distance is greater than the current required distance with the baseline shielding to stay below the specified 5 rem/yr. However, this approach does provide some unique benefits. It could potentially reduce the required shielding mass on the reactor since the large amount of regolith between the personnel and the reactor would provide a more than adequate amount of shielding to reduce the radiation exposure to background levels.

If personnel are required to be in close proximity to the power loads, such as the base camp, then the reactor will need to be placed sufficiently far enough away to keep below the required maximum personnel dose level. As given in Table 22, this would require the reactor to be placed 1.15 km from the base camp and/or oxygen production plant location for the 5-rem/yr dose level with the 10-kWe reactor. However, if multiple reactor systems are needed, this distance will increase. For three 10-kWe reactors, it would be 1.99 km and for six it would be 2.81 km. At this latter distance, the reactors will be over the horizon for most personnel standing on the surface.

To achieve this distancing, a cable will need to be deployed that connects the reactor to the power loads. Also, since the reactor has an output of 120 Vdc, electrical converters at both the reactor and power loads will be needed to raise the output power voltage for transmission and then reduce it at the loads for use. This is done to reduce the overall required cable wire gauge and subsequent mass. The reactor M_w is calculated in a similar manner to the array M_w. The I_w the reactor wire needs to carry is based on the total

power requirement of the loads. For the reactor system, the required power is continuous both day and night. This is similar to the continuous daytime power level used in the array system analysis. The number of wires used to transmit the power is based on the number of 10-kWe reactor systems needed to meet the power system requirements. The reactor power systems are modular systems providing up to 10 kWe of power each. The number of reactor systems needed (n_{rs}) to meet the power demands of the various mission options is given by Equation (101) where the value is rounded up to the next whole number to provide whole reactor units. Subsequently, the required I_w per transmission wire is determined by the voltage of the power wires (V_{rt}) as given by Equation (102).

$$n_{rs} = \left[\frac{P_{dl} + P_{wl}}{10{,}000} + \frac{1}{2} \right] \tag{101}$$

$$I_w = \frac{P_{dl}}{V_{rt} n_{rs}} \tag{102}$$

With the I_w calculated from Equation (102), the G_w and subsequent M_w can then be calculated using Equations (71) and (73), respectively. For the reactor system, the values for the variables used in the wire mass calculation are given in Table 23 and the total n_w used is given by Equation (103).

$$n_w = n_{rs} n_{rw} \tag{103}$$

Due to the L_w between the reactor and the loads, the power transmission loss down the wire (P_{wl}) also needs to be considered. The resistance of a copper wire per meter of length (R_w), as a function of its G_w, is given by Equation (104) and the corresponding P_{wl} is given by Equation (105).

$$R_w = 0.00032 \times 10^{0.23188 G_w} \tag{104}$$

$$P_{wl} = I_w^2 R_w L_w \tag{105}$$

To minimize the transmission line mass, the voltage was boosted from the 120 Vdc output of the fission reactor to 1,500 Vdc for transmission. Each transmission power line needs a direct current (dc) to dc converter at the reactor to raise the voltage from 120 Vdc to 1,500 Vdc and then one at each power load to reduce the voltage from 1,500 Vdc back to 120 Vdc. To scale the converter mass (M_{vc}), data was collected from operating the M_{vc} over a range of power levels and over a similar conversion voltage range as that needed for the fission reactor power transmission as shown in Figure 47. The data was then curve fit to provide an expression to calculate the M_{vc} as a function of the operating power level, as given by Equation (106).

$$M_{vc} = \frac{P_{dl}}{1{,}000 n_{rs} \left\{ 0.0279 \left(\frac{P_{dl}}{n_{rs} 1{,}000} \right) + 0.6816 \right\}} \tag{106}$$

TABLE 23.—FISSION REACTOR POWER TRANSMISSION WIRE SPECIFICATIONS

Number of wires per reactor system, n_{rw}	2
Transmission voltage, V_{rt}, V	1,500
Transmission line length, L_w, m	1,150

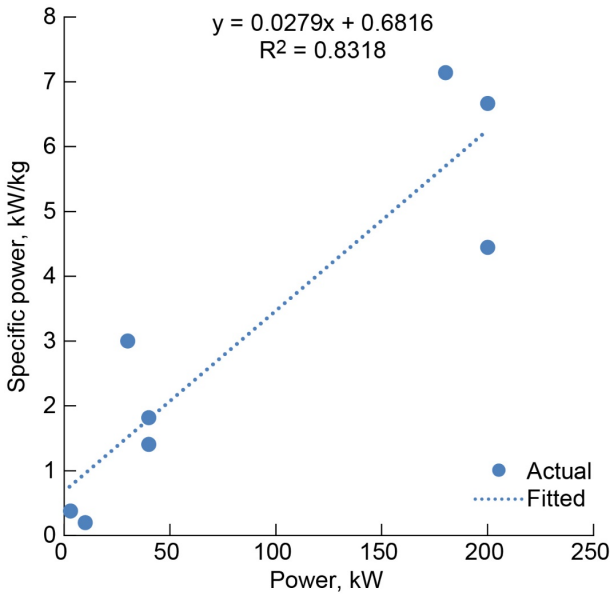

Figure 47.—Direct current (dc) to dc converter specific power versus operating power level.

The total reactor system mass (M_{frt}) is a sum of the reactor components plus the wiring, given by Equation (73), and conditioning. The M_{frt} is given by Equation (107).

$$M_{frt} = n_{rs}M_{fr} + n_{rs}M_{frs} + n_{rs}M_{frb} + M_w + 2n_{rs}M_{vc} \tag{107}$$

6.0 Results

Using the analyses described in the previous sections, results were generated for three cases. Each of the cases compares the mass of the PV array-based power system to that of the Kilopower fission reactor-based system. The first two cases look at the power system sizing for the ISRU oxygen production plant and base camp independently. Whereas the third case combines the power requirements for both applications. It should be noted that the reactor systems are not scaled to directly match the electrical and thermal requirements of the proposed systems but are utilized as building blocks with a fixed output that can be tied together to operate as a single power system if the required power exceeds the output capability of one reactor system. This modular-type power system approach is beneficial in terms of unit cost since the reactor power systems are identical in construction. It can provide excess power capability to a power load beyond the baseline power needs. In that instance, there will be a mass penalty associated with the reactor system over a custom-designed system for the application.

6.1 Case 1—Power System Comparison for ISRU Oxygen Production Plant

The baseline oxygen production rate was selected as 1.63 kg/h. At this rate, over 1 lunar day and night cycle, 1,154 kg of oxygen can be produced. The thermal and electrical power requirements for this baseline oxygen production level are given in Figure 11 and Figure 12 and the mass and power requirements for the oxygen production system are summarized in Table 24.

To meet the power requirements for the ISRU oxygen production system, the solar PV array power system would provide electrical power for both the electrical and thermal requirements of the system. For continuous operation, as discussed in Section 5.1 and as shown in the energy balance diagram of the PV array and battery power system in Figure 48, the array would provide sufficient power during the daytime to operate the oxygen production system as well as recharge the energy storage system to enable ISRU operation during the nighttime.

TABLE 24.—BASELINE OXYGEN PRODUCTION MASS AND POWER REQUIREMENTS AT PRODUCTION RATE OF 1.63 kg/h

Component	Required power, W	Mass, kg
Scoop and delivery conveyors	134	51
Vibrating screen	132	68
Magnetic separator	98	98
Fluidized bed reactor	---------	27
Hydrogen tank	---------	19
Oxygen tank	---------	488
Electrolyzer	8,965	49
Thermal power to process reactor	13,386	-------
Heat of reaction	2,563	-------
Heat loss	552	-------
Thermal control system	---------	326
Total	25,830	1,125

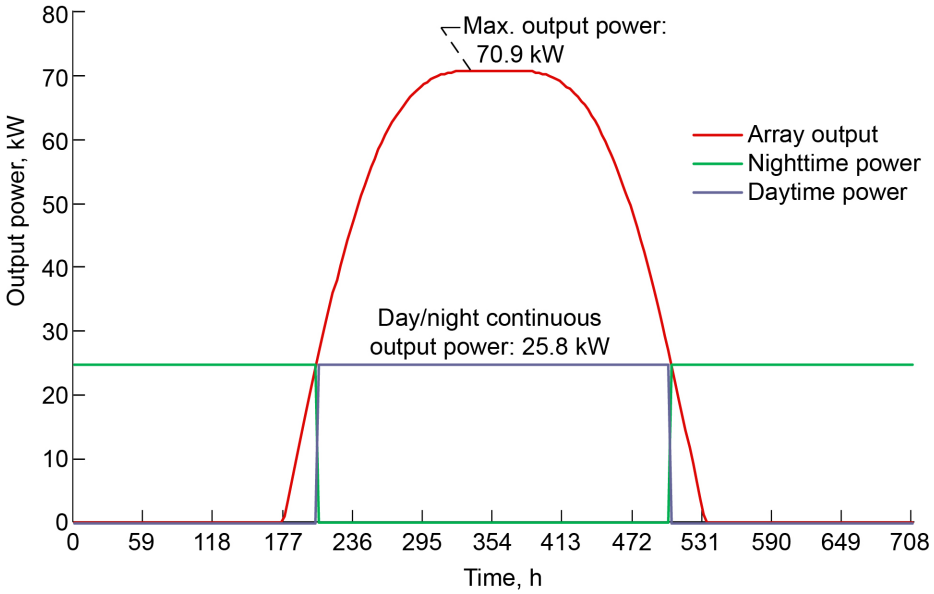

Figure 48.—Photovoltaic (PV) array and battery power system's energy balance for day and night oxygen production at 25.8 kW of continuous output power. Required array area is 208.5 m^2. Total energy required for 1 day and night cycle is 18,288 kWh. The array is at 30° latitude with a fixed 30° tilt angle and 28 percent efficient solar cells. Earth spring equinox is 1,359 W/m^2.

The PV array power system can use either a battery or RFC for energy storage. The mass breakdown of the PV array and battery power system to meet the power and energy requirements are shown in Figure 49. The energy balance for the PV array and RFC system is given in Figure 50 and the corresponding system mass breakdown is given in Figure 51. The energy balance differs between the PV array and battery and the PV array and RFC systems due to their difference in charging and discharging efficiencies. Because of the lower efficiency of the RFC charge and discharge cycle, the PV array area increases to 353.6 m^2 from the 248.5 m^2 required by the battery system. In addition, the corresponding peak operating output power of the PV array increased from 84.4 kW for the battery system to 120.2 kW for the RFC system.

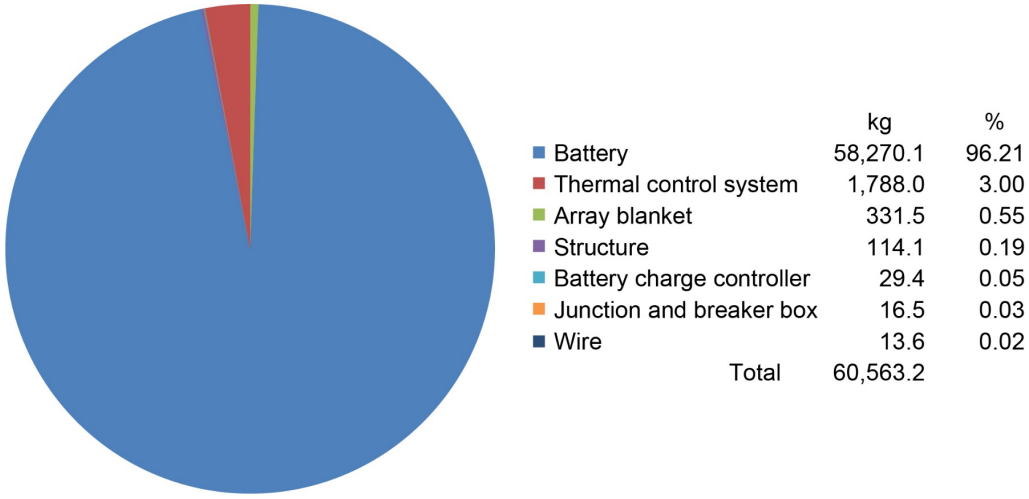

Figure 49.—Photovoltaic (PV) array and battery system mass breakdown for continuous oxygen production at 25.8 kW of continuous output power.

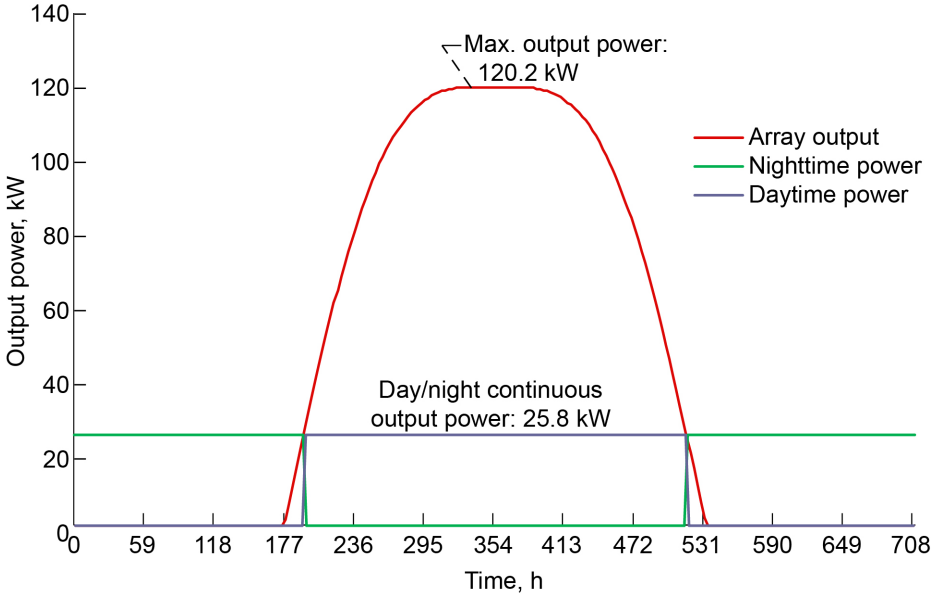

Figure 50.—Photovoltaic (PV) array and regenerative fuel cell (RFC) power system energy balance for day and night oxygen production at 25.8 kW of continuous output power. Required array area is 353.6 m^2. Total energy required for 1 day and night cycle is 18,288 kWh. The array is at 30° latitude with a fixed 30° tilt angle and 28 percent efficient solar cells. Earth spring equinox is 1,359 W/m^2.

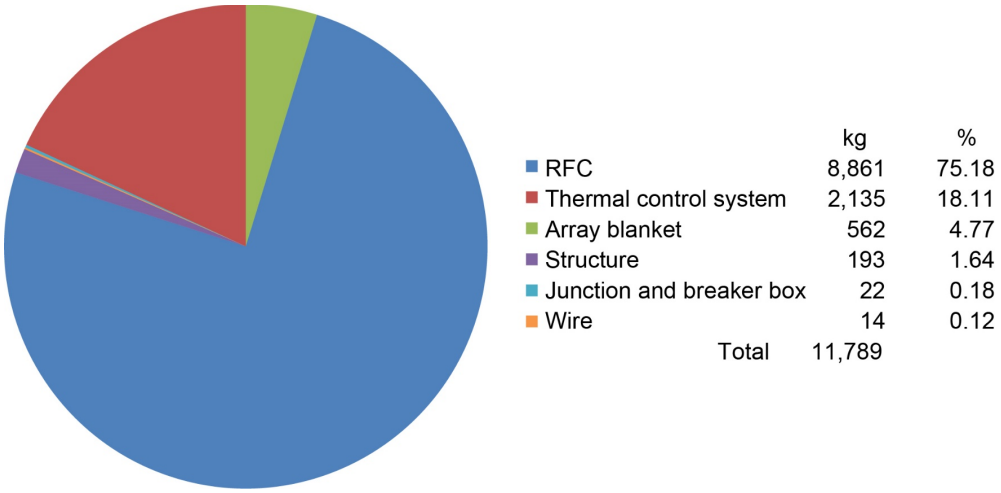

Figure 51.—Photovoltaic (PV) array and regenerative fuel cell (RFC) system mass breakdown for continuous oxygen production at 25.8 kW of continuous output power.

The results show that for continuous operation of the PV array-based power system, the energy storage mass dominates the total mass of the system, 95 percent for a battery and 75 percent for a RFC. The battery specific energy was given as 200 Wh/kg with an 80 percent depth of discharge while the RFC specific energy was 832 Wh/kg based on the mass scaling analysis given in Section 5.1 and the required operating time and power level set by the energy balance curve given in Figure 50. Although the energy storage mass for both the battery and RFC was the dominant mass in their respective power systems, their comparison illustrates the advantage the RFC system has over batteries for long-term operation. For a fixed output power, as in this case, a longer operating time results in a larger energy storage requirement. This causes the specific energy of the RFC system to increase whereas the battery has a constant specific energy regardless of operating time. The reason the RFC system specific energy increases with longer operational time is because all of the components except for the reactants and storage tanks are sized based on the maximum output power level. Only the tanks and reactants scale or increase with longer operation. Therefore, operating for longer duration does not increase the component masses, only that of the tanks and reactants required to support the larger energy storage requirement. This results in the specific energy of the system increasing with increasing operating time at a fixed power level.

Because the nighttime energy storage requirements are such a dominating factor in the sizing of the PV power system, another approach can be taken for powering the ISRU oxygen production system. Oxygen can be produced only during the day and the system can be placed in a hibernation mode during the night utilizing only enough power to maintain the equipment at a temperature sufficient for it to survive the night. However, in order to accurately compare this approach to the baseline case of producing 1,154 kg of oxygen over 1 day and night cycle, the system will need to produce this much while operating just during the daytime. Therefore, the oxygen production system has to be scaled up to operate at a higher production rate during the daytime operation. The production rate needed to achieve a similar total mass of oxygen while operating just during the daytime over the period of 218.3 h identified in Figure 52 is 5.29 kg/h, which produces a total oxygen mass of 1,158 kg. The mass and power breakdown of the oxygen production system at this production rate is given in Table 25. The energy balance shown in Figure 52 for the PV array and battery system describes this approach. The nighttime power requirement will be the power needed to maintain the equipment at a temperature that will allow it to survive the nighttime. This is calculated in a similar manner as the nighttime heat loss for the habitat as given in Section 4.0. Based on this analysis the nighttime heater requirement for the oxygen production system was estimated to be approximately 500 W.

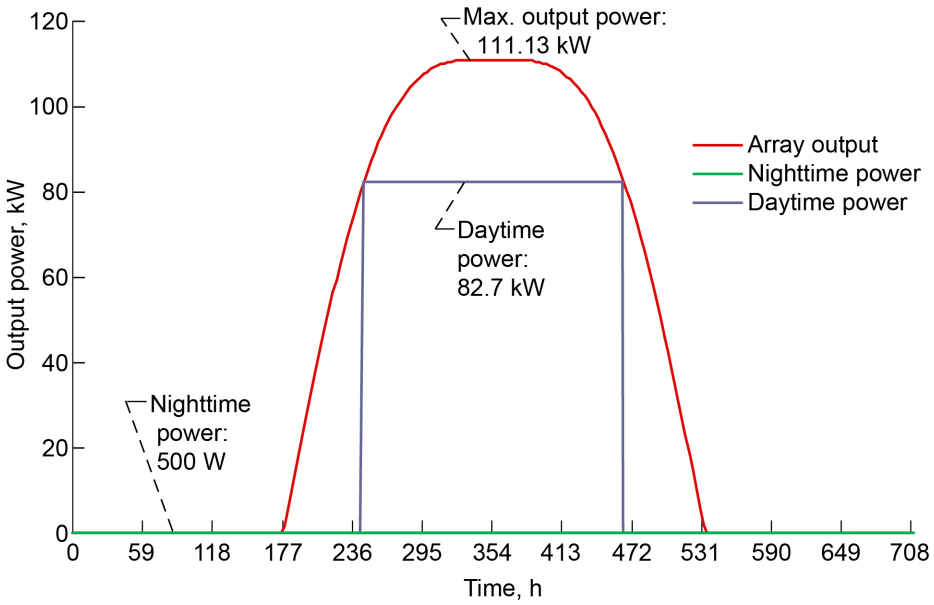

Figure 52.—Photovoltaic (PV) array power system energy balance for daytime-only oxygen production at 82.7 kW daytime operational and 500 W nighttime "keep-alive" power. Required array area is 327 m^2. Total energy required for 1 day and night cycle is 18,288 kWh. The array is at 30° latitude with a fixed 30° tilt angle and 28 percent efficient solar cells. Earth spring equinox is 1,359 W/m^2.

TABLE 25.—DAYTIME-ONLY OXYGEN PRODUCTION MASS AND POWER REQUIREMENTS AT PRODUCTION RATE OF 5.29 kg/h

Component	Required power, W	Mass, kg
Scoop and delivery conveyors	160	51
Vibrating screen	430	91
Magnetic separator	317	98
Fluidized bed reactor	NA	27
Hydrogen tank	NA	19
Oxygen tank	NA	488
Electrolyzer	29,095	159
Thermal power to process reactor	43,446	NA
Heat of reaction	8,316	NA
Heat loss	552	NA
Thermal control system	NA	1,059
Total	82,315	1,989

The daytime-only operational breakdowns of the PV array and battery and the PV array and RFC power system masses are shown in Figure 53 and Figure 54, respectively. The mass breakdown for the RFC system is given in Table 26. The total mass for the PV array systems also includes the increased mass of the oxygen production system needed to produce oxygen at the higher rate to match the day and night continuous operation production amount. The daytime-only operation has significantly reduced the overall system mass for both systems over the continuous operation systems. However, the energy storage mass for both systems, even though it is used only for nighttime keep-alive power, is still a significant item for both systems. For the battery system, it is the largest mass item, and for the RFC system, it is the second largest item behind the array.

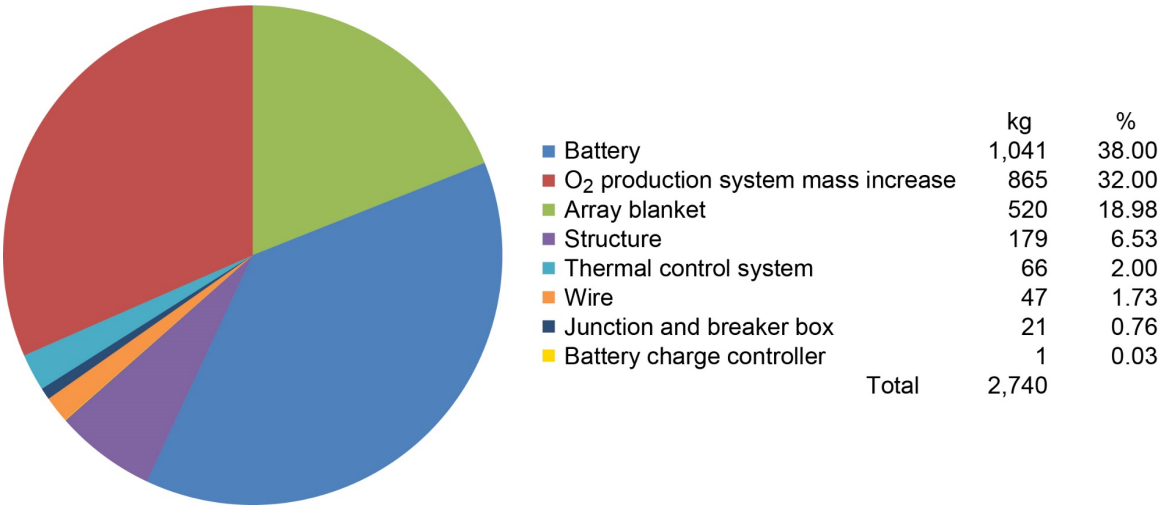

Figure 53.—Photovoltaic (PV) array and battery system mass breakdown for daytime oxygen production for 82.7 kW daytime operational and 500 W nighttime “keep-alive” power.

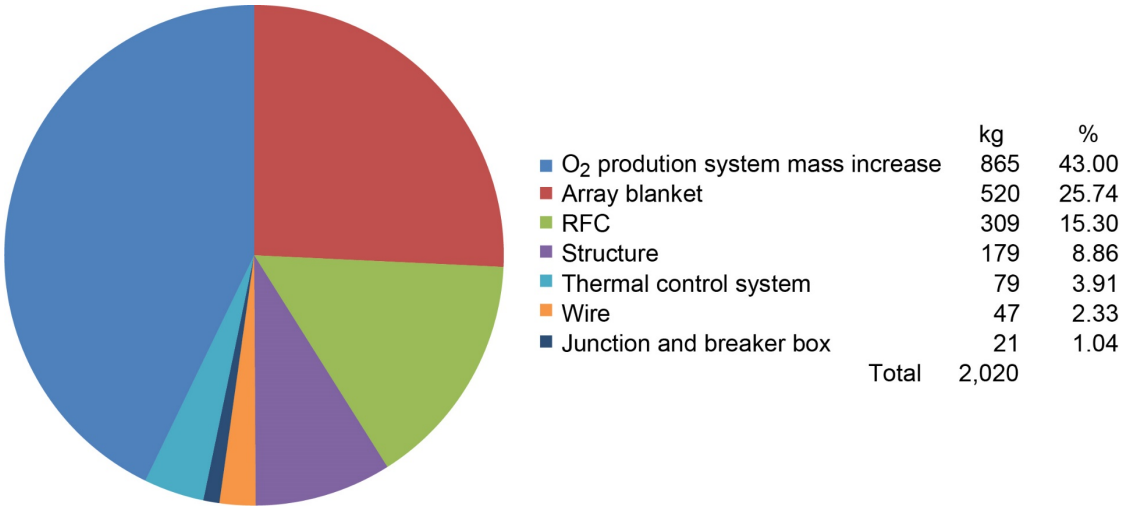

Figure 54.—Photovoltaic (PV) array and regenerative fuel cell (RFC) system mass breakdown for daytime oxygen production for 82.7 kW daytime operational and 500 W nighttime “keep-alive” power.

TABLE 26.—REGENERATIVE FUEL CELL (RFC) SYSTEM
MASS BREAKDOWN FOR NIGHTTIME "KEEP-ALIVE" POWER

Fuel cell	
Fuel cell stack, S_{fc}	1.000
Hydrogen separation tank, S_{hst}	0.100
Filters, S_f	0.060
Propellant lines and fittings, S_{pl}	0.260
Controller unit, S_{cu}	0.080
Wiring, S_w	0.150
Heat exchanger, S_{he}	0.500
Water pump, S_{wp}	0.135
Check valves, S_{chv}	0.040
Flow regulators, S_{fr}	0.310
Control valves, S_{cv}	0.080
Pressure and temperature sensors, S_s	0.040
Flow sensors, S_{fs}	0.030
Hydrogen phase separator, S_{hps}	0.040
Hydrogen regulator, S_{hr}	0.030
Oxygen separation tank, S_{ost}	0.090
Oxygen regulators, S_{or}	0.050
Hydrogen tank	30.700
Hydrogen and residual	12.000
Oxygen tank	12.500
Oxygen and residual	95.900
Total	154.100

Electrolyzer	
Electrolyzer stack, S_{es}	56.9
Water tank and heater	2.9
Filters, S_f	3.4
Propellant lines and fittings, S_{pl}	14.8
Controller unit, S_{cu}	4.6
Wiring, S_w	8.5
Heat exchanger, S_{he}	28.5
Water pump, S_{wp}	7.7
Check valves, S_{chv}	2.3
Flow regulators, S_{fr}	17.5
Control valves, S_{cv}	4.6
Pressure and temperature sensors, S_s	2.0
Flow sensors, S_{fs}	1.7
Total	155.3
System total	309.4

The RFC system specific energy for providing 500 W of electrical power throughout the nighttime with the mass breakdown given in Table 26 was 456 Wh/kg. This is lower than the RFC specific energy calculated for continuous operation due to the smaller total energy storage requirement resulting from operating at only 500 W. In general, as the operating power decreases, the RFC specific power also decreases. This decrease is due to the nonlinear scaling of some of the components at lower operating power levels as well as the effect of the reactants becoming a smaller fraction while the electrical conversion components become a higher fraction of the total RFC mass.

The reactor system was also sized to meet the ISRU oxygen production requirements. For the reactor system, two different approaches were analyzed. One in which the reactor was located near the oxygen production facility, and the second where it was located a distance away, 1.99 km, to maintain the maximum 5 rem/yr dose rate for personnel at the oxygen production facility location.

For the reactor located near the oxygen production facility, it is assumed that the facility is fully automated and that no personnel are needed for its operation. If crew interaction with the facility is required to remove the oxygen produced or for servicing the oxygen production facility, the reactor will need to be shut down during that time to maintain a safe radiation environment for any personnel within the exclusion zone. With the reactor located near the oxygen production facility, it would be possible to utilize the waste heat from the reactor to provide heat for the oxygen production process. The baseline production-rate thermal and electrical power requirements from Figure 11 and Figure 12, respectively, are 16,502 and 9,329 W.

The baseline 10-kWe reactor system can provide the electrical output requirement for the ISRU system but not the thermal requirement. However, if two reactor systems are utilized, there will be sufficient electrical power and heat available to meet the oxygen production system requirements. The heat produced

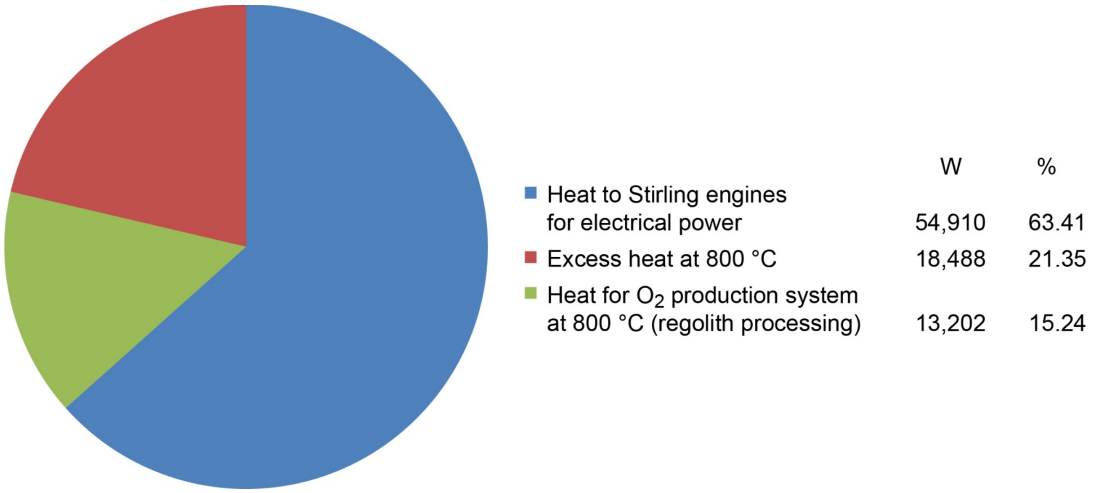

Figure 55.—Baseline reactor system mass and power for the oxygen production plant using waste heat from the reactor for continuous oxygen production.

TABLE 27.—BASELINE REACTOR SYSTEM PARAMETERS

Item	Value
Heat output per reactor at 800 °C, W	43,300
Reactor mass, each, kg	235
Shielding per reactor, kg	547
Balance of plant per reactor, kg	763
Number of reactors	2
Total mass for two reactor power systems, kg	3,090
Electrical power required, W	9,329
Electrical heat needed to raise regolith to 1,000 °C, W	3,300

by the baseline reactor system is at 800 °C. Therefore, electrical heaters will still be needed to add additional heat to 1,000 °C to meet the requirements of the oxygen production system. The breakdown of the heat output of the reactors and the mass of the system is given in Figure 55 and Table 27.

As discussed previously, the reactors are modular power systems that provide fixed output, both thermal and electrical. For Case 1, two reactor systems were able to meet the thermal and electrical requirements of the oxygen production system. However, the reactors also produced an excess 18,488 W of heat. This unused capability will increase the overall mass of the reactor system beyond that of a reactor custom sized for this application.

To better match the reactor to the oxygen production system requirements, an advanced system that operates at a higher temperature and greater Stirling engine efficiency can be conceived. This system, as described in Table 22, would be better matched to the oxygen production system. By utilizing the heat generated by the reactor directly in the oxygen production reactor, only one fission reactor system would be required. The thermal and mass breakdown for this reactor system is given in Figure 56 and Table 28.

The last option for the reactor system is one in which the reactors are located a distance from the oxygen production system in order to maintain a dose level below the 5 rem/yr limit. Due to the distance away from the oxygen production system, thermal heat from the reactor cannot be directly utilized. Therefore, the reactor will need to provide electrical power to meet both the thermal and electrical power requirements of 25,830 W for the oxygen production system as presented by Figure 13. To accomplish this, three 10-kWe fission-power reactor systems will be needed. The dose from the three-reactor system causes the required distance to increase from the 1.15 km for one reactor to 1.99 km. The mass breakdown for this power system is shown in Figure 57.

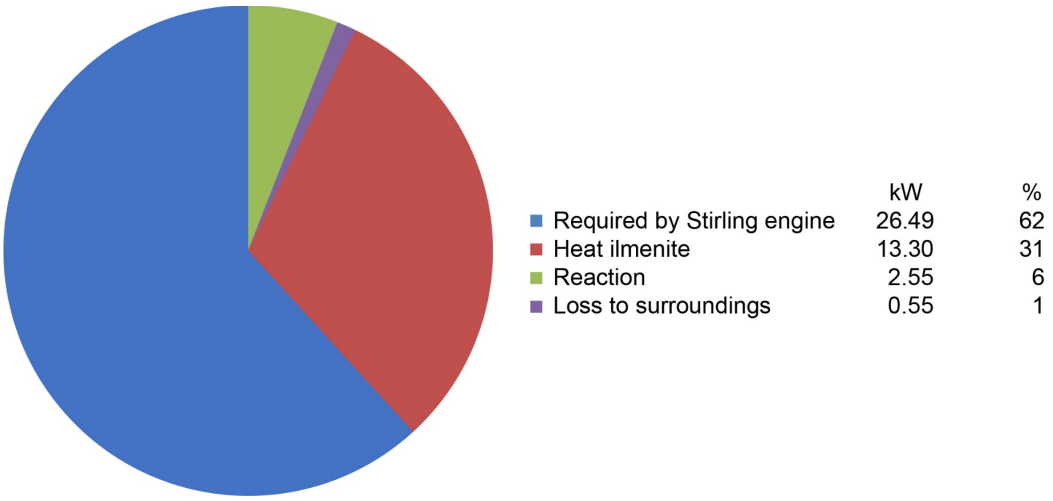

Figure 56.—Advanced reactor system mass and power for the oxygen production plant using waste heat from the reactor.

TABLE 28.—ADVANCED REACTOR SYSTEM PARAMETERS

Item	Value
Heat output at 1,000 °C, W	43,300
Thermal power required at 1,000 °C, W	16,502
Total heat to the Stirling engines for electrical power, W	26,653
Electrical power required, W	9,329
Reactor mass, kg	235
Shielding, kg	547
Balance of plant, kg	763
Total mass, kg	1,545

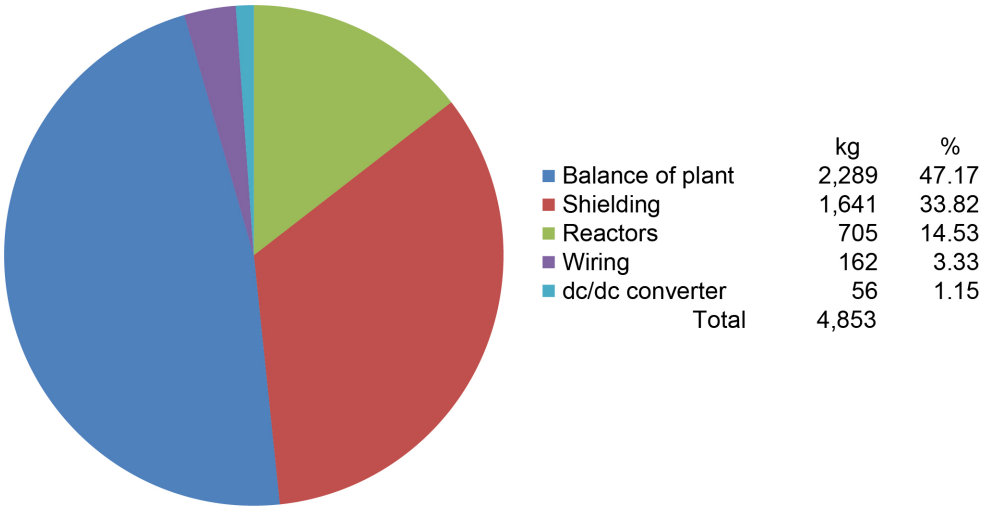

Figure 57.—Baseline three-reactor system mass breakdown for continuous oxygen production at a distance of 1.99 km from the plant. Direct current is dc.

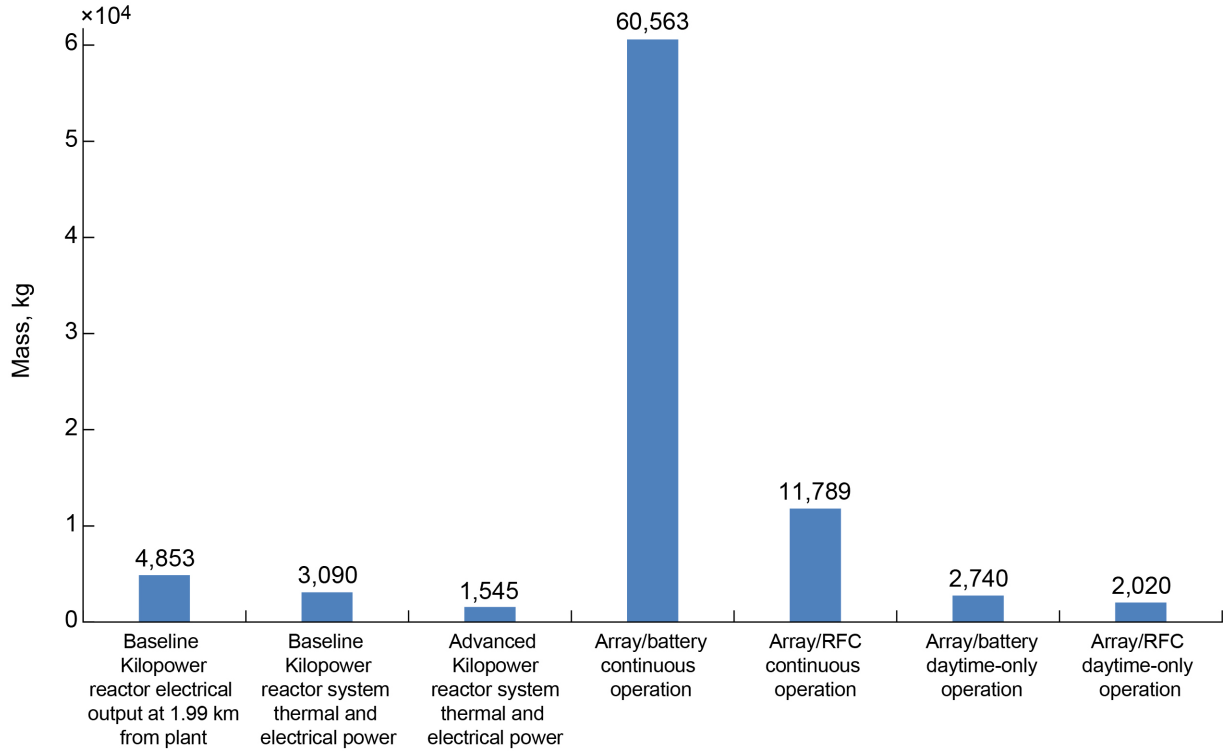

Figure 58.—Power system mass comparison for regolith oxygen production.

The overall power system mass comparison for powering the ISRU oxygen production system is shown in Figure 58. The continuous operation PV array system utilizing batteries for energy storage is by far the largest mass system. Ignoring the continuous operation PV array systems, the remaining systems and operational approaches are all comparable in mass with the advanced fission reactor approach, which has the overall lowest mass. The PV array and RFC system operating only during the daytime has the lowest mass of the PV systems and is lower than that of the currently designed reactor systems.

6.2 Case 2—Base Camp's Power System

Unlike the oxygen production system, the base camp's power system is required to operate continuously day and night at the same power level. Therefore, the PV system for this application must have sufficient storage to operate throughout the night. The energy balance to meet the habitat's continuous day and night power requirement of 28.05 kW, as discussed in Section 4.4 and summarized in Figure 26, is given in Figure 59 for the PV array and battery system. The mass breakdown for the PV array and battery system is given in Figure 60. The battery mass for this system constitutes approximately 95 percent of the total system mass. This is due to the requirement of operating at full power throughout the night.

The energy balance for the PV array and RFC system is given in Figure 61. Based on this energy balance, the power system mass was determined as shown in Figure 62. As seen in Case 1, the RFC provides a lower mass system for energy storage for operation throughout the lunar night than the battery for the base camp operation. However, the RFC still constitutes approximately 92 percent of the total power system mass. The breakdown of the RFC system mass is shown in Table 29. The RFC system has a total specific energy of 831 Wh/kg. The array size was larger for the RFC than the battery system due to the lower charge and discharge efficiency of the RFC. This can be seen in the energy balance diagram for the PV array and RFC system (Figure 61). The required array size for the PV and RFC system is 42 percent larger than the array area needed for the PV and battery system.

For the fission reactor power system to provide adequate shielding for the personnel at the habitat for a maximum dose rate of 5 rem/yr, the reactors were positioned 1.99 km from the habitat. This is similar to the approach used with the crew-tended oxygen production in Case 1. As discussed in Section 5.2, material shielding could also be employed to reduce the separation distance between the reactor and the habitat. However, for this analysis, the 1.99 km distance was utilized with no additional terrain shielding considered.

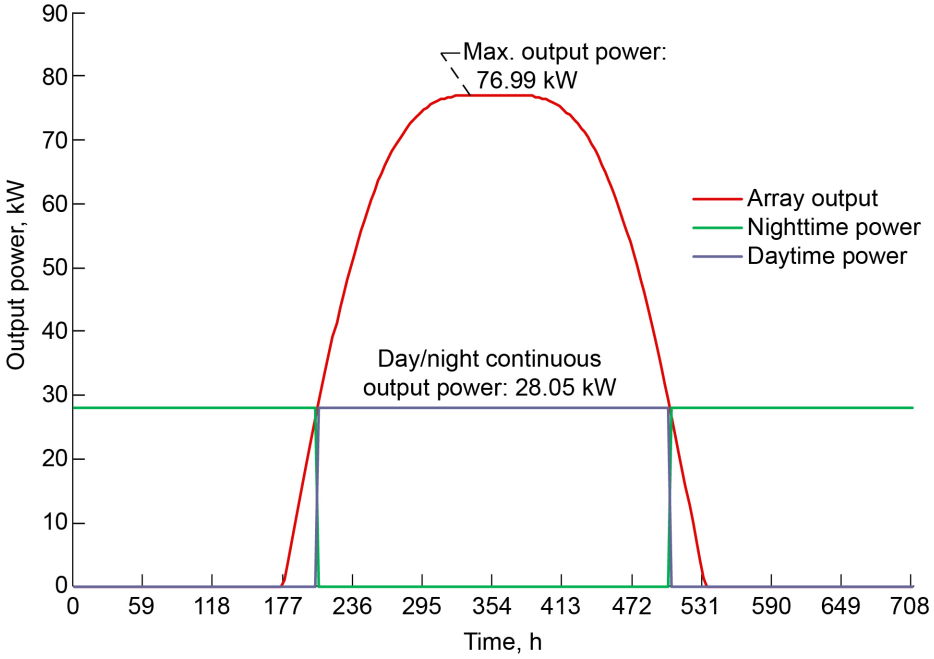

Figure 59.—Photovoltaic (PV) array and battery energy balance for day and night base camp power at 28.05 kW of continuous output power. Required array area is 226.5 m^2. Total energy required for 1 day and night cycle is 19,869 kWh. The array is at 30° latitude with a fixed 30° tilt angle and 28 percent efficient solar cells. Earth spring equinox is 1,359 W/m^2.

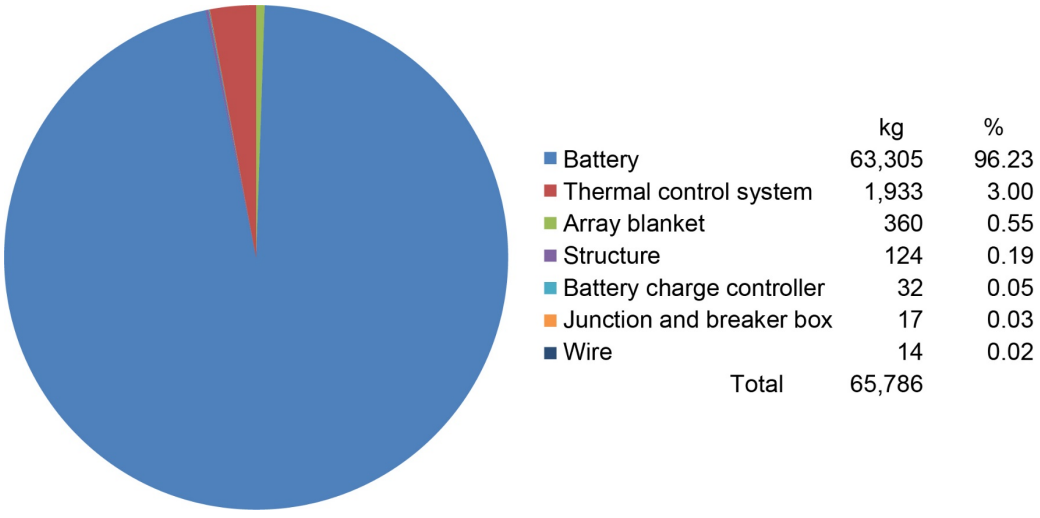

Figure 60.—Lunar base camp photovoltaic (PV) array and battery mass breakdown at 28.05 kW of continuous output power.

TABLE 29.—REGENERATIVE FUEL CELL (RFC) SYSTEM MASS BREAKDOWN FOR BASE CAMP POWER

Fuel cell	
Fuel cell stack, S_{fc}	56.100
Hydrogen separation tank, S_{hst}	5.6
Filters, S_f	3.4
Propellant lines and fittings, S_{pl}	14.6
Controller unit, S_{cu}	4.5
Wiring, S_w	8.4
Heat exchanger, S_{he}	28.1
Water pump, S_{wp}	7.6
Check valves, S_{chv}	2.2
Flow regulators, S_{fr}	17.3
Control valves, S_{cv}	4.5
Pressure and temperature sensors, S_s	2.0
Flow sensors, S_{fs}	1.7
Hydrogen phase separator, S_{hps}	2.0
Hydrogen regulator, S_{hr}	1.4
Oxygen separation tank, S_{ost}	5.1
Oxygen regulators, S_{or}	2.5
Hydrogen tank	1,809.1
Hydrogen and residual	706.1
Oxygen tank	737.1
Oxygen and residual	5,649.0
Total	9,068.1

Electrolyzer	
Electrolyzer stack, S_{es}	205.0
Water tank and heater	10.3
Filters, S_f	12.3
Propellant lines and fittings, S_{pl}	53.3
Controller unit, S_{cu}	16.4
Wiring, S_w	30.8
Heat exchanger, S_{he}	102.5
Water pump, S_{wp}	27.7
Check valves, S_{chv}	8.2
Flow regulators, S_{fr}	63.1
Control valves, S_{cv}	16.4
Pressure and temperature sensors, S_s	7.2
Flow sensors, S_{fs}	6.2
Total	559.2
System total	9,627.3

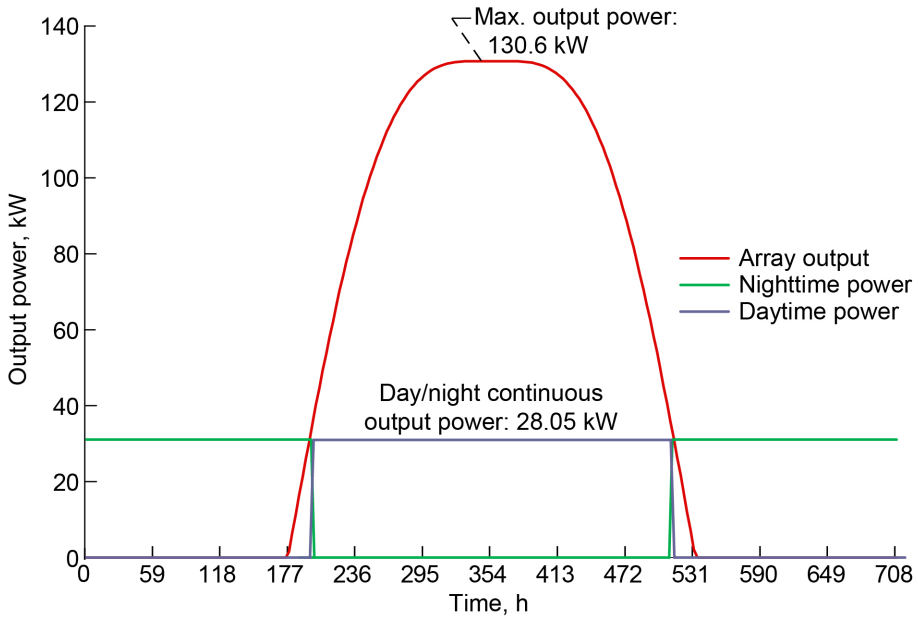

Figure 61.—Photovoltaic (PV) array and regenerative fuel cell (RFC) energy balance for day and night base camp power at 28.05 kW of continuous output power. Required array area is 384.2 m^2. Total energy required for 1 day and night cycle is 19,868 kWh. The array is at 30° latitude with a fixed 30° tilt angle and 28 percent efficient solar cells. Earth spring equinox is 1,359 W/m^2.

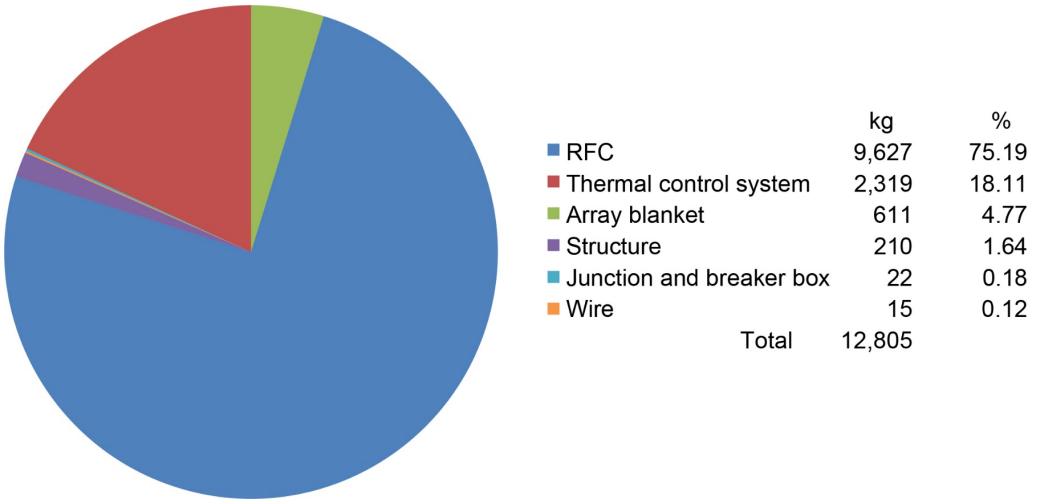

Figure 62.—Lunar base camp photovoltaic (PV) array and regenerative fuel cell (RFC) mass breakdown at 28.05 kW of continuous output power.

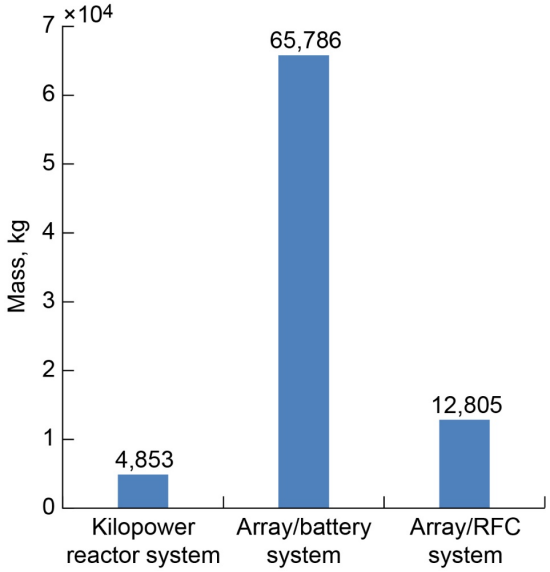

Figure 63.—Power system mass comparison for providing base camp power.

A power cable would be deployed between the reactor and habitat. An exclusion zone of 1.99 km surrounding the reactor would be maintained when it is operational. To meet the 28.05 kWe power requirement for the habitat, three 10-kWe reactors were utilized. The mass breakdown for this system is the same as the reactor power system shown in Figure 57 for the ISRU oxygen production option.

The comparison of the power systems' masses for the base camp's power requirements is given in Figure 63. As seen in the figure, the Kilopower-based fission reactor system provides the lowest mass for the base camp's power system operation. The PV array and battery system is by far the heaviest due to the large battery mass needed to operate throughout the night. The PV array and RFC system had significantly less mass, approximately 80 percent, than the battery system, but was still 2.5 times as massive as the reactor system. This application demonstrates that for lunar missions requiring high power levels throughout the nighttime period, the reactor system provides a significant mass advantage over PV array-based systems that need to store energy for nighttime operation.

6.3 Case 3—Oxygen Production and Base Camp Combined Power System

The final case examines power systems operating both the ISRU oxygen production system and the base camp. For the combined operation, it was assumed that both components were at the same location. For the reactor power system, this eliminated the option of using the reactor waste heat for the oxygen production system. For the PV array-based systems, only the operation of the oxygen production during the daytime was considered, since operating the oxygen production system using stored energy throughout the nighttime was shown to be noncompletive in Case 1. For the PV array and battery power system, the daytime power consumption includes both operating the ISRU oxygen production plant as well as providing power to the base camp. The excess power from the array, above what is used for oxygen production and the base camp, is used to recharge the energy storage system. The corresponding energy balance for the battery system is shown in Figure 64.

From the energy balance diagram (Figure 64), the corresponding operating time for the oxygen production plant is 218.3 h. This requires an oxygen production rate of 5.29 kg/h to meet the 1,154 kg of oxygen production for 1 day and night period. The mass breakdown for the oxygen production system to meet this required production rate is given in Table 30.

The total power system mass breakdown for the PV array and battery power system used to power the combined oxygen production system and base camp is shown in Figure 65. The battery mass still dominates the overall power system mass. Because the battery mass is such a large fraction of the total mass, there is not much difference in the overall mass of this system compared to the PV array and battery system used to power the base camp alone.

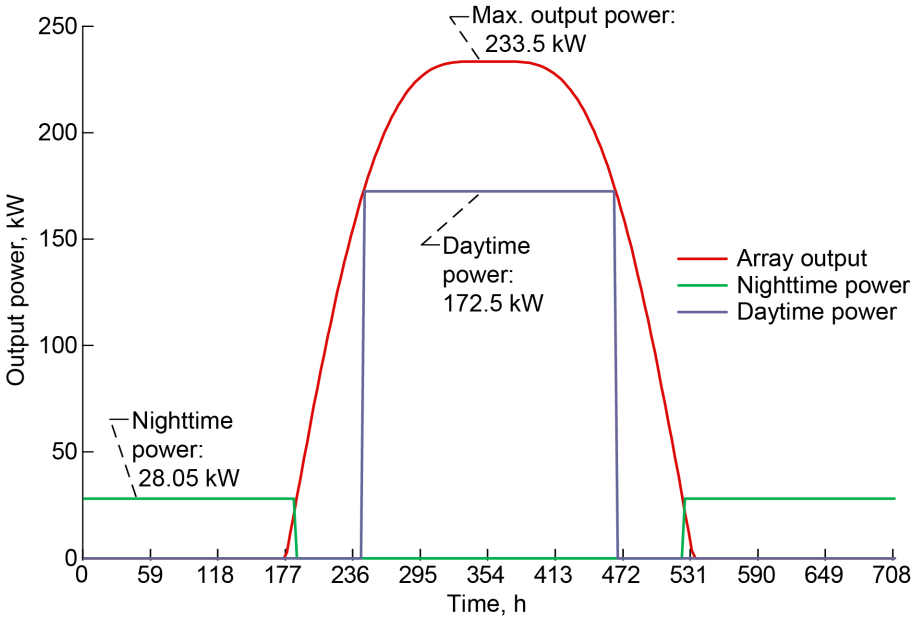

Figure 64.—Photovoltaic (PV) array and battery energy balance for base camp and oxygen production for 172.5 kW daytime and 28.05 kW nighttime operational power. Required array area is 687 m^2. The array is at 30° latitude with a fixed 30° tilt angle and 28 percent efficient solar cells. Earth spring equinox is 1,359 W/m^2.

TABLE 30.—DAYTIME-ONLY OXYGEN PRODUCTION MASS AND POWER REQUIREMENTS FOR COMBINED ISRU PLANT AND BASE CAMP POWER SYSTEM WITH BATTERY ENERGY STORAGE AT PRODUCTION RATE OF 5.29 kg/h[a]

Component	Required power, W	Mass, kg
Scoop and delivery conveyors	160	51
Vibrating screen	430	91
Magnetic separator	317	98
Fluidized bed reactor	---------	27
Hydrogen tank	---------	19
Oxygen tank	---------	486
Electrolyzer	29,095	159
Thermal power to process reactor	43,445	-------
Heat of reaction	8,316	-------
Heat loss	552	-------
Thermal control system	---------	1,059
Total	82,315	1,990

[a]In situ resource utilization (ISRU).

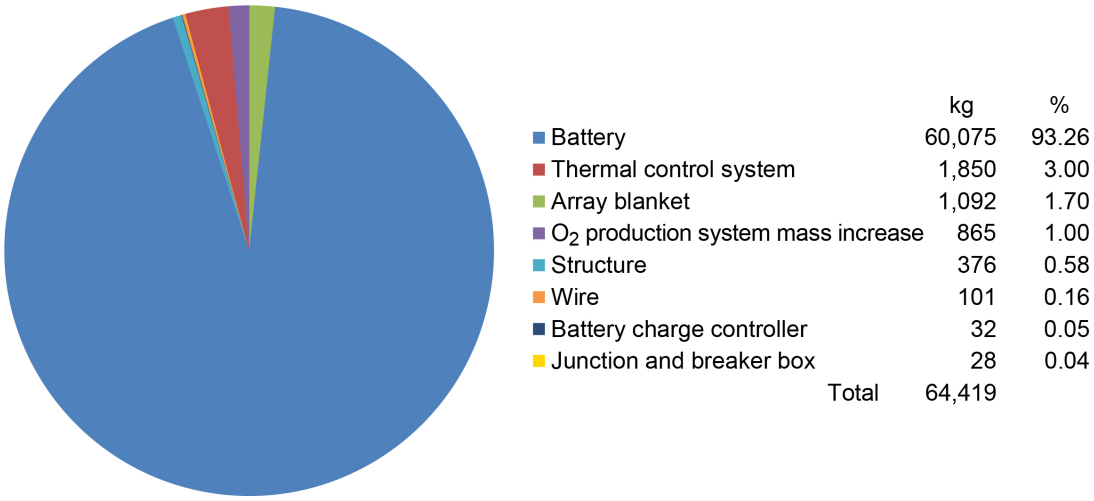

Figure 65.—Photovoltaic (PV) array and battery power system mass breakdown for operating combined in situ resource utilization (ISRU) oxygen production system and base camp for 172.5 kW daytime and 28.05 kW nighttime operational power.

Because of the difference in their charge and discharge efficiencies, the RFC-based energy storage system will have a different energy balance than the battery-based system. The energy balance for the PV array and RFC system to meet the day and nighttime power requirements is shown in Figure 66. The PV array area for the RFC-based system has increased by approximately 50 m^2. The larger array area is needed for the RFC-based system due to its lower charge and discharge efficiencies compared to the battery-based system. However, the larger array does provide some benefits enabling the power system to be operated at a slightly lower peak power level than the PV array and battery system during the daytime. This is due to having sufficient power provided earlier in the morning and later in the evening to operate the oxygen production system. This in turn slightly reduces the required oxygen production rate to 4.66 kg/h and thereby lowers the total power requirement over the daytime operating time. It should be noted

that the total energy produced by the system for oxygen production is the same as for the other cases in order to make the desired 1,154 kg of oxygen over the 1-day period. The mass breakdown for the oxygen production system to meet this production rate requirement is given in Table 31.

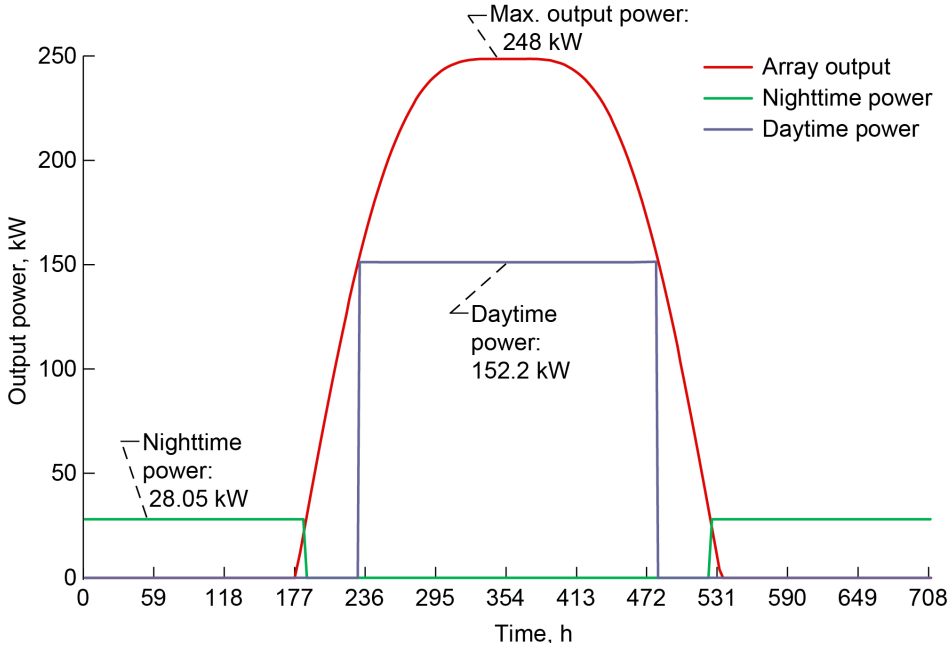

Figure 66.—Photovoltaic (PV) array and regenerative fuel cell (RFC) energy balance for base camp and oxygen production for 152.2 kW daytime and 28.05 kW nighttime operational power. Required array area is 730 m^2. Total energy required for 1 day and night cycle is 38,158 kWh. The array is at 30° latitude with a fixed 30° tilt angle and 28 percent efficient solar cells. Earth spring equinox is 1,359 W/m^2.

TABLE 31.—DAYTIME-ONLY OXYGEN PRODUCTION MASS AND POWER REQUIREMENTS FOR COMBINED ISRU[a] PLANT AND BASE CAMP POWER SYSTEM WITH RFC[b] ENERGY STORAGE AT PRODUCTION RATE OF 4.66 kg/h

Component	Required power, W	Mass, kg
Scoop and delivery conveyors	155	51
Vibrating screen	378	89
Magnetic separator	279	98
Fluidized bed reactor	--------	27
Hydrogen tank	--------	19
Oxygen tank	--------	486
Electrolyzer	25,630	140
Thermal power to process reactor	46,150	-------
Heat of reaction	7,326	-------
Heat loss	552	-------
Thermal control system	--------	933
Total	72,593	1,843

[a]In situ resource utilization (ISRU).

[b]Regenerative fuel cell (RFC).

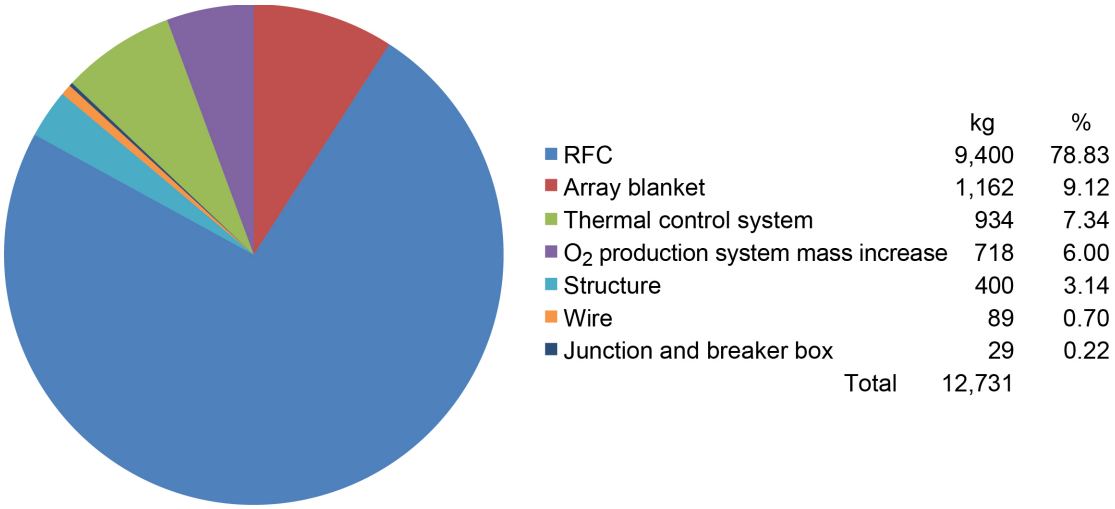

Figure 67.—Photovoltaic (PV) array and regenerative fuel cell (RFC) power system mass breakdown for operating combined in situ resource utilization (ISRU) oxygen production system and base camp for 152.2 kW daytime and 28.05 kW nighttime operational power.

Figure 67 shows the corresponding mass breakdown for the PV array and RFC system to meet the requirements to power the base camp and oxygen production system per the energy balance diagram (Figure 66). The PV array and RFC system provides a significant mass reduction over the solar-powered PV system utilizing batteries for energy storage. The RFC-based system provided a 75-percent decrease in the required mass over the battery-based energy storage system.

The final power system option to consider for powering the base camp and oxygen production system is the Kilopower reactor. With the baseline assumption that the oxygen production system is in close proximity to the base camp, the ability to use the waste heat from the Kilopower reactor as process heat with the oxygen production system is not an option. Therefore, the only option is to provide electrical power for both the habitat and the oxygen production system. The general layout of the reactor system, base camp, and oxygen production system is illustrated in Figure 68.

Since personnel will be working in the vicinity of the base camp and oxygen production system, the reactor was positioned 2.81 km from the habitat to provide adequate shielding as discussed in the previous two cases. A power cable would then be deployed between the reactor and habitat. An exclusion zone of 2.81 km surrounding the reactor would be maintained when it is operational. To meet the 53.84 kWe total power requirement for the habitat and oxygen production system, six 10-kWe reactor systems can be utilized as illustrated in Figure 51. However, this arrangement would provide an excess power capacity of 6.2 kW. The mass breakdown for the six-reactor system is given in Figure 69.

The baseline analysis utilizes the reactor systems as a fixed 10-kWe modular power system block that can be added together to meet the power requirements in increments of 10 kW. However, if the systems were optimized to provide a power output that better matched the power requirements, then a mass savings could potentially be realized. Therefore, an additional reactor system analysis was added in which the reactor mass was scaled linearly to match the total power requirement. The mass breakdown for this scaled case is shown in Figure 70.

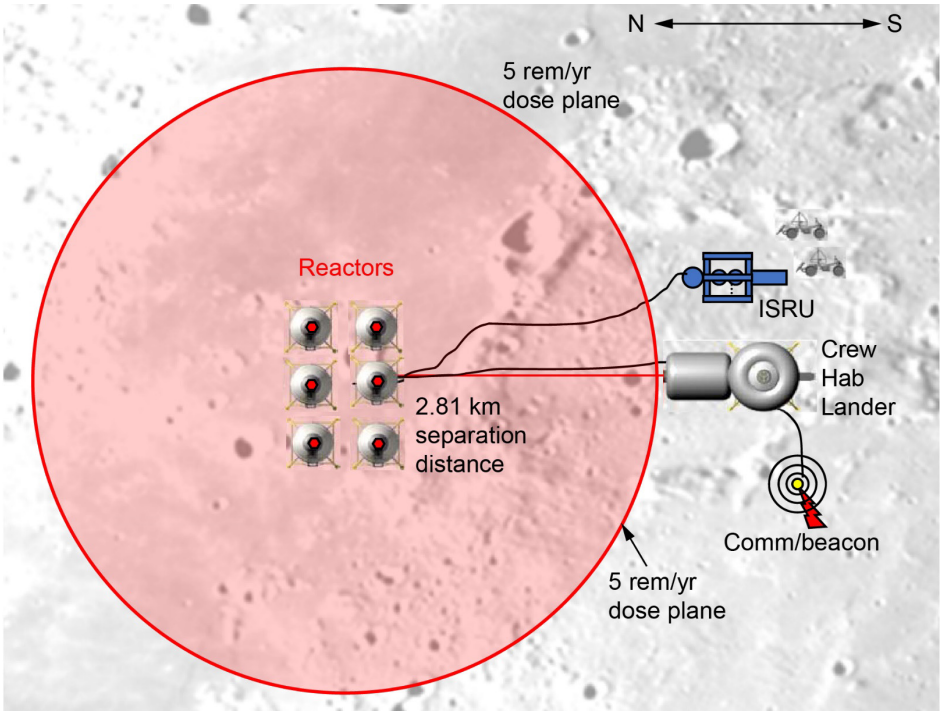

Figure 68.—Kilopower reactor-based power system, base camp, and oxygen production system layout. In situ resource utilization is ISRU.

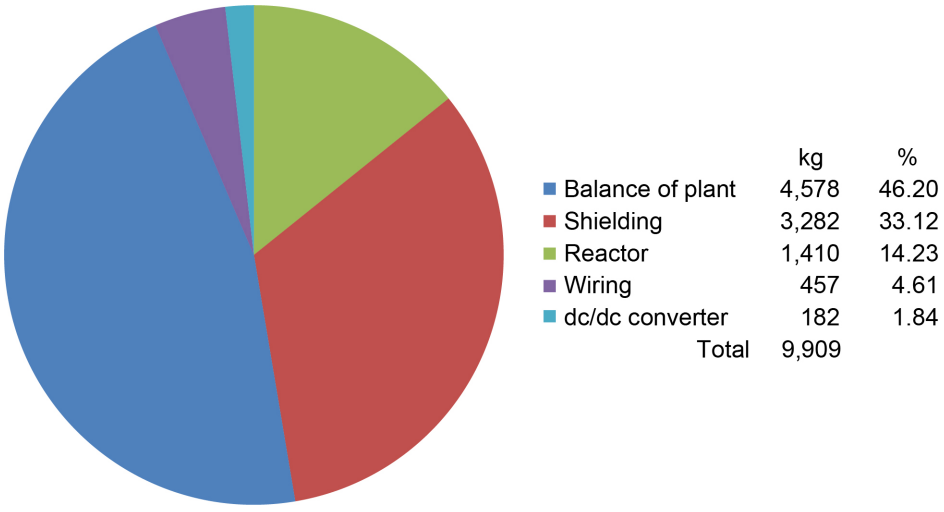

Figure 69.—Baseline reactor system mass breakdown for base camp and oxygen production at distance of 1.15 km from plant for 53.84 kW continuous day and night power production. Direct current is dc.

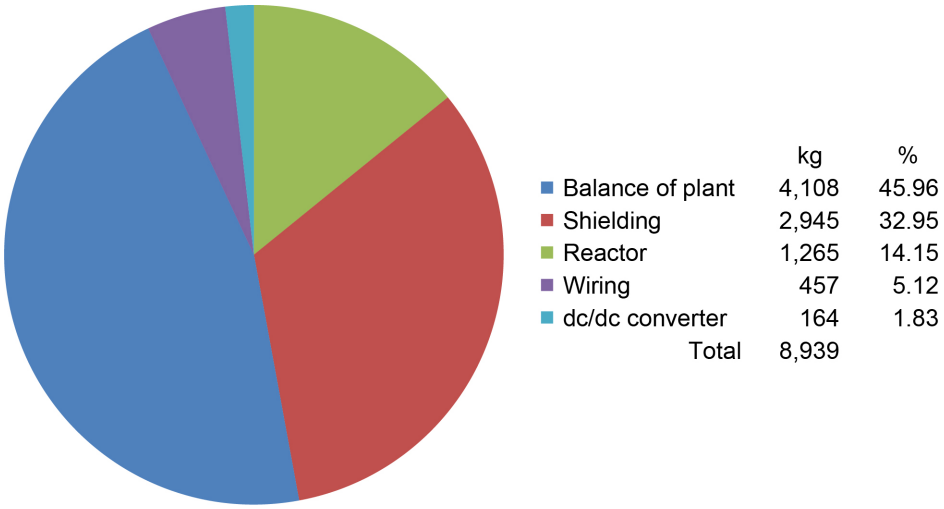

Figure 70.—Scaled reactor system mass breakdown for base camp and oxygen production at distance of 1.15 km from plant for 53.84 kW continuous day and night power production.

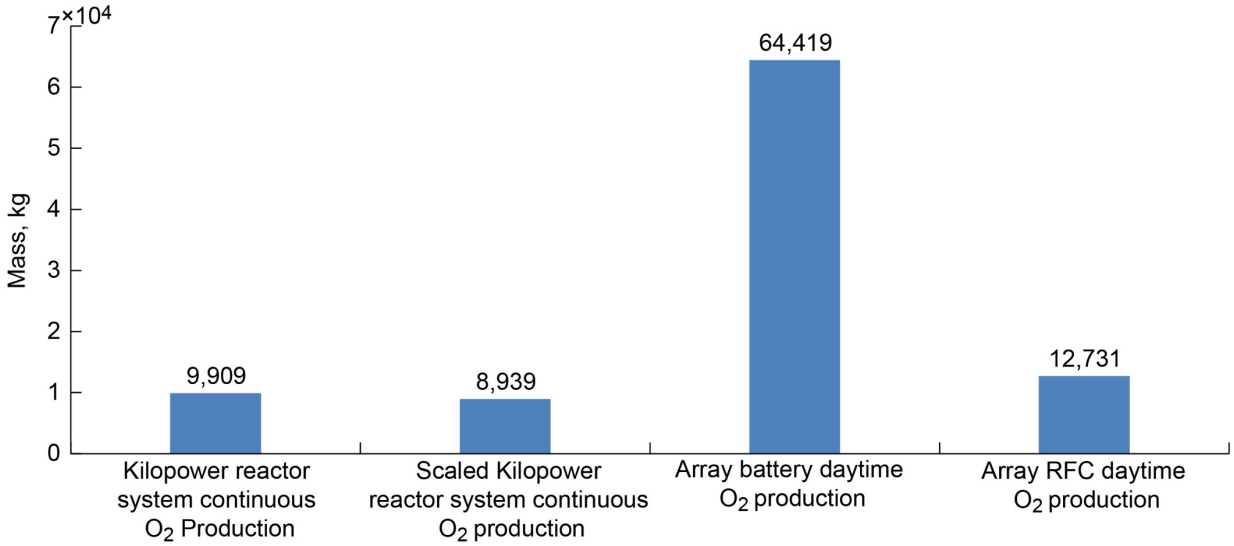

Figure 71.—Power system mass comparison for providing base camp and oxygen production system power.

The comparison of the power system mass for power requirements of the combined base camp and oxygen production system is given in Figure 71. As seen in this figure, the Kilopower-based fission reactor system provides the lowest mass for the base camp and oxygen production power system. To reduce the energy storage mass requirements for the PV array-based systems, the oxygen production system operated only during the daytime as discussed in Case 1. However, the PV array and battery system was still by far the heaviest due to the large battery mass needed to operate the base camp throughout the night. The PV array and RFC system had significantly less mass than the battery-based system, approximately 75 percent less, but was still 30 percent heavier than the baseline reactor system and 37 percent heavier than the scaled reactor system. As with the base camp's power systems comparison, for lunar missions that require high power levels throughout the nighttime period, the reactor

system provides a mass advantage compared to a PV array-based system that needs to store energy for nighttime operation.

7.0 Conclusion

The analysis presented in this report established the power requirements for operating an in situ resource utilization (ISRU) oxygen production system and small base camp on the lunar surface throughout 1 day and night cycle. The power requirements were then used to size a power system and determine its mass to meet them. Three types of power systems were considered: a photovoltaic (PV) array system using batteries for energy storage, a PV array system using a regenerative fuel cell (RFC) for energy storage, and a 10-kWe output power-based Kilopower reactor system.

The first case examined the power system sizing for an oxygen production plant on the lunar surface. For continuous day and night operation of the oxygen production system, the Kilopower-based reactor system provided a significant mass advantage over the PV array-based system with either a battery or RFC as the energy storage method. The Kilopower system's total mass was 4,853 kg for the baseline system providing electrical power only to the oxygen production plant. This is only 8 percent of the mass of the PV array and battery system, which had a mass of 60,563 kg and 41 percent of the mass of the PV array and RFC system, which had a mass of 11,789 kg. This is due mainly to the large energy storage requirements for the PV systems needed to operate the oxygen production plant throughout the night. To address the need for a large amount of energy storage, a variation on the production approach was examined for the PV array-based systems. Since the goal of the oxygen production system is to produce a certain amount of oxygen over a given time period, the production rate was increased so that the baseline total oxygen production of 1,154 kg per 1 day and night cycle was produced only during the daytime for the PV array-based power systems. This significantly reduced the nighttime energy storage requirement to only "keep-alive" power required to maintain the equipment at temperatures needed to survive the lunar night. By eliminating most of the nighttime energy storage requirement, the mass of the PV array-based systems was significantly reduced to less than that needed for the baseline Kilopower reactor-based system. The PV array and battery total system mass dropped to 2,740 kg and the PV array and RFC system to 2,020 kg. These masses included the increased mass associated with scaling the ISRU oxygen production plant to operate at the higher production rate. These masses are much less than the baseline Kilopower system. However, the design of the oxygen production system is intended to be automated. Therefore, it could operate without personnel in the vicinity. If that is the case, then there is the possibility of locating the Kilopower reactor near the oxygen production system and taking advantage of the waste heat produced by the reactor in the oxygen production process. Using this approach with the baseline reactor system reduces the number of systems needed from three to two and reduces the mass to 3,090 kg. This is still more than the daytime-only operation of the PV array systems, but it is more competitive. The requirement for a two-reactor system is due to the operating temperature of the reactor and the Stirling engine conversion efficiency. If the core operating temperature could be increased to 1,000 °C and the Stirling engine efficiency was increased to 35 percent, this would reduce the number of reactor systems needed to one with a system mass of 1,545 kg. This then results in a lower mass system than either the PV array and battery or PV array and RFC systems.

The second case addressed powering a six-person base camp. The base camp power requirements were the same for both the day and nighttime operation. Therefore, there was no means of eliminating or reducing the energy storage requirement for the PV array-based systems. To meet the 28.05 kW continuous power requirement, the PV array and battery system had a mass of 65,786 kg and the PV array and RFC system had a mass of 12,805 kg. Since the camp was manned, operation of the reactor in close

proximity was not possible. The only feasible reactor power system option was to operate the reactor at a distance of 1.99 km from the base camp and provide electrical power to the base camp for all of its power needs. Because of the distance between the reactor and the base camp, the utilization of waste heat from the reactor would not be possible. To provide the desired power, three 10-kWe Kilopower reactor systems would be needed with a total mass of 4,853 kg. This mass is significantly less than both of the PV array cases. It is approximately 7 percent of the mass of the PV array and battery system and 37 percent the mass of the PV array and RFC system.

The last case examined was a combination of powering both the ISRU oxygen production system and the base camp. For this case, the approach considered for the PV array-based systems was producing oxygen only during the daytime since the nighttime oxygen production powered by these systems was not competitive masswise. The power system masses for the combined operation of the base camp and oxygen production system for the PV array and battery and PV array and RFC systems were 64,419 and 12,731 kg, respectively. This compared to a mass of 9,909 kg for the Kilopower reactor system. To meet the power demands of both the base camp and oxygen production, six Kilopower reactor systems were required. However, since these are 10-kWe modular systems, this produced an excess power capacity of 6.2 kWe. To account for this, a fourth power system option was added in which the Kilopower reactor system was scaled or optimized to match the actual power requirement of the base camp and oxygen production. The scaled reactor system had a mass of 8,939 kg.

The results of the comparison between the solar PV array-based and Kilopower reactor-based systems have shown that for missions required to operate throughout the lunar nighttime at power levels comparable to those used during the daytime, the reactor-based system provides a significant mass advantage. However, for applications that can meet their mission requirements while only having to operate during the daytime with minimal power required to survive the nighttime, the PV array-based systems are competitive masswise and provide a mass advantage over the current Kilopower system design.

For the PV array-based systems, the RFC-based energy storage method had a mass advantage over a battery-based method. For higher power nighttime power operation in all three cases, the RFC system's specific energy was just over 830 Wh/kg. For the lower power keep-alive nighttime power level used as part of the analysis for the first case, the specific energy for the RFC was 456 Wh/kg. Both these levels are significantly above the specific energy of 200 Wh/kg for the battery. Because of this higher specific energy, the RFC-based storage system provided significant mass advantages over the battery-based storage system.

The baseline reactor system utilized shielding and separation distance to meet the desired maximum dose level of 5 rem/yr for personnel operating within the vicinity of the power loads, base camp, and oxygen production system. As mentioned, in Section 5.2, there are methods that could be utilized to reduce the shielding requirements and separation distance. Implementing these would reduce the overall system mass for the reactor. Also, as mentioned in the third case, optimizing the reactor output for each specific mission would provide benefits in mass at the expense of modularity.

Appendix—Nomenclature

AEC	Able Engineering Company, Inc.
ASRG	Advanced Stirling Radioisotope Generator
Desert RATS	Desert Research and Technology Studies
DOE	Department of Energy
DOE–NR	DOE Office of Naval Reactors
DSH	Deep Space Habitat
ECLSS	environmental control and life support system
HDU	habitat demonstration unit
ISRU	in situ resource utilization
JIMO	Jupiter Icy Moons Orbiter
MLI	multilayer insulation
MMW	Multimegawatt Space Reactor
NEPSTP	Nuclear Electric Propulsion Space Test Program
NERVA	Nuclear Engine for Rocket Vehicle Applications
NNSA	National Nuclear Security Administration
NREL	National Renewable Energy Laboratory
PDU	power distribution unit
PEM	proton exchange membrane
PV	photovoltaic
RAPDAR	rollout and passively deployed array
RFC	regenerative fuel cell
SDIO	Strategic Defense Initiative Office
SNAP	Systems for Nuclear Auxiliary Power
SNTP	Space Nuclear Thermal Propulsion
SPAR	Space Power Advanced Reactor
TRIGA	Training, Research, Isotope, General Atomic
TRL	technology readiness level
TSRT	Thermionic System Evaluation Test
UV	ultraviolet

Symbols

A_a	solar array area, m^2
A_{be}	battery enclosure surface area, m^2
A_{cp}	conductive path cross-sectional area, m^2
A_{ee}	electrolyzer enclosure surface area, m^2
A_h	habitat surface area, m^2
A_{pt}	passthrough area as a percent of total area
A_r	radiator area, m^2
A_{vs}	vibrating screen area, m^2
a_{ls}	lunar surface albedo

B_{dod} battery depth of discharge
B_w communications transmission bandwidth, Hz
C_a radiator adhesive scaling coefficient, kg/m^2
C_{as} insulation attachment and seals scaling coefficient, kg/m^2
C_{at} radiator attachment scaling coefficient, kg/m^2
C_c radiator coating scaling coefficient, kg/m^2
C_{cf} cold plate coverage coefficient
C_h radiator header scaling coefficient, kg/m^2
C_{hp} heat pipe mass scaling coefficient, kg/m
C_{ic} insulation inner cover scaling coefficient, kg/m^2
C_{lv} radiator louvers scaling coefficient, kg/m^2
C_{oc} insulation outer cover scaling coefficient, kg/m^2
C_p radiator panel scaling coefficient, kg/m^2
C_{rl} insulation reflective layer scaling coefficient, kg/m^2
C_s radiator stingers scaling coefficient, kg/m^2
C_{sp} insulation spacer scaling coefficient, kg/m^2
C_t radiator tubing scaling coefficient, kg/m^2
c speed of light, m/s
c_p specific heat of ilmenite, (J/kg)K
d_h habitat diameter, m
d_{hr} distance to the horizon, m
d_{H_2t} hydrogen tank diameter, m
d_i regolith particle size diameter, m
d_{icp} conductive path inner diameter, m
d_{il} spacing between insulation layers, m
d_n day number, Earth days
d_{nt} total number of Earth days in a lunar year
d_{O_2t} oxygen tank diameter, m
d_r oxygen production reactor diameter, m
d_{rs} travel distance of scoop in regolith, m
d_s maximum regolith particle diameter, m
d_t tank diameter, m
d_{tr} communications transmitter to receiver distance, m
$d_{tr_{max}}$ maximum transmission distance, m
d_1 radiation dose at position 1, rem/yr
d_2 radiation dose at position 2, rem/yr
E_a energy produced by the solar array, Wh
E_d daytime energy requirement, Wh
E_n nighttime energy requirement, Wh
F_{al} radiator louver area adjustment factor

f_{cl} centerline frequency, Hz
f_{ls} view factor to the lunar surface
f_n passthrough constant 1
f_p passthrough constant 2
f_s material yield strength factor of safety
f_{sc} solar cell fill factor
G_w wire gauge
g lunar surface gravity, m/s^2
g_r ratio of lunar to Earth gravitational constants
H_r oxygen production heat of reaction, kJ/kg
h height above the surface, m
h_r oxygen production reactor height, m
h_{re} communications receiver height, m
h_{rs} height of the oxygen production reactor above the surface, m
h_t communications transmitter height, m
I_m mean solar intensity at the Earth/Moon system, W/m^2
I_s solar intensity at the Earth/Moon system, W/m^2
I_w wire current, A
K transmission adjustment factor
k thermal conductivity o material, W/(m·K)
k_b Boltzmann constant, J/K
L_c cold plate length, m
L_{cb} regolith and ilmenite conveyor belt length, m
L_{cp} conductive path length, m
L_w length of the wire runs, m
M_{ab} solar array and battery system total mass, kg
M_{apv} solar array blanket mass, kg
M_{arfc} solar array and RFC system total mass, kg
M_{as} solar array structure mass, kg
M_b battery mass, kg
M_{bb} breaker box mass, kg
M_{bcc} battery charge controller mass, kg
M_{cb} conveyor belt mass, kg
M_{cp} cold plate mass, kg
M_e electrolyzer mass, kg
M_{es} energy storage mass, kg
M_{fc} fuel cell mass, kg
M_{fr} fission reactor mass, kg
M_{frb} fission reactor balance-of-plant mass, kg
M_{frs} fission reactor shield mass, kg

M_{frt} fission reactor system total mass, kg
M_{H_2} hydrogen mass, kg
M_{H_2t} hydrogen tank mass, kg
M_{hp} heat pipe mass, kg
M_{mli} insulation mass, kg
M_{ms} magnetic separator mass, kg
M_{O_2} oxygen mass, kg
M_{O_2t} oxygen tank mass, kg
M_r radiator mass, kg
M_{rfc} regenerative fuel cell mass, kg
M_{rt} oxygen production total reactor tank mass, kg
M_{sw} specific mass of the wire, kg/m
M_t reactor tank mass, kg
M_{tc} thermal control system mass, kg
M_{vc} direct current (dc) to dc voltage converter mass, kg
M_{vs} vibrating screen mass, kg
M_w wire mass, kg
$\dot{M}_i$ rate at which ilmenite is separated from the regolith, kg/h
$\dot{M}_o$ rate of oxygen production, kg/h
$\dot{M}_r$ rate at which regolith is acquired from the surface, kg/h
$\dot{M}_w$ rate of water production, kg/h
n_{cp} number of conductive paths
n_l number of layers of insulation
n_{ri} regolith particle size distribution
n_{rs} number of fission reactor systems
n_{rw} number of wires per fission reactor system
n_w number of wire runs between array and junction box
P_a solar array output power, W
P_{ahc} habitat air conditioning power, W
$P_{a_{max}}$ maximum solar array output power, W
P_{bc} base camp power requirement, W
P_{bm} biomass processing power, W
P_{com} communications power requirement, W
P_{dl} daytime power level required by the loads, W
P_e electrolyzer power, W
P_{eva} extravehicular activity support power, W
P_{fd} food processing and storage power, W
P_{H_2} hydrogen gas pressure, Pa
P_{ht} habitat nighttime heater power, W
P_{il} power to lift the ilmenite, W

P_{ls} environmental control and life support power, W
P_{ms} magnetic separator power, W
P_n noise power level, W
P_{nl} nighttime power level required by the loads, W
P_{oe} operational equipment power, W
P_r heat rejection power to the radiator, W
P_{rl} power to lift regolith, W
P_{ro} surface-to-satellite receiver power, W
P_{rs} power to scoop regolith, W
P_{ss} communications signal strength, W
P_t tank internal pressure, Pa
P_{te} electrolyzer waste heat, W
P_{th} habitat thermal control power, W
P_{tm} communications transmitter power, W
P_{tO_2} total oxygen production system electrical power required, W
P_{vs} vibrating screen power, W
P_{wl} transmission wire power loss, W
P_{wp} water processing power, W
P_{wst} waste processing power, W
Q_{as} airlock structure heat leak to the surroundings, W
Q_{cp} conductive path heat loss, W
Q_h habitat total nighttime heat loss, W
Q_{hi} thermal power required to heat the ilmenite, W
Q_i insulation heat loss, W
Q_{ls} oxygen production reactor heat loss to the surroundings, W
Q_{ps} passthrough heat loss, W
Q_r heat consumed by the oxygen production process, W
Q_{ra} heat leak to the radiator during nighttime, W
Q_{sl} support leg heat leak to the surface, W
Q_{tO_2} total oxygen production system thermal power required, W
R_{H_2} hydrogen gas constant
R_m ratio of mass of ilmenite to mass of regolith
R_{max} maximum achievable communications data rate, bit/s
$R_{m'}$ average amount of small grain ilmenite in mare by weight
R_{res} hydrogen and oxygen reactant residual fraction
$R_{v'}$ average amount of small grain ilmenite in mare by volume
R_w power transmission wire resistance per length, Ω/m
$\dot{R}_{vs}$ regolith screening rate, kg/(h·m^2)
r_m radius of the Moon, km
r_{orb} solar orbital radius of the Earth/Moon system, km

r_{orbm} average solar orbital radius of the Earth/Moon system, km
r_1 distance from reactor for dose level 1, m
r_2 distance from reactor for dose level 2, m
S_a spacing between the array modules, m
S_b battery specific energy, Wh/kg
S_{chv} check valve specific mass, kg/kW
S_{cu} controller unit specific mass, kg/kW
S_{cv} control valve specific mass, kg/kW
S_{es} electrolyzer stack specific mass, kg/kW
S_f filter specific mass, kg/kW
S_{fc} fuel cell stack specific mass, kg/kW
S_{fr} flow regulator specific mass, kg/kW
S_{fs} flow sensor specific mass, kg/kW
S_{he} heat exchanger specific mass, kg/kW
S_{hps} hydrogen phase separator specific mass, kg/kW
S_{hr} hydrogen regulator specific mass, kg/kW
S_{hst} fuel cell hydrogen separation tank specific mass, kg/kW
S_{or} oxygen regulator specific mass, kg/kW
S_{ost} oxygen separation tank specific mass, kg/kW
S_{pl} propellant line and fittings specific mass, kg/kW
S_{rti} oxygen production reactor tank scaling factor
S_s pressure and temperature sensor specific mass, kg/kW
S_{vb} battery specific volume, kg/m^3
S_{ve} electrolyzer specific volume, kg/m^3
S_w wiring specific mass, kg/kW
S_{wp} water pump specific mass, kg/kW
S_{wt} electrolyzer water tank specific mass, kg/kW
T_{H_2O} electrolyzer water temperature, K
T_{hi} habitat internal temperature, K
T_i reactor ilmenite and hydrogen temperature, K
T_{io} regolith surface temperature at collection time, K
T_{ls} maximum lunar surface temperature, K
T_m mean insulation temperature, K
T_r radiator operating temperature, K
T_s sink temperature, K
T_{sd} lunar surface average daytime sink temperature, K
T_{sn} lunar surface average nighttime sink temperature, K
t_c cold plate thickness, m
t_{cp} conductive path wall thickness, m
t_d lunar day length, h

t_h time to heat ilmenite, h

t_i instantaneous day time, h

t_{rt} time ilmenite is maintained at the reaction temperature, h

t_{sc} fraction of batch processing time used to scoop the regolith

t_t tank wall thickness, m

U_{H_2} hydrogen gas velocity within the oxygen production reactor, m/s

V_a array operating voltage, V

V_{H_2t} hydrogen tank volume, m^3

V_{O_2t} oxygen tank volume, m^3

V_{rt} power wire voltage, V

V_{tm} tank material volume, m^3

$\dot{V}_{ir}$ rate ilmenite is replaced in the oxygen production reactor, kg/hr

w_c cold plate width, m

Z_{H_2} hydrogen gas compressibility factor

α solar elevation angle

α_{rls} radiator lunar infrared (IR) absorptivity

α_{rs} radiator solar infrared (IR) absorptivity

β array inclination angle

γ day angle

ΔG Gibbs free energy, kJ/mol

ΔH change in enthalpy, kJ/mol

ΔS change in entropy, (kJ/K)mol

ΔS_{H_2} hydrogen entropy change, (J/K)mol

ΔS_{H_2O} water entropy change, (J/K)mol

ΔS_{O_2} oxygen entropy change, (J/K)mol

ε eccentricity of the Earth/Moon system

ε_{hw} habitat wall emissivity

ε_i insulation layer emissivity

ε_l lunar orbital eccentricity

ε_p fluidized bed porosity

ε_r radiator emissivity

ε_{rO_2} oxygen production reactor emissivity

η_{bc} battery charge efficiency

η_c energy storage system charge efficiency

η_d energy storage system discharge efficiency

η_e electrolyzer efficiency

η_{em} electric motor efficiency

η_{fc} fuel cell efficiency

η_s ilmenite separation process efficiency

η_{sc} solar cell efficiency

θ	hour angle
θ_{rs}	maximum solar incident angle to the radiator
μ_{H_2}	hydrogen gas viscosity, kg/(m·s)
μ_r	regolith coefficient of friction
ρ_a	solar array areal density, kg/m^2
ρ_{as}	solar array structure specific mass, kg/m^2
ρ_c	cold plate material density, kg/m^3
ρ_{H_2}	hydrogen gas density, kg/m^3
ρ_i	granular ilmenite density, kg/m^3
ρ_{ip}	ilmenite particle density, kg/m^3
ρ_r	average regolith density, kg/m^3
ρ_{tm}	tank material density, kg/m^3
σ	Stefan-Boltzmann constant, W/(m^2·K^4)
σ_y	tank material yield strength, Pa
τ	ilmenite particle shape factor
ϕ	latitude
χ_d	percent dust coverage
ψ	lunar declination angle in degrees
ψ_{max}	maximum lunar declination angle in degrees

References

1. National Aeronautics and Space Administration: Explore Moon to Mars: Earth's Moon. 2009. https://www.nasa.gov/multimedia/imagegallery/image_feature_1538.html Accessed Nov. 4, 2019.
2. Bussey, D.B.J., et al.: Permanent Sunlight at the Lunar North Pole. Presented at the Lunar and Planetary Science XXXV Meeting, Houston, TX, 2004.
3. Choi, Charles Q.: Moon Facts: Fun Information About the Earth's Moon. Space.com, 2017. https://www.space.com/55-earths-moon-formation-composition-and-orbit.html Accessed Nov. 7, 2019.
4. Berry, Patrick L.: A Hithchiker's Guide to the Moon. 2005. https://www.nasa.gov/vision/universe/solarsystem/24may_lola.html Accessed Nov. 1, 2019.
5. Jet Propulsion Laboratory: Solar Cell Array Design Handbook: Volume 1. JPL SP 43–38, 1976.
6. Williams, J.-P., et al.: The Global Surface Temperatures of the Moon as Measured by the Diviner Lunar Radiometer Experiment. Icarus, vol. 283, 2017, pp. 300–325.
7. Smith, R.E.; and West, G.S.: Space and Planetary Environment Criteria Guidelines for Use in Space Vehicle Development, 1982 Revision (Volume 1). NASA TM–82478, 1983. http://ntrs.nasa.gov
8. Eagle Engineering, Inc.: Conceptual Design of a Lunar Oxygen Pilot Plant Lunar Base Systems Study (LBSS) Task 4.2. EEI Report 88–182, 1988.
9. Colozza, Anthony J.: Analysis of Lunar Regolith Thermal Energy Storage. NASA CR–189073, 1991. http://ntrs.nasa.gov
10. Colozza, Anthony J.: Hydrogen Storage for Aircraft Applications Overview. NASA/CR—2002-211867, 2002. http://ntrs.nasa.gov
11. Weiss, Norman L., ed.: SME Mineral Processing Handbook. Vols. 1 and 2, American Institute of Mining, Metallurgical, and Petroleum Engineers, Englewood, CO, 1985.
12. Guangzai, Nong; Yijing, Li; and Yin, Yongjun: Energy Analysis on the Water Cycle Consisting of Photo Catalyzing Water Splitting and Hydrogen Reacting With Oxygen in a Hydrogen Fuel Cell. Chem. Phys. Lett. X, vol. 4, 2019.
13. Hanford, Anthony J.: Advanced Life Support Research and Technology Development Metric—Fiscal Year 2005. NASA/CR—2006-213694, 2006. http://ntrs.nasa.gov
14. Bhasin, Kul; and Hayden, Jeffrey L.: Evolutionary Space Communications Architectures for Human/Robotic Exploration and Science Missions. NASA/TM—2004-213074, 2004. http://ntrs.nasa.gov
15. Lindsey III, Jefferson F.: Lunar Surface Transmission Loss for the Apollo Astronaut. NASA TN D–4915, 1968. http://ntrs.nasa.gov
16. Stallings, William: Data and Computer Communications. Macmillan Publishing Co., New York, NY, 1985.
17. National Renewable Energy Laboratory: Photovoltaic Research. 2019. https://www.nrel.gov/pv/ Accessed Jan. 8, 2019.
18. Barrett, Rory, et al.: Development of a Passively Deployed Roll-Out Solar Array. AIAA 2006–4011, 2006.
19. Duchek, Matthew E., et al.: Self-Deploying Tent Array for Mars Surface Solar Power. AIAA 2018–1943, 2018.
20. Crutchik, M.; Colozza, Anthony J.; and Applebaum, J.: A Photovoltaic Catenary-Tent Array for the Martian Surface. NASA TM–106306, 1993. http://ntrs.nasa.gov
21. Epec Engineered Technologies: Lithium Battery Technologies and Battery Chemistry. 2019. https://www.epectec.com/batteries/ Accessed Nov. 4, 2019.

22. Luo, Xing, et al.: Overview of Current Development in Electrical Energy Storage Technologies and the Application Potential in Power System Operation. Appl. Energy, vol. 137, 2015, pp. 511–536.
23. Mallon, Kevin R.; Assadian, Francis; and Fu, Bo: Analysis of On-Board Photovoltaics for a Battery Electric Bus and Their Impact on Battery Lifespan. Energies, vol. 10, 2017, p. 943.
24. Herron, David: Gasoline, Electricity, and the Energy to Move Transportation Systems, Green Transportation. 2019. https://greentransportation.info/energy-transportation/introduction.html Accessed Feb. 1, 2019.
25. Idaho National Laboratory: Atomic Power In Space II. INL/EXT–15–34409, 2015.
26. NASA Space Technology Mission Directorate: Kilopower. 2019. https://www.nasa.gov/directorates/spacetech/kilopower Accessed Nov. 4, 2019.
27. NASA Facts: Space Technology: Game Changing Development: The Fission System Gateway to Abundant Power for Exploration. FS–2018–01–291–LaRC, 2018. https://www.nasa.gov/sites/default/files/atoms/files/ns_kilopower_fs_180111.pdf Accessed Nov. 4, 2019.
28. NASA COMPASS Team: ISRU Power System Demonstrator: Final Draft. 2016.
29. United States Nuclear Regulatory Commission: Information for Radiation Workers. 2018. https://www.nrc.gov/about-nrc/radiation/health-effects/info.html Accessed Nov. 4, 2019.